ABSTRACT

Title: The impact of agricultural irrigation on land surface characteristics and near surface climate in China

Xiufang Zhu, Doctor of Philosophy, 2012

Directed by: Dr. Shunlin Liang, Professor

Department of Geography

It is well known that land cover and land use change can significantly influence the climate system by modulating surface-atmosphere exchanges. Land management, such as irrigation, also has a profound influence on the climate system. Irrigation can alter the water and energy flux from ground surface to the atmosphere and further influence near surface climate. Considering its dramatic expansion during the last century, the widespread use of irrigation has had an ongoing impact on our climate system. However, until now, this relationship between increased irrigation and its effect on climate system has not been well examined.

The main objective of this dissertation is to quantify the irrigation impacts on land surface characteristics and near surface climate over China by using both observational (remote sensing and meteorological observation) and modeling studies with four specific questions: Where are the irrigated areas in China? What might have happened in the past? What will happen as a result of irrigation expansion in the future? And what is the relationship between the land cover land use change (LCLUC) impact and the irrigation impact on near surface climate in China?

To answer these questions, I 1) developed three irrigation potential indices and produced a high resolution irrigation map of China; 2)analyzed and compared meteorological and remote sensing observations in irrigated and non-irrigated

agriculture areas of China; 3) simulated both irrigation and LCLUC impact on land surface energy balance components (i.e., land surface temperature, latent flux, and sensible flux) and near surface climate (i.e., air temperature, water vapor, relative humidity) of China in the past (1978-2004) and also in two future time periods (2050 and 2100) by using the Community Land Model and compared the impact of irrigation with that of LUCC.

Meteorological observations in Jilin Province show that the temperature differences between highly and lightly irrigated areas are statistically significant. The differences are highly correlated with the effective irrigation area (EIA) and sown area of crop (CSA). Results from satellite observations show that highly irrigated areas corresponded to lower albedo and daytime land surface temperature (LST), and higher normalized difference vegetation index (NDVI) and evapotranspiration (ET). The difference between highly and lightly irrigated areas is bigger in drier areas and in drier years.

The modeling studies show that the irrigation impact on temperature is much less in the future than in the 20th century and that irrigation impacts more on the maximum air temperature than on the minimum air temperature. Both contemporary and future irrigation simulations show, nationally, irrigation decreases daily maximum temperature (Tmax) but increase daily minimum temperature (Tmin). Daily mean temperature (Tmean) decreases in contemporary irrigation simulations but increases in most of the cases in future irrigation simulations. In the 20^{th} century, nationally, the spray irrigation leads to a decrease in Tmax of 0.079K and an increase in Tmin of 0.022K. Nationally, the spray irrigation leads to a decrease in Tmax

between 0.022K and 0.045K and an increase in Tmin between 0.019K and 0.057K under future scenarios.

This study demonstrates that the irrigation patterns (flood irrigation and spray irrigation) have statistically significant impacts on local climate. Moreover, this study suggests that, in the national respective, the impacts of changes in land management on climate are not comparable to the impacts of changes in land cover land use.

This dissertation on irrigation and its impact is the first study which focuses solely on China using observational and modeling methods. The results from this dissertation contribute to a better understanding of the irrigation impact on near-surface climate which can improve our knowledge of how human activities influence climate, guide future policies aimed at mitigating or adapting to climate change, and help design a precise model to project the impact of irrigation on the climate system and irrigation requirements in the future. It can also be useful in assessing future food and water security issues.

THE IMPACT OF AGRICULTURAL IRRIGATION ON LAND SURFACE CHARACTERISTICS AND NEAR SURFACE CLIMATE IN CHINA

By

Xiufang Zhu

Dissertation submitted to the Faculty of the Graduate School of the
University of Maryland, College Park, in partial fulfillment
of the requirements for the degree of
Doctor of Philosophy
2012

Advisory Committee:

Dr. Shunlin Liang, Chair
Dr. Christopher Justice
Dr. George C. Hurtt
Dr. Stephen Prince
Dr. Ning Zeng

Dedication

For my parents.

And for my husband, Dejin Bie.

Thank you for your love and support.

Acknowledgements

I am extremely grateful to my advisor, Dr. Shunlin Liang, for his continuous support, encouragement, guidance, and suggestions throughout this project. It has been a great experience to work with Professor Liang. Besides the help in my research, he also helps me a lot in my everyday life. I also would like to thank the other members in my advisory committee: Dr. Christopher Justice, Dr. George C. Hurtt, Dr. Stephen D. Prince and Dr. Ning Zeng. Their valuable suggestions helped to improve the quality of my dissertation work.

In addition, I would like to thank the encouragement and help from my colleagues in our research group including Dr. Dongdong Wang, Dr. Wonkook Kim, Tao He, Xin Tao, Xiangge Liu, Qinqing Shi, Zan Dodson, Hongyi Wu, Xiaotong Zhang, Shen Gui, Bo Li, Tongren Xu, and Bo Jiang. I benefited a lot from discussions with all of them.

Finally, I would like to thank my husband who quit his decent job in China and accompanied me during my studies. After the birth of my daughter, he put more energy and time into taking care of her than I did. I appreciate him for all of his support and encouragement so that I could work on my dissertation. His selfless and endless love makes all this possible, and I promise I will pay him back.

I am also funded by the Chinese Scholarship Program.

Table of contents

List of tables

List of figures

Chapter 1

Chapter 2

Chapter 3

Chapter 4

Chapter 1 Introduction

1.1Background

It is well known that land cover and land use change can significantly influence the climate system by modulating surface-atmosphere exchanges. These changes include urbanization (Carlson and Arthur 2000; Owen et al. 1998; Paul and Meyer 2001), deforestation (Dirmeyer and Shukla 1994; Lean and Rowntree 1997; Nobre et al. 1991), crop land expansion (Bondeau et al. 2007; Kucharik et al. 2001; Lobell et al. 2006b), and desertification (Xue 1996; Xue and Shukla 1993). Land management can also make great impact on the climate system, but current studies are thus far inadequate. Irrigation is one of most important land management techniques by which people try to grow crops in dry areas, or increase food production. It is reported that agricultural irrigation accounts for 84 percent of the global water used by the world population (Shiklomanov 2000), and has rapidly grown over the past 200 years. Irrigated areas are estimated to have increased from about 8 Million ha around 1800, to 47 Million ha around 1900 (Shiklomanov 2000), and now to about 274 Million ha around 2000 (Siebert et al. 2005b) (Figure 1-1).

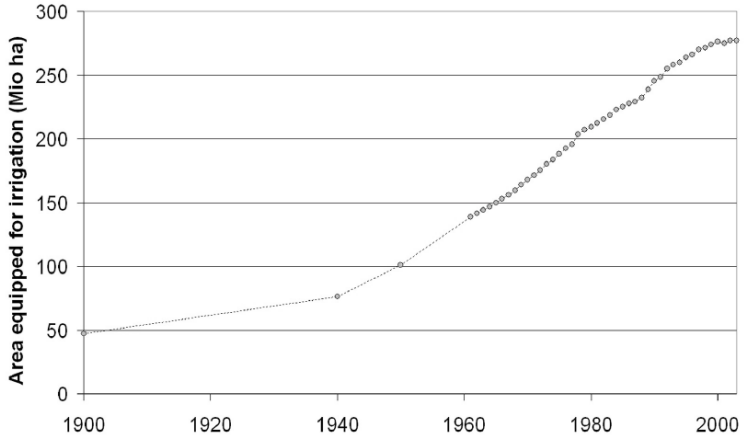

Figure 1-1 Global extent of areas equipped for irrigation in the period 1900–2003

(Data sources: Shiklomanov 2000; FAOSTAT)

Theoretically, an agricultural irrigation system can impact climate in several ways both directly and indirectly (Figure 1-2). Excessive evapotranspiration (ET) from irrigation in an agricultural system increases water vapor in the atmosphere. Water vapor is the most dominant greenhouse gas and thus amplifies the warming effect of increased atmospheric levels of carbon dioxide which is regarded as a positive feedback in our climate system (Rangwala et al. 2009; Rind 1998; Rind et al. 1991). Some reports have linked water vapor to changes in convection and precipitation patterns (Barnston and Schickedanz 1984; Chow et al. 2008; Douglas et al. 2009). ET also causes changes in the land surface energy partition (de Rosnay et al. 2003; Devries 1959) and cools the land surface and near-surface air temperature (Kueppers et al. 2007; Lobell and Bonfils 2008; Mahmood et al. 2006; Mahmood et al. 2004). Irrigation also increases soil moisture, which can modify the radiative properties of the soil such as albedo, control the partitioning of the heat flux, impact land surface processes, and therefore, influence the regional climate system.

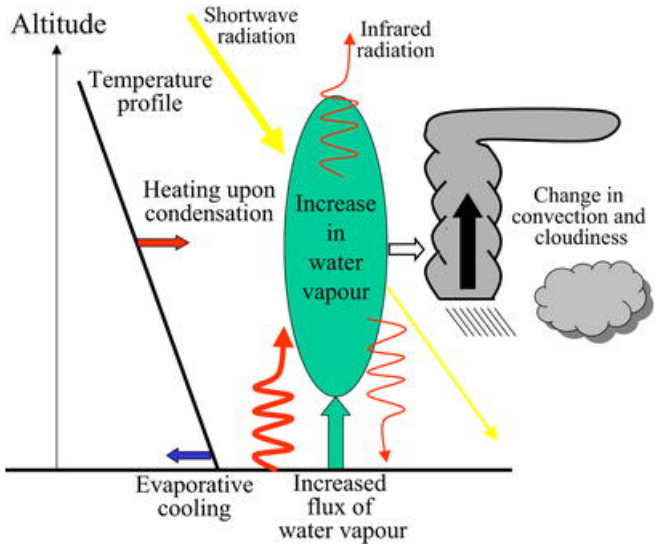

Figure 1-2 Schematic of the atmospheric properties and processes potentially induced by irrigation (Boucher et al. 2004)

The tremendous increase in irrigated areas and the potential impact of irrigation on the climate system may have contributed to the formation of the current climate system and could continue to influence our future climate system. Hence, it is important to explore the irrigation impact on near-surface climate. Such information can improve our understanding about how human activities affect climate, guide policies aimed at mitigating or adapting to climate change, and help build a precise model to project the future impact of irrigation on climate system and irrigation requirements under future scenarios as well.

So far, there have been some reports about the impact of irrigation on near-surface air temperature (Bonfils and Lobell 2007; Kueppers et al. 2007; Lobell and Bonfils 2008; Mahmood et al. 2006), energy fluxes (Devries 1959; Douglas et al. 2006), groundwater (Kendy et al. 2004), water vapor (Boucher et al. 2004), and precipitation (Barnston and Schickedanz 1984; Lee et al. 2009; Lohar and Pal 1995; Moore and Rojstaczer 2001; Segal et al. 1998) based on climate observations and modeling studies (Table 1-1). Observational studies usually make comparison between pre- and post-irrigation temperature trends in irrigated areas (Adegoke et al. 2003; Mahmood et al. 2004), or between irrigated and non-irrigated areas (Christy et al. 2006; Segal et al. 1998). Modeling studies usually compare the output from different models (regional or global, coupled or uncoupled) with and without irrigation, for example, fixing a high value of soil moisture (Kanamaru and Kanamitsu 2008; Lobell et al. 2006a), imposing a fixed amount of ET from irrigated areas (Boucher et al. 2004; Segal et al. 1998; Wauer 2007), and designing an

irrigation model based water balance between water demand and supply (de Rosnay et al. 2003; Haddeland et al. 2006) throughout the growing season.

Table 1-1 Recent Studies on irrigation impacts

Author	Method	Basic conclusion
de Rosnay et al. (2003)	Modeling	Intensive irrigation increased annual mean latent heat fluxes by 3.2w/m^2 over India during 1987–1988.
Gordon et al. (2005)	Modeling	The vapor flows increased around 2600km^3/yr globally during 1961-1990 due to irrigation.
Douglas et al. (2006)	Modeling	Mean annual vapor fluxes increased by 17% (340km^3) and mean increase of latent heat flux was estimated to be 9w/m^2 over Indian because of irrigation.
Haddeland et al. (2006)	Modeling	In the Colorado and Mekong river basins, irrigation caused mean annual latent heat flux increase by 1.2 and 1.3w/m^2, respectively, and corresponding, mean annual temperature decreased by 0.04 °C during the period 1979–1999.
Biggs et al. (2008)	Modeling and Meteorological observation	Irrigation increased annual evaporation by 166 ± 32 mm and decreased sensible heat flux by 12.7 ± 2 w/m^2 in the Krishna Basin during 1990–2005.
Douglas et al. (2009)	Modeling	Mean sensible heat flux decreased 11w/m^2 because of irrigation during 16 to 20 July 2002 over the Indian region.
Lee et al. (2009)	Satellite observation	The NDVI increased as long the increase of irrigated area in India during 1982-2003 and their correlation coefficient was high up to 0.87.
Boucher et al. (2004)	Modeling	Irrigation caused water vapor increased by 0.12-0.18% and net radiative forcing increased by 0.03-0.1w/m^2 globally for the year 1990.
Bonfils and Lobell (2007)	Meteorological observation	The maximum temperature decreased by 0.14 to -0.25 °C per decade in heavily irrigated area of California.
Geerts (2002)	Meteorological observation	The annual range of monthly-mean temperatures decreased by 1-2 K due to irrigation in southeastern Australia.
Kanamaru and Kanamitsu (2008)	Modeling	Daily minimum temperature increased by 3.5 °C in July in the California Central Valley.
Lobell et al.(2009)	Modeling	In global respective, the cooling effect of irrigation varied in different regions, and the highest temperature decrease could be up to 10 °C.
Lobell and Bonfils (2008)	Meteorological observation	Daily maximum temperature decreased by 5.0 °C in fully irrigated area of California during 1934-2002.
Mahmood et al (2006)	Meteorological observation	Mean maximum growing season temperature decreased by 1.01 °C in the northern Great Plains after 1945 when irrigation expansion occurred.
Sacks et al (2009)	Modeling	Globally, annual latent heat fluxes increased by 0.656w/m^2. Air temperature decreased by 0.061 k averaged over irrigated areas, and by 0 averaged globally.
Ozdogan et al (2010)	Modeling	Latent heat flux, ground heat flux, net radiation, ET, runoff increased by 9 w/m^2, 0.05w/m^2 and 1.2w/m^2, 0.3mm/day, 0.01mm/day respectively and Sensible heat flux decreased by 8 w/ m^2 due to irrigation over the growing season in USA.
Puma and Cook (2010)	Modeling	Annual, globally averaged decrease in temperature was 0.095 k, and the increase in precipitation was 0.026 mm d-1 during 1980-2000.

However, both observational and modeling studies are facing some challenges

(Bonfils and Lobell 2007; Lobell and Bonfils 2008). For example, meteorological observations essentially provide point measurements, which usually do not represent area means. It is difficult to clearly distinguish the impact of irrigation on climate from other factors since the background of irrigated sites such as land cover type, altitude, latitude, and longitude, distance from urban/ocean, and black carbon concentration, may vary considerably. The results from modeling rely heavily on the input parameters associated with four key aspects of irrigation: where to irrigate, when to irrigate, how much to irrigate and how to irrigate (e.g., rain, spray, drip; and rate), causing over- or under-estimation To date, efforts have been made to map the irrigated area at a global scale (where to irrigate): FAO/University of Frankfurt global map of irrigated areas for the fraction of 5 arc minutes by 5 arc minutes cells (Siebert et al. 2005b), International Water Management Institute (IWMI)'s Global Map of Irrigated Area (Thenkabail et al. 2008; Thenkabail et al. 2006) with 10 km grid resolution, and Global data set of monthly irrigated rainfed crop areas (MIRCA2000) with 5 arc-minutes by 5 arc-minutes (Portmann et al. 2010). All of them are for around the year 2000. The FAO/UF map was produced by combining irrigation statistics for 10825 sub-national statistical units and geo-spatial information on the location and extent of irrigation schemes (Siebert et al. 2005a; Siebert et al. 2005c). The IWMI map was produced through twenty years of AVHRR data and other additional data including SPOT VEGETATION, Japanese Earth Resources Satellite (JERS-1), and Landsat GeoCover 2000 data. MIRCA 2000 is produced by combining irrigation statistics, the FAO/UF map and other sources. It describes monthly growing areas of 26 irrigated and rainfed crops including wheat, rice, maize, barley, rye,

millet, sorghum, soybeans, sunflower, potatoes, cassava, sugar cane, sugar beet, oil palm, rape seed/canola, groundnuts/peanuts, pulses, citrus, date palm, grapes/vine, cocoa, coffee, as well as related crop calendars for 402 spatial units. However, these global irrigation maps were assessed by limited ground-truth data. Some regions without ground-truth data may be less reliable.

Another problem in current observational studies is that most evidence about irrigation impact on climate is reported in intensive irrigated areas of the USA (Bonfils and Lobell 2007; Kanamaru and Kanamitsu 2008; Kueppers et al. 2007; Lobell and Bonfils 2008; Lobell et al. 2008; Mahmood et al. 2006; Mahmood et al. 2004; Weare and Du 2008) and India (Biggs et al. 2008; de Rosnay et al. 2003). Little meteorological observation evidence is reported in other places including China, the second largest irrigation area (53.8 M ha), following India (57.3 M ha), in the world (Siebert et al. 2005b), which may be caused by several reasons. First, it is limited by direct observation. Most Chinese meteorological stations are located within, or near cities, and the urbanization influence is highly significant (Zhou et al. 2004). Second, the Asian Monsoon sweeps across China during June to July each year, the growing season for major crops in China, which causes the impact of irrigation to be less obvious. Third, the main irrigation pattern in China is supplemental irrigation that adds small amounts of water to rainfed crops when rainfall fails to provide sufficient moisture for normal plant growth. Hence, it also weakens the atmospheric signature of irrigation. Fourth, rapid urbanization along with irrigation expansion during past decades exacerbates the difficulty in distinguishing the climatic impact of irrigation. Lastly, black carbon aerosol emissions from household burning of biofuels, coal and

biomass—which are also theorized as a cause of global climate change—are reported to be very high in China (Menon et al. 2002), and thus make the study of irrigation's impact on climate change particularly difficult (Bonfils and Lobell 2007).

Considering the weaknesses in current studies mentioned above, future studies should consider the following several points in order to better evaluate irrigation impact on our climate system:

First, an irrigation map is one of the most important model inputs; it directly decides which grids will be irrigated during simulation. The small uncertainties or errors in the irrigation map may lead to great differences of simulation outputs, especially at the regional scale. Hence, it is necessary to produce a reliable irrigation map.

Second, to avoid over- or under- estimation of irrigation impact, modeling study should reflect reality as much as possible taking into account such factors as irrigation patterns (spray irrigation, flood irrigation or drop irrigation), rate and time.

Third, remote sensing observation is a promising tool since it can provide land parameter information on a large scale including soil moisture, albedo, land surface temperature, vegetation cover and so on. It could be a valid method for determining the impact of irrigation on the local surface climate—especially in those regions where direct observations are limited or obscured by other factors, such as urbanization in China. It also can be integrated into models to better represent reality.

Fourth, a comprehensive evaluation method needs to be developed, in which evidence from both observational studies (remote sensing and meteorological measurement) and modeling studies can validate each other.

Based on the above considerations, this study proposes a comprehensive framework for China to address four questions:

1. Where are the irrigated areas in China?
2. What might have happened?
3. What will happen due to irrigation expansion?
4. Is the impact of irrigation comparable to that of land cover land use change (LCLUC)?

1.2 Objectives

The overall objective is to quantify the irrigation impact on land surface characteristics and near surface climate by using both observational (remote sensing and meteorological observation) and modeling studies. To be specific, I will:

1. Develop and implement a new methodology to produce a high resolution irrigation area distribution map of China.
2. Analyze meteorological and remote sensing observations in irrigated and non-irrigated agricultural areas of China for finding evidence of irrigation impacts in China.
3. Use the Community Land Model (CLM) to simulate irrigation impact on land surface energy balance components (e.g., land surface temperature, latent flux, and sensible flux) and near surface climate (e.g., air temperature, water vapor,

relative humidity etc.) of China by using a high resolution irrigation map produced from objective 1.

4. Estimate the irrigation impact in the future scenarios by CLM with the IPCC 4 future scenarios.
5. Simulate the impact of land cover land use change impact on near surface climate in China, and compare the impact with that of irrigation.

1.3 Outline of the Dissertation

The dissertation consists of five chapters (**Error! Reference source not found.**). The first chapter is the introduction. The second to fourth chapters are presented in the self-contained format of a journal article. Chapter 5 concludes the findings and contributions of this dissertation and also discusses the limitations of the current study as well as future study directions.

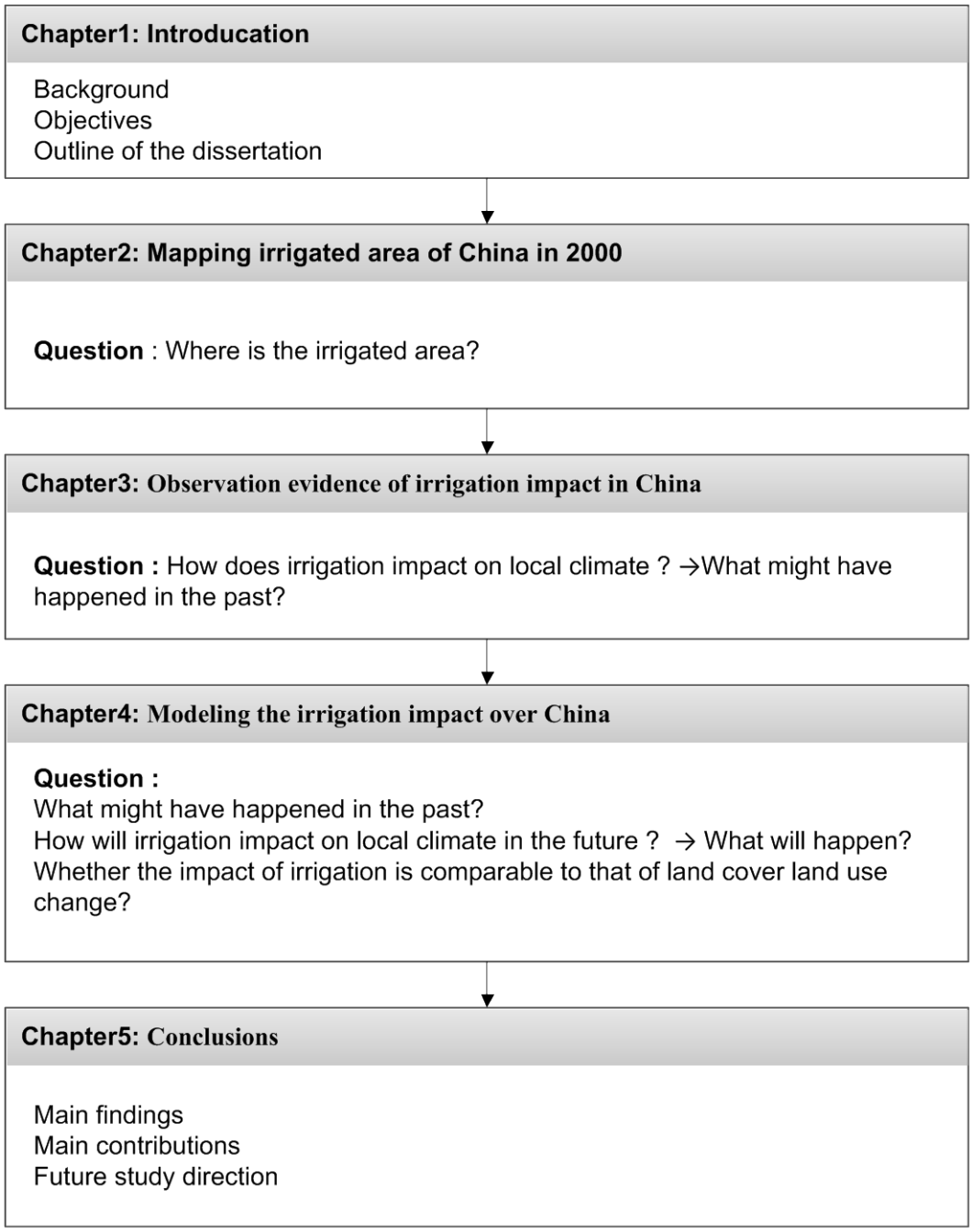

Figure 1-3 Dissertation structure

Chapter 2 Mapping Chinese irrigation in 2000

In addition to global-scale irrigation maps mentioned in the introduction, irrigated area studies at other scales have also been reported (Beltran and Belmonte 2001; Biggs et al. 2006; Boken et al. 2004; Dheeravath et al. 2010; El-Magd et al. 2003; Ozdogan and Gutman 2008; Thenkabail et al. 2005; Wriedt et al. 2009). Current methods for producing irrigated area datasets can be divided into three basic types: census data (such as FAO's method), remote-sensing-derived maps (IWMI's method), and GIS-derived maps (such as FAO/FU's method). Census data do not provide locational information about irrigated areas (Döll and Siebert 1999; FAO 2003). Remote-sensing-derived maps exploit advanced remote sensing technology to determine both the spatial location and extent of irrigated areas; however, some challenges exist. For example, for patchy irrigated areas, remote sensing data with fine spatial resolution is needed to accurately detect which fields are irrigated in a given year or growing season. Meanwhile, in some cropping systems, a certain field can be planted once, twice, or even three times in one year, so the remote sensing data used to detect irrigated areas must have a high temporal resolution. However, data with both high spatial and high temporal resolution are difficult to obtain for large-scale studies. Additionally, traditional classification methods sometimes cannot effectively distinguish irrigated areas from non-irrigated areas owing to the spectral mixture between them, especially for supplemental irrigated areas, causing over- or underestimation. On the other hand, collecting a large number of high-quality training samples is costly and time-consuming. GIS-derived maps allocate census data on irrigated areas from geopolitical units to grids on the basis of predefined rules and

have not taken advantage of remote sensing technology in past work, such as the FAO/FU's method.

In this study, I developed three irrigation potential indices and proposed a spatial allocation model for mapping irrigated areas of China. China was selected as the study area because no study has attempted to map the irrigated areas of China, although it has the second highest irrigated area in the world. The global irrigation maps cover China; however, they are perhaps less reliable owing to the lack of ground-truth data for China (Ozdogan and Gutman 2008). If a more detailed irrigated area map of China can be produced, it will contribute to efforts to map global irrigated areas, and also to the study of irrigation water requirements, food and water security issues in China.

Here, I will introduce the proposed method for developing irrigation indices and the irrigation spatial allocation model in section 2.1. Section 2.2 describes the data used for mapping Chinese irrigation in 2000, and section 2.3 shows irrigation map of China in 2000 by using the proposed method. Discussion and conclusions are presented in Section 2.4. A manuscript about the work in this chapter has been prepared and submitted for review (Zhu et al. 2011d).

2.1 Methodology

It is difficult to distinguish irrigated areas from non-irrigated areas, especially for supplemental irrigated areas, since the water that croplands accept can come from rainfall, irrigation, or both. An irrigation index indicating how likely cropland is to accept water from irrigation is helpful in mapping irrigated areas. Therefore, I built up three irrigation indices based on an assumption, and then developed an automatic

classification routine to downscale the irrigated area census data from a given political unit to each pixel within the unit with the help of the irrigation indices and the existing land cover map.

2.1.1 Assumptions

My assumption is that the crop productivity is high and stable over a long time series in irrigated areas compared with rainfed areas in a given land unit. In other words, agricultural areas with little variation in productivity but high irrigation demand over a long time period are more likely to be irrigated than agricultural areas with great variation in productivity but low irrigation demand (Figure 2-1). In this assumption, I emphasize two points: a given land unit and a long time series.

A land unit here is defined as land with the same characteristics, such as productivity, irrigation requirements, climate condition, fertilizer and pesticide use, weed control, etc. In this work, I used the boundaries of the administrative units to define the land units mainly because the statistics are reported based on the administrative units (province, city, or county). Obviously, the smaller the administrative unit, the higher the expected accuracy.

Second, I emphasize that the productivity of crops is stable over a long time series in irrigated areas compared with rainfed areas. In other words, I emphasize the mean status of the productivity of crops over a long time period. In China, the term “irrigated area” refers to land “where there are water sources or complete sets of irrigation facilities to lift and move adequate amounts of water for irrigation purposes under normal conditions,” and irrigated area statistics are an indication of “drought resistance capacity” (China Statistical Yearbook 2008). Therefore, irrigated areas can

better resist disasters such as drought. Moreover, farmers are more likely to keep cropland with an irrigation system than without an irrigation system, and they are more likely to maintain better field management such as fertilizer and pesticide use and weed control in the irrigated areas because of a much higher crop yield in those areas than in the non-irrigated areas especially in dry regions.

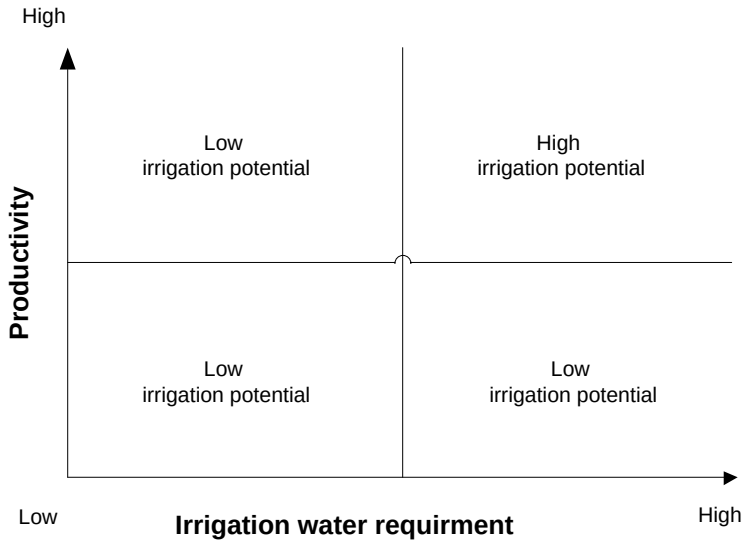

Figure 2-1 Assumption for developing the irrigation indices

2.1.2 Irrigation index

The Normalized Difference Vegetation Index (NDVI) is strongly related to canopy biophysical properties and is often used as a proxy for vegetation productivity (Fensholt et al. 2004; Paruelo et al. 1997; Zhao et al. 2005). Here, I use it as a proxy for crop productivity. Irrigation demands can be indicated by the aridity index or precipitation. Finally, I developed the following formulae to estimate the likelihood of irrigation. In Equation 2-1, the pixel with a higher precipitation, but larger NDVI variation, has less potential to be irrigated. In Equation 2-2, the pixel with high precipitation variation, but stable NDVI, is more like to be irrigated. In Equation 2-3, the pixel with stable NDVI, but deceasing precipitation, is more like to be irrigated.

$$IP_{1,i} = \frac{1000 - CV'_{NDVI_i}}{u_{PI_i}} \quad \textbf{Equation 2-1}$$

$$IP_{2,i} = (1000 - CV'_{NDVI_i}) \times CV_{PI_i} \quad \textbf{Equation 2-2}$$

$$IP_{3,i} = \frac{1000 - CV'_{NDVI_i}}{S'_{PI_i}} \quad \textbf{Equation 2-3}$$

Here, IP is the irrigation potential index. There are three irrigation potential indices: $IP_{1,i}$, $IP_{2,i}$, and $IP_{3,i}$.The term CV'_{NDVI_i} represents the quantile-normalized CV_{NDVI_i} obtained using Equation 2-4 to Equation 2-6, and $\mathrm{NDVI_i}$ CV_{NDVI_i} is the coefficient of variance of the growing season NDVI over the studied period at pixel *i*. The quantile-normalization of NDVI aims to reduce the effect of the extreme NDVI values. The terms μ_{PI_i} and CV_{PI_i} are the mean and coefficient of variation of precipitation (mm/year), respectively, in the past several decades. S'_{PI_i} is the normalized S_{PI_i} obtained by the min-max normalization (Equation 2-8), and S_{PI_i} is the regression coefficient of precipitation (Equation 2-7) in the past several decades at pixel i. The value of S_{PI_i} could be negative or positive, where negative S_{PI_i} indicates a decreasing precipitation trend and positive S_{PI_i} indicates an increasing trend. To ignore the impact of the sign of S_{PI_i} on the calculation of the likelihood of irrigation S_{PI_i} is first normalized as S'_{PI_i} by min-max normalization. The value of S'_{PI_i} is

between 0 and 1, where 0 represents the strongest decreasing trend of precipitation and 1 represents the strongest increasing trend of precipitation.

if $CV_{NDVI_i} \le CV_{NDVI_{q10}}, CV'_{NDVI_i} = CV_{NDVI_{q10}}$ **Equation 2-4**

if $CV_{NDVI_i} \ge CV_{NDVI_{q90}}, CV'_{NDVI_i} = CV_{NDVI_{q90}}$ **Equation 2-5**

else $CV'_{NDVI_i} = \frac{CV_{NDVI_i} - CV_{NDVI_{q10}}}{CV_{NDVI_{q90}} - CV_{NDVI_{q10}}}$ **Equation 2-6**

Where, $NDVI_i$ $CV_{NDVI_{q10}}$ and $CV_{NDVI_{q90}}$ are the CV_{NDVI_i} values of the 10th and 90th percentiles, respectively. To reduce the effect of extreme values, the 10th and 90th percentiles of CV_{NDVI_i} were set to 0 and 1000, respectively, and the other pixel percentile values were scaled linearly between 0 and 1000. To do this, CV'_{NDVI_i} equals $CV_{NDVI_{q10}}$ if CV_{NDVI_i} is less than or equal to $CV_{NDVI_{q10}}$, and it equals $CV_{NDVI_{q90}}$ if CV_{NDVI_i} is greater than $CV_{NDVI_{q90}}$.

$$PI'_{i,j} = S_{PI_i} \times PI_{i,j} + Bias_{i,j}$$ **Equation 2-7**

$$S'_{PI_i} = \frac{S_{PI_i} - Min(S_{PI_i})}{Max(S_{PI_i}) - Min(S_{PI_i})}$$ **Equation 2-8**

Where $PI_{i,j}$ represents the precipitation observation for year *j* at pixel *i* (mm/year), and it was derived by interpolating precipitation records at observation sites to pixels. The terms S_{PI_i}, $Bias_{i,j}$, and $PI'_{i,j}$ are the regression coefficient, bias, and estimate, respectively, of precipitation during the past several decades at pixel *i*.

Of those three variables, only S_{PI_i} is further used to calculate the likelihood of irrigation.

2.1.3 An automatic allocation model

After estimating the likelihood of irrigation of each pixel in a given unit using the three possible irrigation indices developed in section 2.2, I downscaled the irrigated area census data from a given political unit to each pixel within the unit with the help of the irrigation indices and the existing land cover map, in the four steps as described below.

Step 1. The pixel with the highest irrigation potential within the crop grids was firstly identified as an irrigated pixel. The irrigation percentage in the irrigated pixel equals the crop percentage of this pixel, which is determined using land cover maps. In this study, the land cover maps are from the National Land Cover Database (NLCD) for China (2000).

Step 2. The total area covered by the irrigated pixels was calculated and was compared with the target number of hectares provided by the census of irrigated areas in the Statistical Yearbook. If the total area of the selected pixels was less than the target area, the pixel with the next highest irrigation potential was selected.

Step 3. These steps are repeated until the total irrigated area is greater than the target area in a given political unit.

Step 4. All the irrigated pixels in each given geopolitical unit are combined to obtain the irrigation map of the whole study area.

2.1.4 Mapping irrigated area

My method for deriving the final irrigation map is shown in Figure 2-2. For each irrigation index, I used the automatic allocation model described in section 2.1.3 to generate a preliminary irrigation map in which the pixel value ranges from 0–100, and then transferred the preliminary irrigation map to a binary map by a simple rule: If the value of a pixel in the preliminary irrigation map was greater than 0, I defined it as 1; otherwise it was given a value of 0 in the binary map. Thus, I generated three binary irrigation maps from three different irrigation indices. I summed the three binary irrigation maps to produce a new "Irrigation Potential Intensity Map," in which the pixel values range from 0 to 3. A pixel value of 0 indicates that all three irrigation indices show that no irrigation occurred in that pixel; a pixel value of 3 in the Irrigation Potential Intensity map indicates that all three irrigation indices show irrigation may occur in that pixel. For pixels with a value of 3, I then reused the irrigation potential calculated from the Irrigation Index 1 ($IP_{1,i}$) and the automatic allocation model to downscale the irrigated area census data from the given political units to each pixel within the unit. The procedure terminates if the total irrigated area calculated from that pixel with a value of 3 in the Irrigation Potential Intensity map is already greater than the target area in a given administrative unit; otherwise, I continue to use the automatic allocation model for the pixels with a value of 2. Similar procedures are repeated for pixels with a value of 2 (and then 1) in the Irrigation Potential Intensity map until the total irrigated area calculated from the automatic allocation model is greater than the target area.

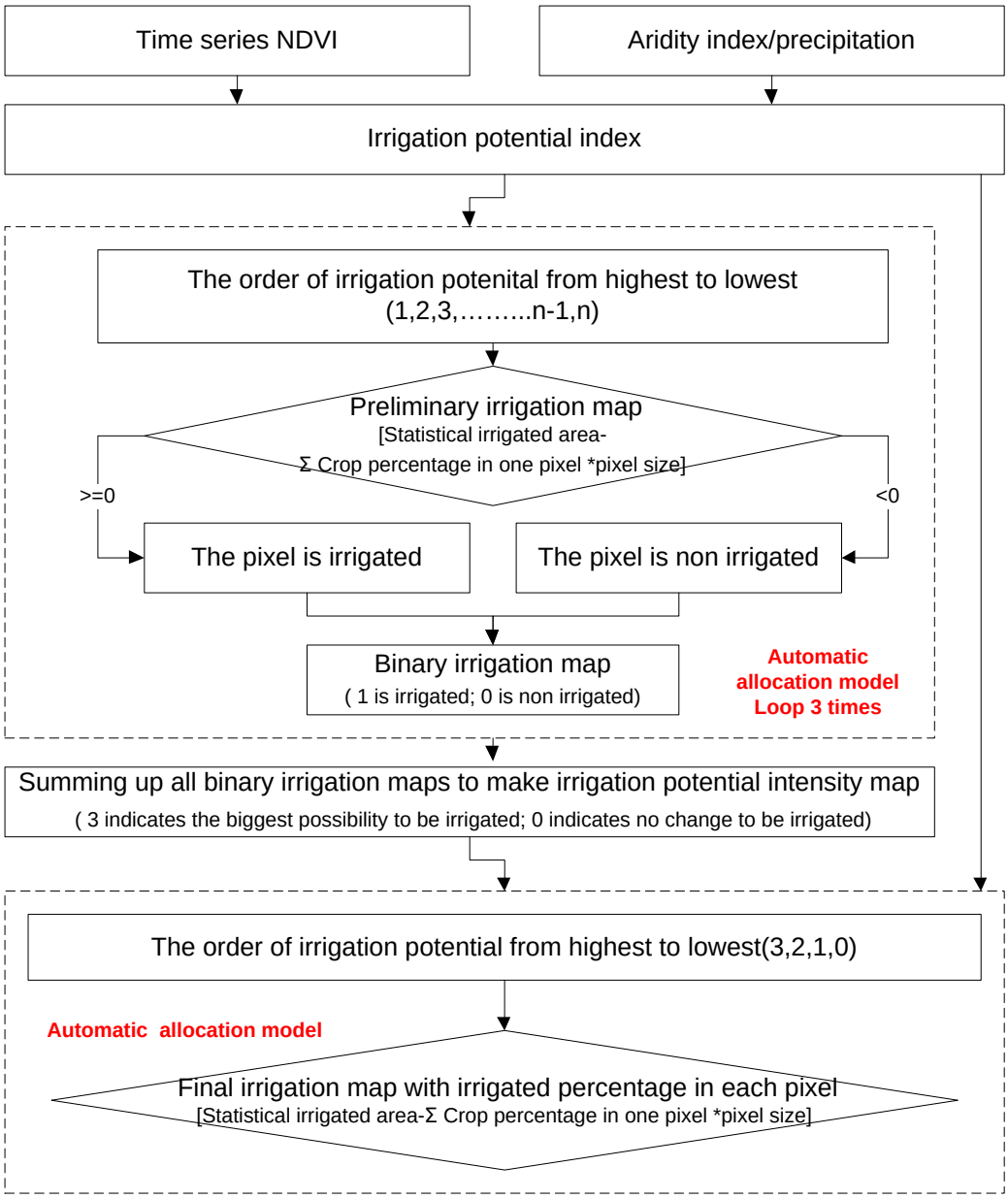

Figure 2-2 Procedures for developing irrigation map of China

2.2 Data and Processing

2.2.1 Irrigation census data and recalculation

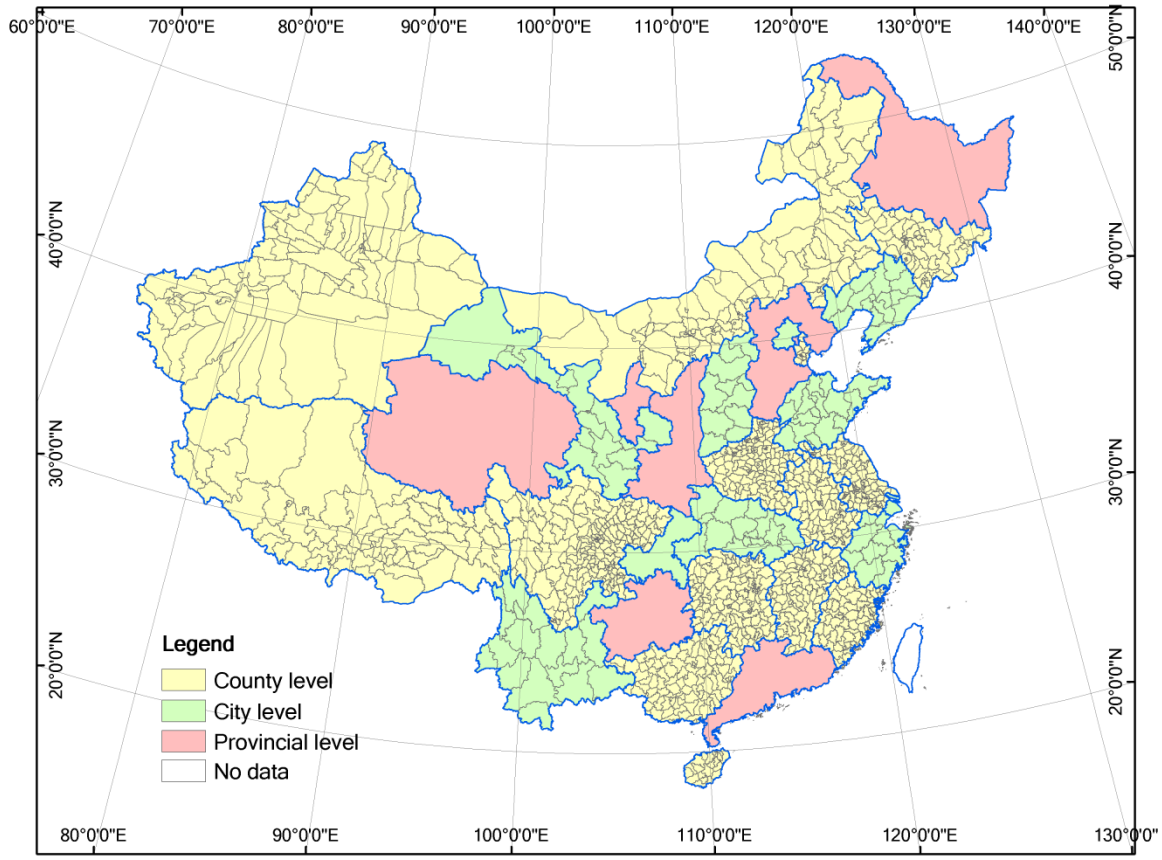

Figure 2-3 Available census of irrigated areas of each province in China from the Statistical Yearbook 2001. Yellow indicates provinces with county-level irrigation data; green indicates provinces with city-level irrigation data; pink shows that the province has only irrigation data for the entire province; white indicates that no data are available.

In China, irrigated areas are reported on the basis of census data. Traditional local-level Bureaus of Statistics report irrigation census data at the village level, which are then aggregated to higher levels, such as the county, city, province, and national levels. The National Bureau of Statistics regularly releases data on the provincial-level irrigated area in its Statistical Yearbook. Local Bureaus of Statistics might release the county- or city-level irrigated area. Considering that the IWMI and FAO/UF maps are all from around 2000, in this study, I tried to collect all the

available irrigated area data for each province in 2000 (Figure 2-3). I obtained county-level irrigated areas in 14 provinces (Jiangsu, Inner Mongolia, Sichuan, Tianjin, Anhui, Xinjiang, Henan, Hunan, Fujian, Jilin, Guangxi, Jiangxi, Hainan, and Tibet), city-level irrigated areas in 7 provinces (Shandong, Zhejiang, Yunnan, Shanxi, Hubei, Liaoning, and Gansu) and 3 municipalities (Chongqing, Beijing, and Shanghai), and provincial-level irrigated area in 7 provinces (Ningxia, Guizhou, Qinghai, Heilongjiang, Guangdong, Hebei and Shaanxi). No data are available for Taiwan, Hong Kong, and Macao. The geopolitical units (city, county, and province) are used as land units as described in Section 2.1 to map irrigated areas.

Before using the irrigation census data to map irrigated areas in China, I preprocessed the census data, for two reasons. First, the boundaries and names of some areas have been changed since 2000. For example, a county may have been upgraded or merged into a city. Therefore, I amended the boundary polygon map and update its attributes. Second, in some provinces, such as Xinjiang, Heilongjiang, and Hainan, the irrigated area reported in the Yearbooks contains two parts: one from the local Bureau of Statistics, which reports city- or county-level irrigated areas, and another from the Production and Construction Corps, which reports only the total irrigated area in the agricultural land it manages. The agricultural lands managed by Production and Construction Corps are distributed across the entire province, and there is no polygon map showing their location. Thus, I combined these two parts. My method for combining them is as follows:

$$IRR\_C_i^{'} = IRR\_P \times \frac{f_i}{\sum_{i=0}^{n} f_i} + IRR\_C_i \qquad \textbf{Equation 2-9}$$

IRR_P is the total irrigated area of agricultural land managed by the Production and Construction Corps in a target province. IRR_C_i is the irrigated area reported by the local Bureau of Statistics in the county or city i. f_i represents attributes of the county or city i that are strongly related to the irrigated area, such as the acreage of agricultural land and the agricultural population. In this study, I used the acreage of agricultural land as an eigenvalue in Hainan province and the agricultural population in Xinjiang province to calculate the total irrigated area in a target city. Table 2-1 shows an example of the recalculated city-level irrigated area in Hainan province.

Table 2-1 Recalculated city-level irrigated area in Hainan province

Regions	IRR_C_i (kha)	f_i (kha)	$f_i \Big/ \sum_{i=0}^{n} f_i$	$IRR\_C_i^{'}$
Haikou	1.07			1.07
Sanya	6.84	2.24	0.06	7.76
Wuzhishan	1.84	0.09	0.00	1.87
Qiongshan	16.78	5.00	0.14	18.84
Wenchang	12.59	1.93	0.05	13.38
Qionghai	13.64	0.56	0.02	13.87
Wanning	8.68	1.02	0.03	9.10
Ding'an	9.61	1.54	0.04	10.24
Tunchang	4.05	1.54	0.04	4.68
Chengmai	10.31	4.11	0.11	12.00
Lingao	10.62	6.19	0.17	13.16
Danzhou	16.38	7.08	0.19	19.29
Dongfang	11.15	0.24	0.01	11.25
Ledong	15.55	0.99	0.03	15.95
Qiongzhong	4.25	1.12	0.03	4.71
Baoting	3.19	0.62	0.02	3.44
Lingshui	9.14	0.92	0.02	9.52
Baisha	3.59	1.49	0.04	4.21
Changjiang	5.30	0.33	0.01	5.43
IRR_P	15.22	36.98	1.00	
Total	179.78			179.78

Note: Here, f_i is agricultural land occupied by the Production and Construction Corps of Hainan province (Kha). IRR_C_i is the effective irrigated area in a target city (Kha), and IRR_P is the total agricultural land occupied by the Production and Construction Corps of Hainan province (Kha).

2.2.2 Time series NDVI

I acquired 10-day composite, 1-km SPOT-VEGETATION satellite images for 1998–2010 at http://free.vgt.vito.be/. The VEGETATION products fall into three categories: VGT-P (Primary), VGT-S (Synthesis), and VGT-D (Directional) (Maisongrande et al. 2004). VGT-P products provide top of the atmosphere (TOA) reflectances that are corrected by radiometric and geometric corrections. VGT-S products are derived from P products and provide daily and 10-day MVC (Maximum Value Composite) syntheses. VGT-D products are bidirectional composite syntheses. In this study, I used VGT-S10 data to calculate the coefficient of variation of NDVI (CV'_{NDVI_i}) during a growing season. The growing season is from April to September.

2.2.3 Precipitation and interpolation process

The precipitation data used in this study include monthly mean precipitation averaged from 1950 to 2000 from WorldClim Global Climate Data at http://www.worldclim.org/ (Hijmans et al. 2005) and precipitation observations from the National Meteorological Center of the China Meteorological Administration (NMCCMA). China has a total of 726 observation sites, 11 of which were excluded from further processing in this study because of inconsistent or short-term observations. The precipitation obtained from WorldClim Global Climate Data has a resolution of 1 km and therefore, does not require further interpolation. It was used as μ_{PI_i} to calculate the first irrigation potential index using Equation 1. However, the WorldClim Global Climate Data only provides mean precipitation, and so cannot be

used to calculate the coefficients of variation of precipitation (CV_{PI_i}) and regression coefficients of precipitation (S_{PI_i}). Therefore, I used the precipitation observations from NMCCMA to estimate CV_{PI_i} and S_{PI_i} and then interpolated the CV_{PI_i} and S_{PI_i} values from the observation sites to 1-km resolution grids by the inverse distance weighting method (**Error! Reference source not found.**).

2.2.4 Other data sets and preprocessing

The other data used in this study include the FAO/UF map, the IWMI map, and the intensively validated National Land Cover Data of China (NLCD2000) produced by visual interpretation and digitization of Landsat TM/ETM+ data in 2000 (Liu et al. 2002; Liu et al. 2005a).

The FAO irrigation map used in this study is version 4.0.1, which can be downloaded at http://www.fao.org/nr/water/aquastat/irrigationmap/index10.stm. It showed the fraction of 5′ × 5′ cells that was equipped for irrigation in about the year 2000. The area equipped for irrigation includes areas equipped for full control irrigation, equipped lowland areas, and areas equipped for spate irrigation. It does not include non-equipped cultivated wetlands and inland valley bottoms or non-equipped flood recession cropping areas. The data collected for China in FAO's AQUASTAT-programme (available at http://www.fao.org/nr/water/aquastat/irrigationmap/cn/index.stm) is actually the same as mine (available at http://www.stats.gov.cn/tjsj/ndsj/). The numbers used in the FAO/UF map and in my map are consistent in all the provinces except Xinjiang (3094.8 Kha in FA map and 3094.3 Kha in our map). Therefore, I can conclude that

the area equipped for irrigation shown in the FAO/UF map has the same meaning as the effective irrigated area in my map and that those two maps are comparable. However, the irrigated areas on a county and city level in the FAO/UF map are not consistent with the census data (Figure 2-4), which indicate that the FAO/UF map still has room for improvement.

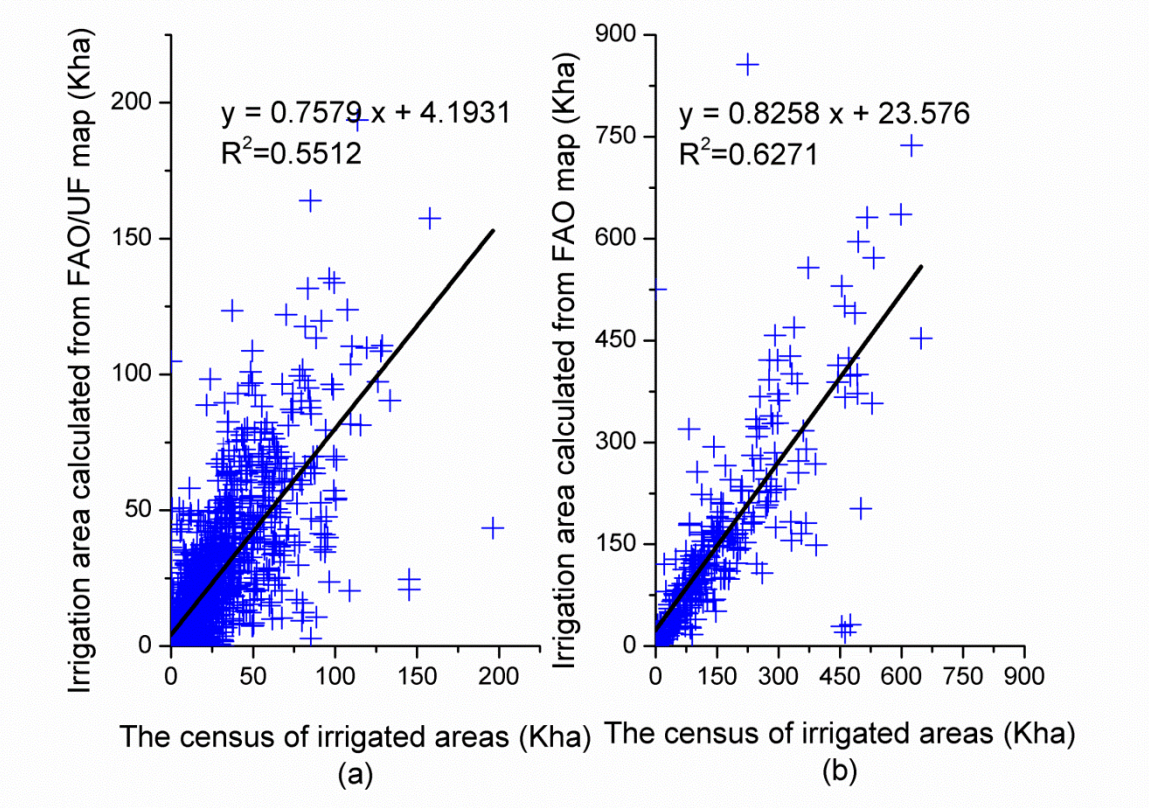

Figure 2-4 Regression of irrigated areas between census data and the FAO/UF map at the county level (a) and city level (b) **(**Note: only the cities and counties with available census data were used to produce this figure.)

The IWMI map used in this study is version 2.0, which can be downloaded at http://www.iwmigiam.org/info/main/index.asp. The area statistics reported by IWMI include annualized irrigated areas (AIA) and total area available for irrigation (TAAI). The former considers the intensity of irrigation and the latter does not. In my comparison, I used TAAI, which refers to the irrigated areas at any given point in

time as well as the areas left fallow but “equipped for irrigation” at the same point in time. From the definition, we can see that the IWMI map and my map are also comparable. Therefore, The FAO and IWMI maps were used for comparison with the newly produced irrigation map.

The cropland area of China around the year 2000, as derived by remote sensing images, was reported in several previous studies. It was estimated to be 204 million ha by using the Global Land-use Model (GLM) (Hurtt et al. 2006), 133 million ha by HYDE from the History Database of the Global Environment (Goldewijk et al. 2011), 140 million ha by Houghton and Hackler (Houghton and Hackler 2003) and Ramankutty et al. (Ramankutty et al. 2008), and 141.1 million ha by NLCD2000 (Liu et al. 2005c). The census data of the cropland area is reported as 156.3 million ha in the National Statistical Yearbook 2001. The estimate of the cropland by NLCD2000 is closest to the census data. Therefore, the NLCD was used to provide the crop percentage information in detected irrigated pixels. NLCD2000 has six land cover types: cultivated land, forest, grassland, residence, unused land, and water body, and 1 km spatial resolution in Albers equal-area conic projection. Cultivated land has two sub categories: paddy land and dryland.

2.3 Results, validation and product intercomparisons

2.3.1 Results

Using the method described in Section 2.1, I produced an irrigation map of China for the year 2000. In terms of my method, after a pixel was identified as an irrigated pixel, the irrigation percentage of this identified irrigation pixel was set as equal to the crop percentage of this pixel. The crop percentage is the sum of paddy

land and dryland percentages in this pixel. As a result, I obtained three values in one irrigated pixels: the percentage of irrigated paddy fields, the percentage of irrigated dryland and the total irrigation percentage. Accordingly, I generated three secondary products: irrigated dryland area, irrigated paddy fields, and rainfed area (Figure 2-5). The total irrigated land is the sum of the irrigated dryland area and irrigated paddy fields, and the rainfed land is the cropland minus the irrigated area.

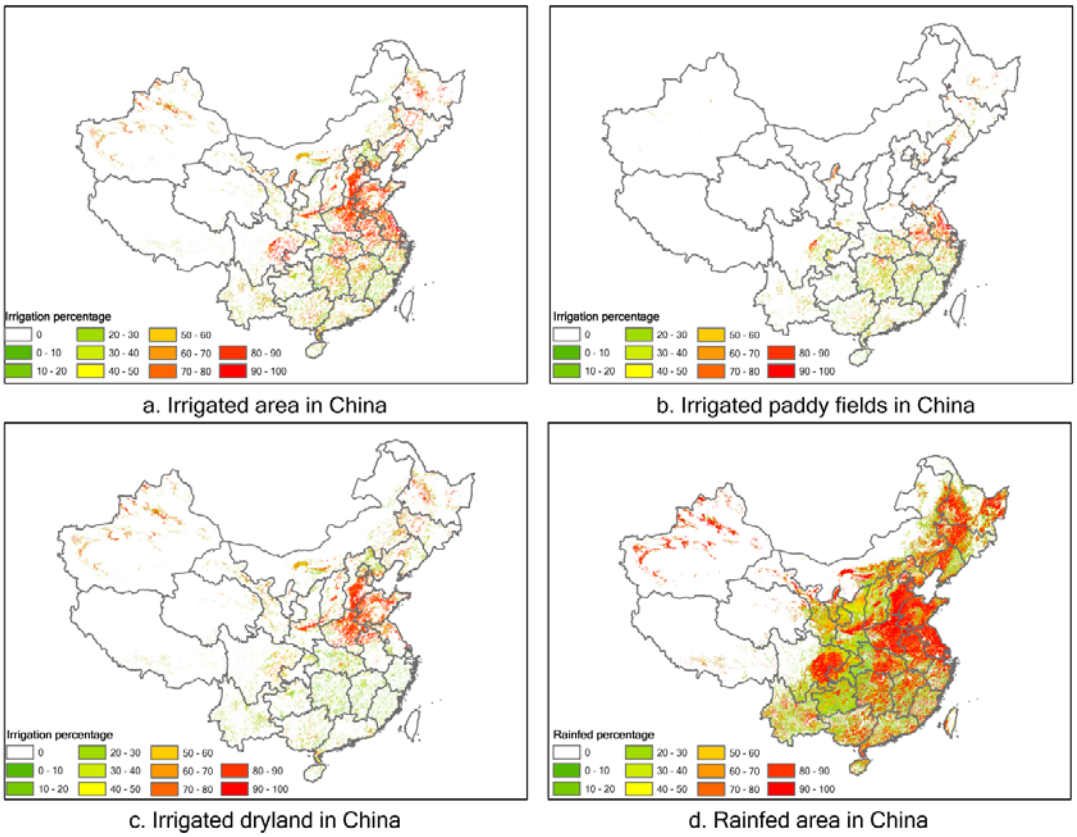

Figure 2-5 Irrigated and rainfed areas in China in 2000

2.3.2 Validation

To validate the accuracy of the new map and facilitate comparison with the FAO and IWMI maps, I collected 614 validation samples (262 irrigated samples, 352 non-irrigated). The samples were obtained from two sources: The first source was the crop growth and soil moisture dataset provided by the China Meteorological Data

Sharing Service System (CMDSSS). This dataset records the crop type, developmental phase, the date of the developmental phase, plant height, plant density, soil moisture in the top 10 cm, 20 cm, 50 cm, 70 cm, and 100 cm and the irrigation label (irrigated or non-irrigated) of 778 observational sites since 1991. All sites with an irrigation labels were used in this study, and they are totally 352 non-irrigated samples and 156 irrigated samples. The irrigated samples from this source are mainly located in North China and Southwest China; Southeast China does not have irrigated samples. I therefore collected another 106 irrigated samples by identifying and labeling them using Google Earth and irrigation information on large irrigated areas provided by the China Irrigation and Drainage Development Center (CIDDC) at http://www.dxgq.org.cn/other/AllIrrInfo.aspx. A large irrigated area in China is defined as an area where the effective irrigated area is greater than 0.3 million acres. This website releases the information on 443 large irrigated areas distributed over the whole of mainland China including the name, location, the total cultivated land, the irrigation and drainage development history in this area, water resource, crop types, and so on. The Google Earth data and CIDDC data were the second source. Unlike CMDSSS, CIDDC does not provide the latitudes and longitudes of the irrigated sites, but it does describe the irrigation water source of the large irrigated area (e.g., lake, canal, reservoir, and river). Therefore, I searched for the location of the irrigation water sources by name, using Google Earth, then zoomed in on the high-resolution Google Earth images and labeled the farmlands near the irrigation water sources as irrigated sites. Figure 2-6 shows the locations of the sites of my validation samples in mainland China;

Figure 2-7 shows three examples of irrigated sites that I collected using Google Earth and CIDDC data.

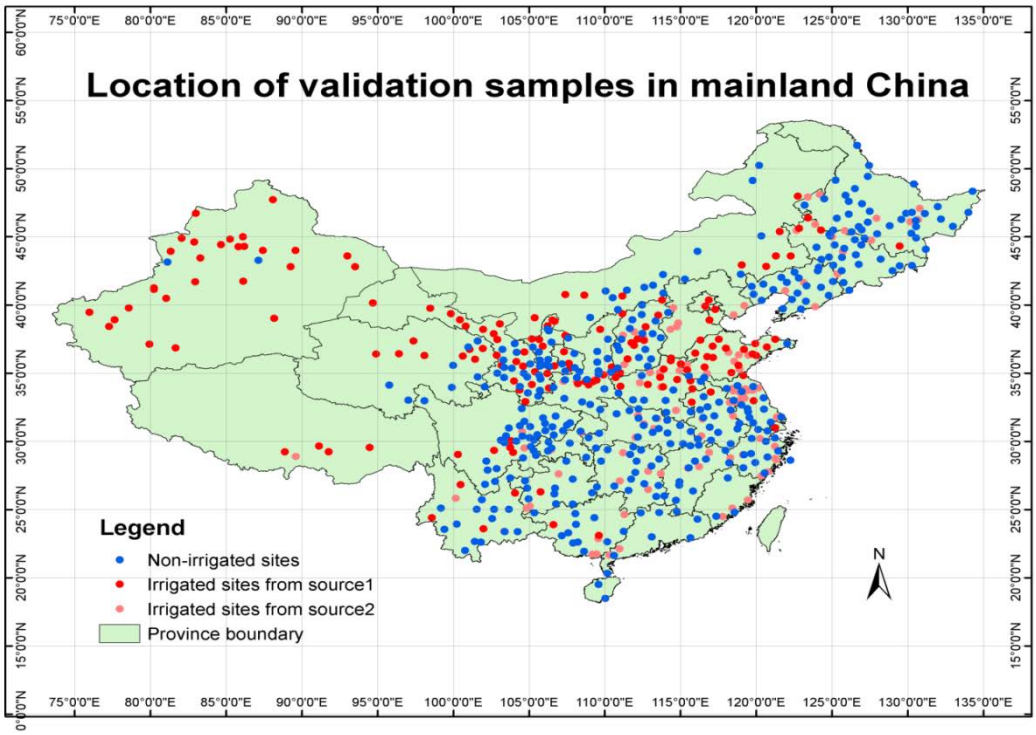

Figure 2-6 Validation samples in mainland China. The first data source is crop growth and soil moisture dataset, provided by the China Meteorological Data Sharing Service System; the second data source is visual interpretation from Google Earth data and China Irrigation and Drainage Development Center data

a b c

Figure 2-7 Three examples of irrigated sites labeled using Google Earth: (a) Wusi Jiang, Guangxi Province; (b) The People's Victory Canal, Henan Province; and (c) Xingkai Lake, Heilongjiang Province

In the new irrigation map and the FAO/UF map, the pixel value is the percentage of irrigation while the pixel value of IWMI is the class label for the irrigation type. In order to validate the data, these irrigation maps need to be transformed into binary maps (irrigation and non-irrigation), wherein pixels in these three maps with a value greater than 0 were coded as 1, representing irrigated areas; other pixels were coded as 0, representing non-irrigated areas. I then compared the class label of each sample in the reference data to the class label of the pixel extracted from the irrigation maps at the same location.

The resolutions of the three irrigation maps are different. The resolution of FAO/UF map, IWMI map and new map are 5' (0.0833333º), 0.0089282º, and 1km, respectively. Validating the non-irrigated pixels is more difficult for the FAO/UF map because the non-irrigation samples collected in a small region within the 5' × 5' grid may not represent that the whole 5' × 5' grid is non-irrigated. Therefore, we calculated the error matrices for the IWMI map and the new irrigation map (Table 2-2), but for FAO/UF map, we only reported the producer accuracy (Table 2-3). In addition, we resampled the IWMI map and the new irrigation map to the same spatial resolution of FAO/UF map, and then computed the producer accuracies of the resampled irrigation maps.

Table 2-2 Confusion matrices for the new irrigation map, IWMI map, and FAO/UF map

		Reference		
		Irrigated	Non-irrigated	Total
IWMI map(0.0089282º)	Irrigated	173	151	324
	Non-irrigated	89	201	290
	Total	262	352	614
Overall Accuracy = 60.91%				
Kappa Coefficient = 0.23				

New map(1km)	Irrigated	164	96	260
	Non-irrigated	98	256	354
	Total	262	352	614
Overall Accuracy = 68.40%				
Kappa Coefficient = 0.35				

Table 2-3 Producer accuracies of FAO/UF map, resampled IWMI map and resampled new irrigation map of China

	FAO/UF map	Resampled IWMI map	Resampled new map
Correctly classified irrigation pixels	218	218	228
Validation irrigation samples	262	262	262
Producer accuracy	83.2%	83.2%	87.0%

Note: FAO/UF map, resampled IWMI map and resampled new irrigation map of China have the same spatial resolutions (0.0833333º).

2.3.3 Intercomparisons

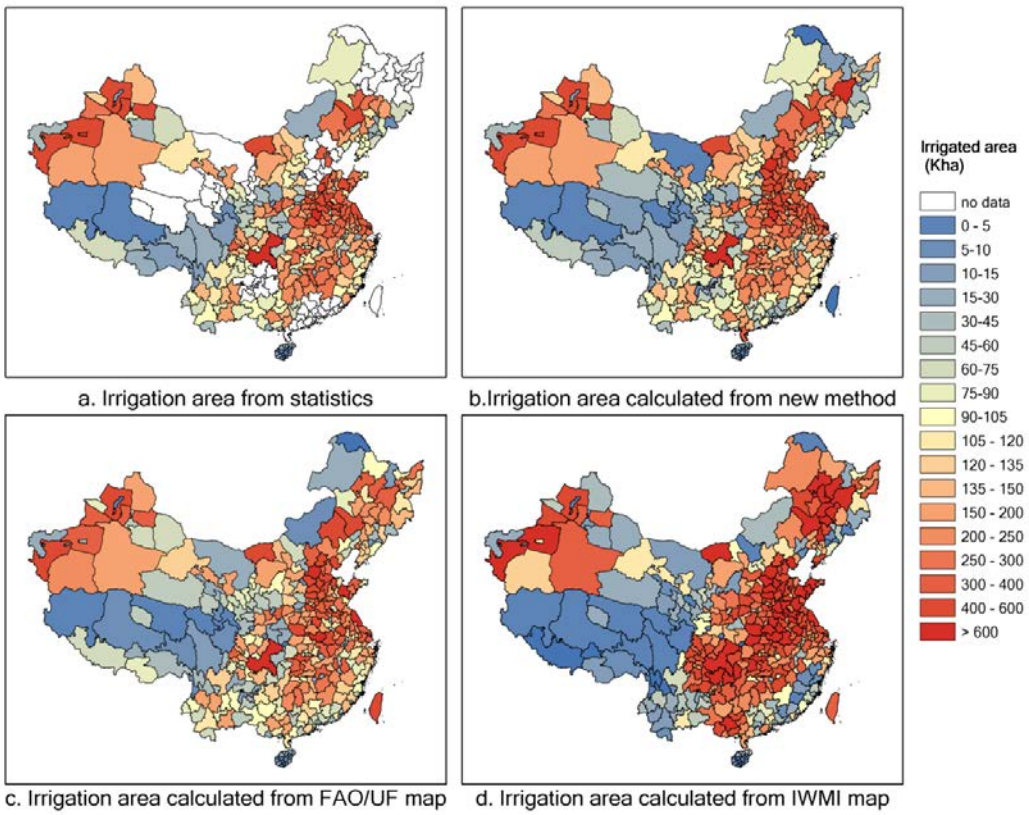

Figure 2-8 An example of the city-level polygon maps aggregated from three irrigation maps and statistics

I aggregated these three maps into two levels (city and county) of subnational polygon maps and then compared their similarity and dissimilarity by using the Cluster and Outlier Analysis and Hot Spot Analysis tools in ArcGIS. Figure 2-8 shows an example of the city-level polygon maps. Details about the comparison results are shown in following sections.

2.3.3.1 Similarity between irrigation maps

I analyzed the distribution patterns of the irrigated areas as summarized by county from the three different irrigation maps by using the Cluster and Outlier Analysis and Hot Spot Analysis tools in ArcGIS. The Cluster and Outlier Analysis tool was used to identify clusters of irrigated areas. For each feature, it calculates a local Moran's I value, a Z score, a p-value, and a code representing the cluster type (Mitchell 2005). The cluster types include HH, LL, HL, and LH. HH and LL are statistically significant (0.05 level) clusters of high values and low values, respectively. HL is a cluster of high values surrounded by low values, and LH is a cluster of low values surrounded by high values. The Hot Spot Analysis tool calculates the Getis-Ord Gi* statistic. The G-statistic is a Z Score, which is a test of statistical significance, and is used to decide whether features with high values or features with low values tend to cluster in a study area. Z scores are measures of standard deviation. There is no pattern in the area at the 95% confidence level if the Z score is between -1.96 and +1.96 standard deviations (SD). There is a clustering of high values in the area at the 95% confidence level if the Z score is greater than +1.96 standard deviations. There is a clustering of low values in the area at the 95% confidence level if the Z score is less than -1.96 standard deviations.

Figure 2-9 shows the distribution patterns of irrigated areas estimated from the three irrigation maps. The figure suggests that both the new map and the FAO/UF map effectively depict irrigation patterns with similar types of spatial distributions. The North China plain, the Hetao plain, northwestern Xinjiang province, and Songnen Pingyuan are four heavily irrigated areas where the HH pattern is dominant. Southwestern and southeastern China are lightly irrigated areas where the LL pattern is dominant. The IWMI map shows more irrigated area in the Dongting Hu pingyuan, Jiang Han pingyuan, and Chengdu pingyuan and less irrigated area in Xinjiang province and the Hetao plain than the other two maps.

2.3.3.2 Dissimilarity among irrigation maps

To analyze the dissimilarity between the irrigation maps, I summarized the irrigated area by county in each map and then subtracted the maps from each other. The results are shown in Figure 2-10(a), (c), and (e). Next, I used the Hot Spot Analysis tool in ArcGIS to analyze the cluster patterns of the dissimilarity between the irrigation maps (Figure 2-10 [b], [d], and [f]). The figure suggests that the new map agrees well with the FAO/UF map; the greatest difference between the two appears in northeastern China, especially in Jilin and Heilongjiang provinces, Hainan province, the Huaihe River, and the lower reaches of the Yangtze River. The IWMI map differs greatly from both the FAO/UF map and the new map.

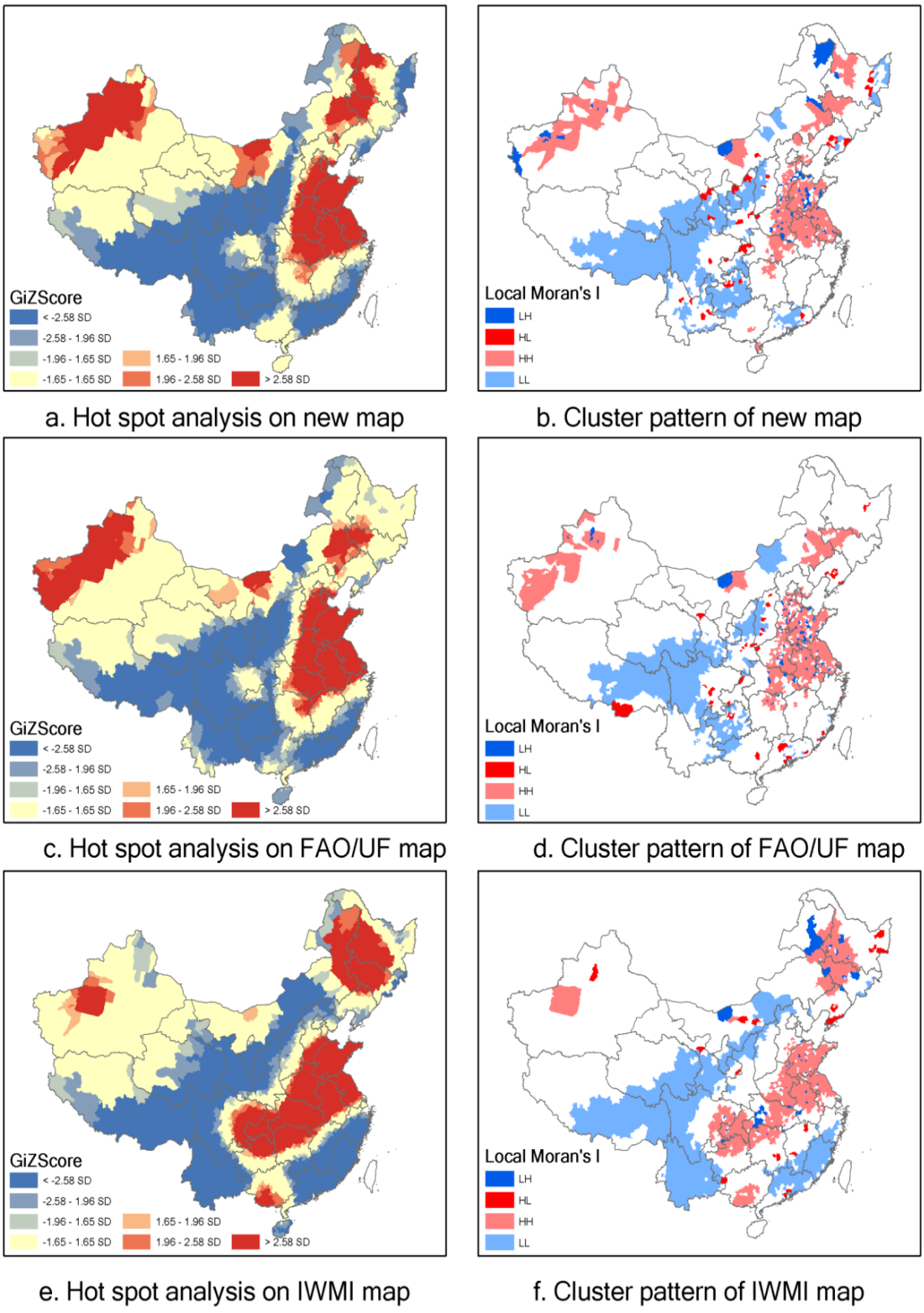

Figure 2-9 Hot spot analyses and cluster pattern analyses of three irrigation maps (GIZScore is the Z score calculated by Getis-Ord Gi* statistic in the Hot Spot Analysis tool of ArcGIS, and SD is standard deviations.)

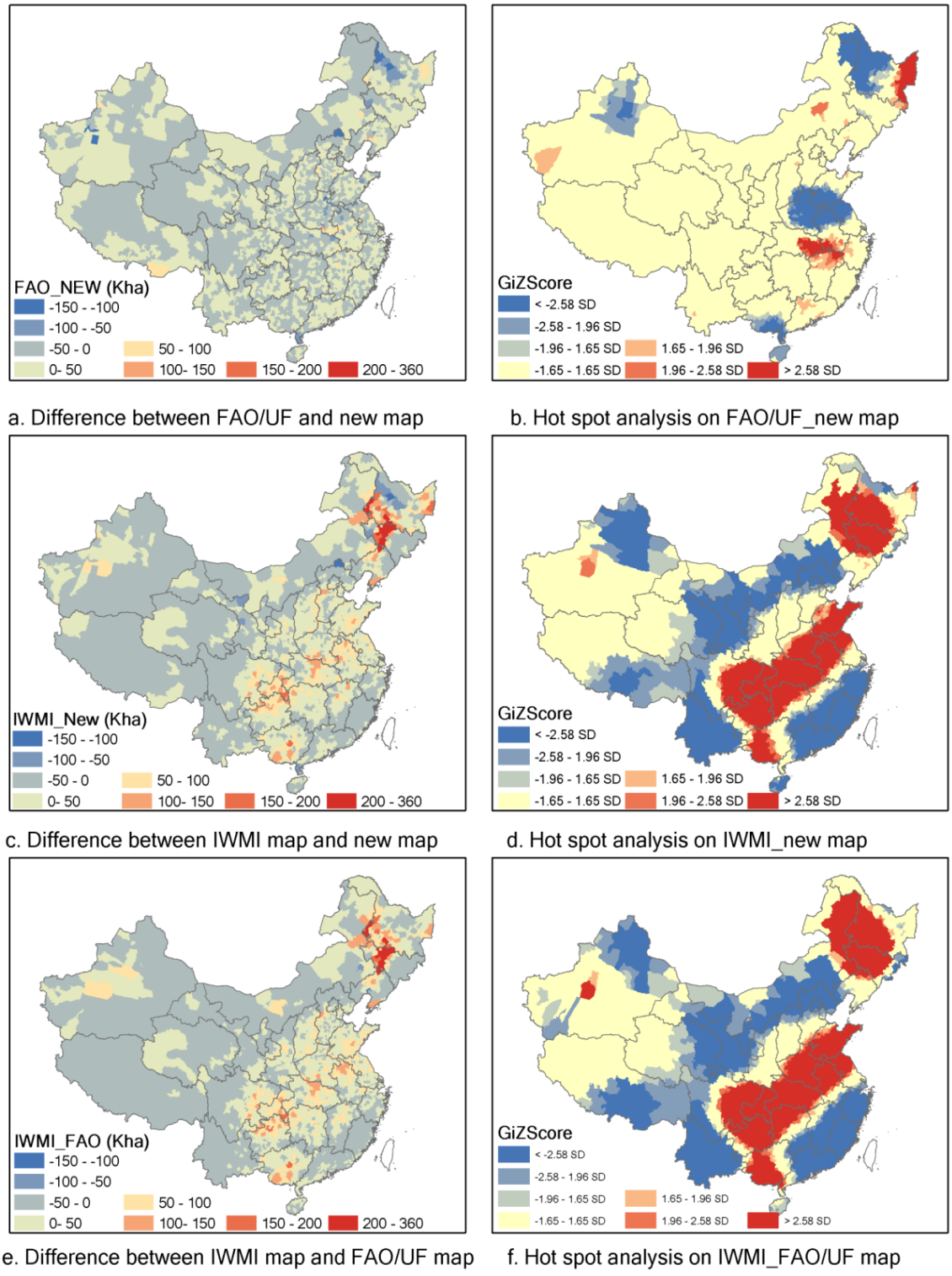

Figure 2-10 The differences between irrigation maps. (a) FAO/UF map minus new map (FAO/UF_NEW), (c) IWMI map minus new map (IWMI_NEW) , and (e) IWMI map minus FAO/UF map (IWMI_FAO/UF); (b), (d), and (f) are hot spot analyses of (a), (c), and (e), respectively. (GIZScore is the Z score calculated by Getis-Ord Gi* statistic in the Hot Spot Analysis tool of ArcGIS, and SD is standard deviations.)

2.4 Discussion and conclusions

In this study, I developed three irrigation potential indices by using time series NDVI and precipitation data. Using these indices and a spatial allocation model, I downscaled the census data on irrigation from geopolitical units to individual pixels in China.

I validated the new irrigation map and also two global irrigation maps (IWMI map and FAO/UF map) in China using 614 reference samples including 262 irrigated samples and 352 non-irrigated samples. The overall accuracy of the IWMI map (0.0089282º) and the new map (1km) are 60.91% and 68.40%, respectively. I also resampled the IWMI map and the new map to the spatial resolution of the FAO/UF map (0.0833333º), and calculated the producer accuracies for the FAO/UF map, the resampled IWMI map and the resampled new irrigation map. They are 83.2%, 83.2% and 87.0%, respectively. My validation is the first report on the accuracy of global irrigation maps in China, as far as we know. However, in order to validate the data, I transferred fraction irrigation maps to binary maps in which a pixel with an irrigation percentage great than 0 is defined as 1 (irrigated area). The detailed information regarding the acreage of the irrigated area is lost during this transfer process. For example, a pixel with an irrigation percentage of 100 and a pixel with an irrigation percentage of 1 are both defined as an irrigated pixel, but the acreage of the irrigated area in those two pixels differs a lot. Besides, my validation samples are point samples. There is a scale problem when validating grids by point samples because it is unknown to what extent the point samples could be representative. Therefore, point

samples are better for validating high resolution maps than for coarse resolution maps. In the future, I need to investigate square samples rather than point samples in order to make a more objective validation on the fractional irrigation map.

I also made intercomparisons among the three maps. The comparison results suggest that my new map agrees most with the FAO/UF map. Both these maps differ greatly from the IWMI map. The greatest differences between the new map and the FAO/UF map occur in northeastern China, especially in Jilin and Heilongjiang provinces, Hainan province, the Haihe River, and the lower reaches of the Yangtze River.

My method has several advantages. First, its inputs are quite simple, and no training samples are needed. Training samples are one of the most important factors for successful classification of satellite imagery, but collecting them by field investigation is costly and time-consuming. As a result, it is very expensive to update these samples regularly.

Second, my method is general and repeatable. Repeatability is pivotal to an approach's practical applicability. Traditional classification methods always require prior knowledge or ground-truth information regarding the study area. The classification results vary considerably because of differences in the classifiers or training samples. As a result, classification is more likely to be idiosyncratic and lack repeatability. In contrast, my method is a standardized procedure and could easily be repeated in other similar studies.

Third, my method can be used to map historically irrigated areas as long as the simple inputs needed for equations can be obtained. The case study in China

described in this paper demonstrated the procedure for mapping historically irrigated areas.

However, my model also has some weaknesses. First, the NDVI and the variation in NDVI depends not only on irrigation but also on other factors such as fertilizer use, plant protection, soil properties, weeds, diseases, and the change of crop rotation system. However, irrigation is regarded as the major factor affecting NDVI in China for the following three reasons: 1) China constantly faces challenges of food security and has undertaken large-scale programs to increase agricultural production in order to achieve self-sufficiency in food production. Among those measures, irrigation contributes most to increased crop production (Pu-te 2010). Chinese farmers are already accustomed to increasing crop productivity using chemical fertilizer, insecticides, and herbicides on both irrigated and rainfed areas (Khan et al. 2009); 2) Drought is the biggest agrometeorological hazard in China, following by flood (Simelton 2011). An irrigation system serves both flood control and drought relief functions in China. In other words, irrigated areas can better resist natural disasters than rainfed areas. Therefore, NDVI in irrigated areas is expected to be more stable than in rainfed areas; 3) Changing crop rotation systems within an irrigated pixel will increase the variation of NDVI in this pixel, and my method may misclassify it as a non-irrigated area. The use of double-cropping techniques was reported to decrease by 9% from 1978 to 2008 due to climate change and other factors (Yu and Zuo 2010), with a corresponding increase in the use of single-crop techniques. The previous study cited in this work did not describe the locations where (irrigated or rainfed areas) double-crop agriculture changed to singe crop. However, it

is reasonable to infer that the change from double to single crop is more likely in rainfed areas because of the decrease in precipitation. In summary, the assumption that crop productivity is high and stable over a long time-series in irrigated areas compared with rainfed areas in a given land unit is reasonable in China, but may differ in other regions, where irrigation is not the major factor influencing NDVI.

Second, my method is expected to perform better in dry areas than in humid areas, where less irrigation water is required and supplemental irrigation is the dominant irrigation type. However, this problem of accuracy is not limited to my method; the traditional classification methods are also unable to effectively distinguish between irrigated areas and non-irrigated areas planted with identical crops, due to the spectral mixture between them, especially in supplemental irrigated areas. For example, rainfed corn fields have little spectral difference compared to irrigated corn fields. The greatest spectral difference between rainfed and irrigated corn occurred in the irrigation period. In supplemental irrigation, irrigation water is only applied in key periods of crop growth and development. The key period is short, and the spectral differences caused by the extra soil moisture from irrigation are less distinct with time, following irrigation. In addition, adjacent farmlands may even be irrigated at different times because they are owned by different farmers. Therefore, it is very difficult to identify optimal temporal satellite images, especially for detecting irrigated areas on a large scale. It is also impossible to effectively distinguish irrigated crops from rainfed crops based only on a spectral difference. However, as irrigation greatly increases crop yield and irrigation requirements are closely associated with climatic conditions, my method used time series NDVI and precipitation data to

estimate the irrigation potential of each crop pixel. I emphasize the average precipitation condition, which aims to reflect the irrigation requirements; and the average NDVI condition, which aims to reflect the difference in yield between irrigated and non-irrigated crops over long time periods. My method may not perform better in humid areas than traditional classification methods, but it may still provide an alternative approach to assessment.

Third, the subpixel irrigated area (irrigation percentage) in a detected irrigated pixel is inherited from the crop percentage of the land cover map, which assumes that the crops in one pixel are all either irrigated or non-irrigated. However, this may not be true, especially in agricultural lands that are being irrigated through informal sources, say, from ground water. However, the approach can be improved to some extent if one uses an NDVI dataset with higher spatial resolution NDVI (such as MODIS 250 m NDVI) and a land cover map.

Finally, the amount of irrigated area is controlled by the irrigation census data, which may not represent the real irrigated area. For example, the Statistical Yearbooks published in China release data on the effective irrigated area (EIA). The EIA refers to an area of land where water sources or complete sets of irrigation facilities exist to lift and move sufficient water for irrigation purposes under normal conditions; an EIA may not be irrigated in a given year, causing overestimation. On the other hand, the EIA does not include land cultivated using informal irrigation sources, causing underestimation. However, in China, the EIA is regularly reported in the national census data. Therefore, it can be easily used as an input to update the irrigation map regularly.

Chapter 3 Seeking observational evidence of irrigation impact in China

In this observation study, I will analyze and compare meteorological and remote sensing observation in irrigated (/highly irrigated area) and non-irrigated (/lightly irrigated) agriculture areas. Meteorological observations will mainly focus on daily air temperature, and satellite observations will include albedo, LST, NDVI, soil moisture, and evapotranspiration. Here, I will introduce my method and results by two studies: one is in Jilin Province, and another is in North China. Two manuscripts about the work in this chapter have been prepared; one was published (Zhu et al. 2011e) and another one was accepted (Zhu et al. 2012).

3.1 Case study in Jilin Province

Jilin is one of the main dryland grain production provinces in China; supplemental irrigation is responsible for contributing to a vast increase of food production and resistance to drought disasters. Spring corn, middle rice, and soybeans are predominant crops in Jilin Province, and irrigation water is used in their growing season (April to late September). Like other regions in China, Jilin Province features an array of issues that challenge the study of the irrigation cooling effect in China, such as a rapid urbanization process and continuously increased coal energy consumption, the biggest contributor of black carbon (Figure 3-1). Fortunately, the effective irrigation area (EIA) and sown area of crop (CSA) in Jilin Province fluctuated during last 50 years. The effective irrigated area underwent three phases: a rapid increase after 1949, because the new nation invested significant capital towards fostering agricultural development, including construction of irrigation systems; a

decrease starting in 1978, when China began a series of economic reforms (with a greater decrease from 1991-1996); and then resumed again after 1996. The mean crop sown area was around 4.47 M ha from 1955-1965, increasing to about 17 percent over the next 12 years (1966-1978), and then decreasing again, remaining at approximately 4.07M ha from 1979-1999.

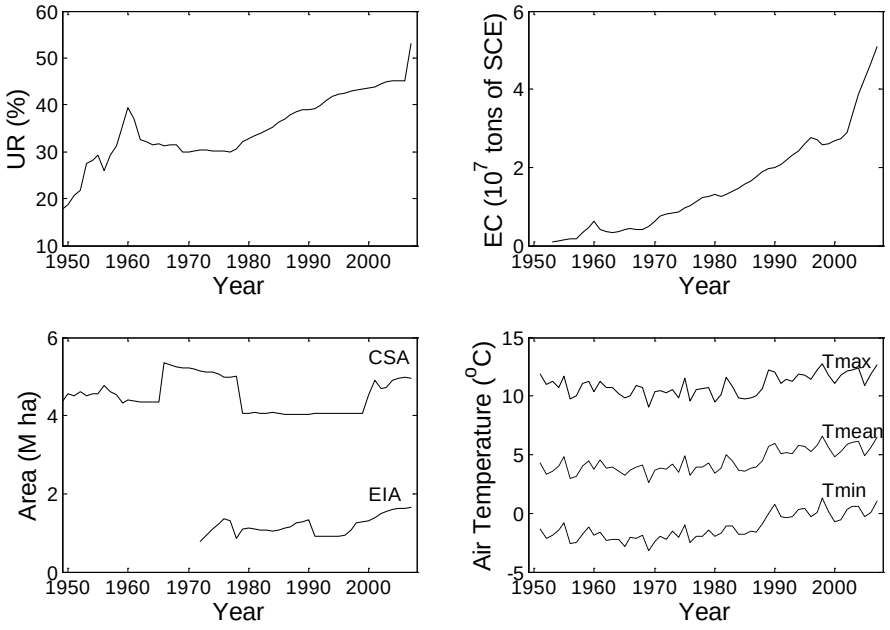

Figure 3-1 Background of study area

(a. urbanization ratio (UR) (%); b. Energy consumption (EC) ($\times 10^7$ tons of standard coal equivalents (SCE); c. EIA and CSA (M ha)); d. Average maximum, mean, and minimum temperature of Jilin province. Note: UR is equal to urban population divided by total population. Urban population and total population of Jilin Province are taken from the Jilin statistical yearbook 2007 compiled by Jilin Bureau of Statistics. EC for Jilin Province is calculated by unit EC ($\times 10^7$ ton SCE/person) multiplied by total population in Jilin Province in a given year; and unit EC is total EC divided by total population of China in a given year. Total EC and the population statistics before 1991 are from the China Statistical Yearbook 1992, and after 1991 are from China Statistical Yearbook 2008; both of which are published by the National Bureau of Statistics of China. The cultivated area over 1949-2007, and effective irrigation area over 1972-2007, are from the Chinese website http://www.zzys.gov.cn/. Average maximum, mean, and minimum temperature of Jilin provinces are derived from observations of 28 meteorological stations located in Jilin Province.

Jilin is one of thirteen provinces in China that are major grain producers (Figure 3-2). It has a temperate continental climate with cold winters, and warm and

wet summers. There are approximately 120 frost-free days each year. Annually, there is an average of 2259 to 3016 hours of sunshine. The active accumulative daily air temperatures are 2700–3600ºC which satisfies the sunshine requirement for single cropping (Yao et al. 2009). Rainfall averages are 400 to 1000mm yearly, mostly occurring in the summer and in the eastern area of Jilin. The rainfall amount during April and May accounts for 13 percent of the yearly total rainfall. Hence, the frequency of drought is high during spring, especially within the western areas of this province.

Spring corn, mid-season rice, and soybean are the predominant crops in Jilin Province. The growing season lasts from April to late September (Table 3-1). For spring corn, the leaf to jointing stage occurs early June to middle July, and the teaseling to filling stage occurs during late July to middle August, which encompasses 30 to 33 percent of the water consumed over the course of the growing cycle. For middle rice, most evaporation is lost during the transplanting stage in middle and late May, and transpiration is primarily lost during booting to tasting stage in late July and early August. For soybean, the flowering to seed filling stages, which occur from late July to early September, used 61 to 66 percent of the water consumed in its growing cycle. In these key crop phenological stages, people in Jilin province, especially in the western areas, often use supplemental irrigation to meet crop water requirements. During the past 50 years, the sown area of crops in Jilin province has increased from 4.38 M ha in 1949 to 4.94M ha in 2007. Additionally, the effective irrigation area increased from 0.796 M ha in 1972 to 1.6137 M ha in 2005.

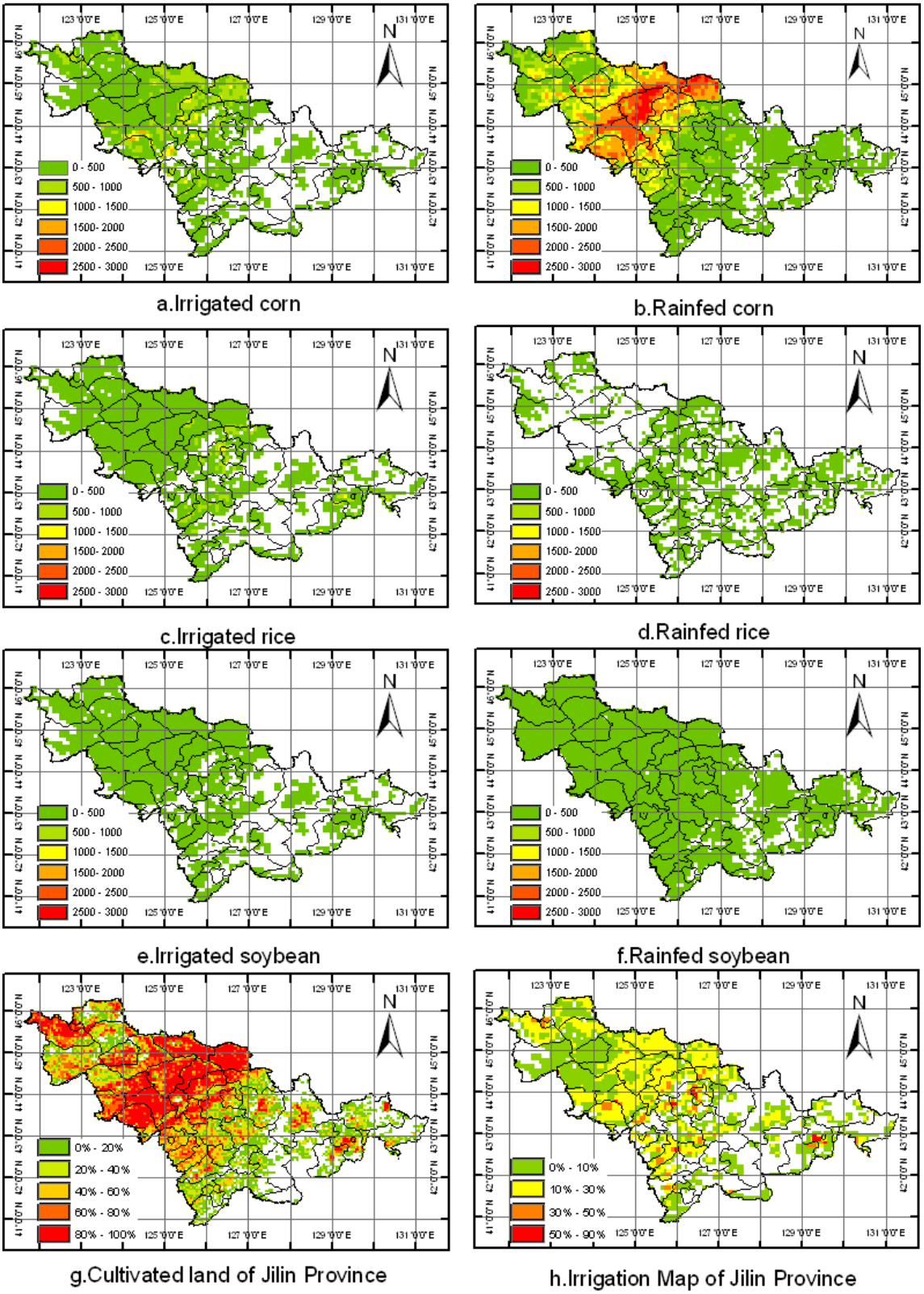

Figure 3-2 Study area (Note: Irrigated and rainfed corn, rice and soybean maps are subset of MIRCA2000 data(Portmann et al. 2010); cultivated land of Jilin is a subset of Land Cover Dataset (NLCD) of China; irrigation map of Jilin province is a subset of FAO/UF MAP.)

Table 3-1 Crop phonological stages (1, 2, and 3 mean the first, second and third ten days of each month, respectively)

Month	April			May			June	July			August			September		
	1	2	3	1	2	3		1	2	3	1	2	3	1	2	3
Spring corn			Sowing		Seedling		Leaf -Jointing			Tasseling-filling			Ripening		Maturity	
Middle rice	Sowing		Seedling Nursing		Transplanting		Tillering			Booting -filling			Ripening		Maturity	
Soybean			Sowing		Seedling		Leafing-Branching			Flowering-Podding-Seedfilling					Maturity	

3.1.1 Data

Spring corn, middle rice, and soybean are the principal crops in Jilin Province; irrigation water is used during the growing season (April to late September) for these crops. Hence, my study focused on April to late September.

The data used here include three parts: meteorological observations, satellite observations and three ancillary maps. The first dataset was used to calculate the long-term growing season mean yearly maximum, minimum, and mean air temperature. The second dataset was used to calculate the growing season land surface biogeophysical parameters. The three ancillary maps were used to choose suitable meteorological observation sites and to classify the areas with high irrigation percentages and those with low irrigation percentages.

3.1.1.1 Meteorological observations

The meteorological observations include daily maximum, minimum and mean air temperatures and precipitation for the period 1956-2008 from the National Meteorological Center of the China Meteorological Administration. In this study, the mean temperature is not the average between maximum and minimum daily temperature, but an average of observations at the local times: 02:00, 08:00, 14:00, and 20:00.

3.1.1.2 Satellite observations

The satellite observations (Table 3-2) include albedo, land surface temperature (LST), the Normalized Difference Vegetation Index (NDVI), soil moisture (SM), and evapotranspiration (ET).

Surface albedo is the fraction of solar energy (shortwave radiation) reflected from the earth back into space, and measures the reflectivity of the earth's surface (Liang 2004). Since water absorbs solar energy, and irrigation increases the soil wetness, it is expected that irrigation decreases surface abledo. The surface albedo dataset we used is from the MODerate-resolution Imaging Spectroradiometer (MODIS) Albedo product (MCD43C3: Albedo 16-Day L3 Global 0.05Deg CMG). MCD43C3 provides both Black-Sky Albedo (BSA), which denotes directional-hemispheric reflectance (at local solar noon), and White-Sky albedo (WSA) for bi-hemispheric reflectance. WSA represents reflectance under conditions of isotropic illumination for seven spectral bands (MODIS channels 1–7), and another three broadbands: visible (VIS, 0.3–0.7μm), near-infrared (NIR, 0.7–5.0μm) and shortwave (SW, 0.3–5.0μm).

LST is a key parameter in the physics of land surface processes, combining surface-atmosphere interactions and the energy fluxes between the atmosphere and the ground. Irrigation decreases LST, and the LST will decrease further in daytime, compared with nighttime, due to two factors. First, irrigation increases evapotranspiration in daytime which will reduce the energy for heating the land surface, causing lower LST. Correspondingly, irrigation increases near-surface water vapor and decreases the shortwave radiation absorbed by the land surface, which also

causes lower LST. Second, the evapotranspiration in nighttime is lower than daytime, so more energy is necessary to heat the land surface during nighttime. At the same time, the increased near-surface water vapor during nighttime absorbs longwave radiation, which increases near-surface air temperature and slows the cooling of the land surface temperature. The LST dataset I used in this study is from MODIS/Aqua Land Surface Temperature/Emissivity Monthly L3 Global 0.05Deg CMG (MYD11C3) products.

Table 3-2 Land surface parameters data used in this study

	Spatial resolution	Temporal resolution	time period	Projection	Source
Albedo	0.05°	8-day	02/ 2000-2008	Geographic	MODIS (MCD43C3)
LST	0.05°	monthly	08/2002 -2008	Geographic	MODIS (MYD11C3)
NDVI1	0.05°	monthly	02/2000-2008	Geographic	MODIS (MOD13C2)
soil moisture	25 km	daily	2003-2008	EASE	AMSR-E L3
*NDVI2	0.05°	16-day	2000-06/2005	Geographic	MODIS (MOD13C1)
$*R_s \downarrow R_s \uparrow$ $*R_l \downarrow R_l \uparrow$	1 °	daily	2000-06/2005	Geographic	GEWEX (SRB)
*T	1 °	daily	2000-06/2005	Geographic	NMCMA
*Tmax, *Tmin	1.875°	daily	2000-06/2005	Geographic	NCEP/NCAR Reanalysis 1: Surface Flux

Note: MODIS (MCD43C3): MODerate-resolution Imaging Spectroradiometer (MODIS) Albedo product (MCD43C3: Albedo 16-Day L3 Global 0.05Deg CMG).MODIS(MYD11C3): MODIS/Aqua Land Surface Temperature/Emissivity Monthly L3 Global 0.05Deg CMG (MYD11C3) products. MODIS (MOD13C2): MODIS Vegetation Indices Monthly L3 Global 0.05Deg CMG (MOD13C2) product. MODIS (MOD13C1): MODIS Vegetation Indices 16-Day L3 Global 0.05Deg CMG(MOD13C1) product. GEWEX (SRB): NASA/GEWEX Surface Radiation Budget (SRB) Release-3.0 data sets. NMCMA: National Meteorological Center of the China Meteorological Administration AMSR_E: AMSR-E L3 Surface Soil Moisture products. EASE: Grid global cylindrical projection. The parameters with asterisk were used to calculate daily ET.

NDVI, defined as the ratio of (NIR-Red) and (NIR+Red), is still a frequently used tool for evaluating changes in vegetation and assessing the impact of environmental phenomena. Irrigation assists in growing crops in dry areas, or

increasing food production. Thus, the crops within areas that include irrigation facilities have a greater ability to resist dry climate conditions, and are expected to be healthier in dry areas. Correspondingly, NDVI values of areas with irrigated facilities are expected to be higher compared to non-irrigated areas in dry areas. The NDVI dataset I used in this study is from MODIS Vegetation Indices Monthly L3 Global 0.05Deg CMG (MOD13C2) product.

Soil moisture is the most important component of the metrological memory. Soil moisture can modify the radioactive properties of the soil, control the partitioning of the heat flux, impact land surface processes, and therefore, influence the regional climate system. The soil moisture data I used in this study are from the Advanced Microwave Scanning Radiometer - Earth Observing System (AMSR-E) L3 Surface Soil Moisture products provided by National Snow and Ice Data Center (Njoku 2005).

ET, a combination of evaporation from land surface and transpiration from plant leaves, has a complex influence on the hydrologic cycle and land surface energy budget by changing vapor and energy flux. It is frequently used when estimating irrigation water requirements, planning water resource management, and when improving hydrological, land surface, and weather/climate prediction models. Many algorithms have been developed to estimate ET. In this study, ET was calculated using the statistical equation (Wang and Liang 2008):

$$ET = R_n \times (0.1440 + 0.6495 \times NDVI + 0.0090 \times T - 0.0163 \times (T\max - T\min)) \quad \textbf{Equation 3-1}$$

$$R_n = \mathrm{R_S}\downarrow - \mathrm{R_S}\uparrow + R_l\downarrow - R_l\uparrow \quad \textbf{Equation 3-2}$$

Where R_n is monthly-average net radiation (W/m^2). $R_S\downarrow$, $R_S\uparrow$, $R_l\downarrow$, $R_l\uparrow$ are daily incoming shortwave radiation, outgoing shortwave radiation, incoming longwave radiation, and outgoing longwave radiation (W/m^2). All of these are of 1°x1° spatial resolution and from the NASA/GEWEX Surface Radiation Budget (SRB) Release-3.0 data sets (available at http://eosweb.larc.nasa.gov/PRODOCS/srb/table_srb.html.) T is the daytime-averaged air temperature with a 1°x1° resolution from National Meteorological Center of the China Meteorological Administration. NDVI is the 16-Day Normalized Difference Vegetation Index. T_{max} and T_{min} are daily maximum and minimum temperature from NCEP/NCAR Reanalysis (available at: http://www.esrl.noaa.gov/psd/data/gridded/data.ncep.reanalysis.surfaceflux.html.)

3.1.1.3 Other data sets

Other data sets used in this study include the global irrigation map derived by the Food and Agriculture Organization (FAO/UF MAP) (Siebert et al. 2005b), which shows the fraction of 5' by 5' cells that were equipped for irrigation in 2000, the global irrigated area map (GAIM) and global map of rainfed cropland areas (GMRCA) generated by the International Water Management Institute (IWMI) (http://www.iwmigiam.org), and the intensively validated National Land Cover Dataset (NLCD) of China produced by visual interpretation and digitization of Landsat TM/ETM+ data from around 2000 (Liu et al. 2005b), which has six land cover types: cultivated land, forest, grassland, residence, unused land, and water body. The NLCD has 1 km spatial resolution in Albers equal-area conic projection.

3.1.2 Methodology

Temperature changes could be caused by many factors besides irrigation, such as longitude and latitude, terrain, land cover type, aerosols, and urbanization. Some of these factors, such as irrigation, could change with time. Therefore, some authors suggested that evaluation of the impact of irrigation on temperature should be conducted both temporally and spatially (Bonfils and Lobell 2007; Lobell and Bonfils 2008). In accordance with this point, I conducted my study both temporally and spatially. Temporally, I used meteorological observations because they provide a long-term dataset. Spatially, I used satellite observations because of their large spatial coverage.

3.1.2.1 Temporal dimension test

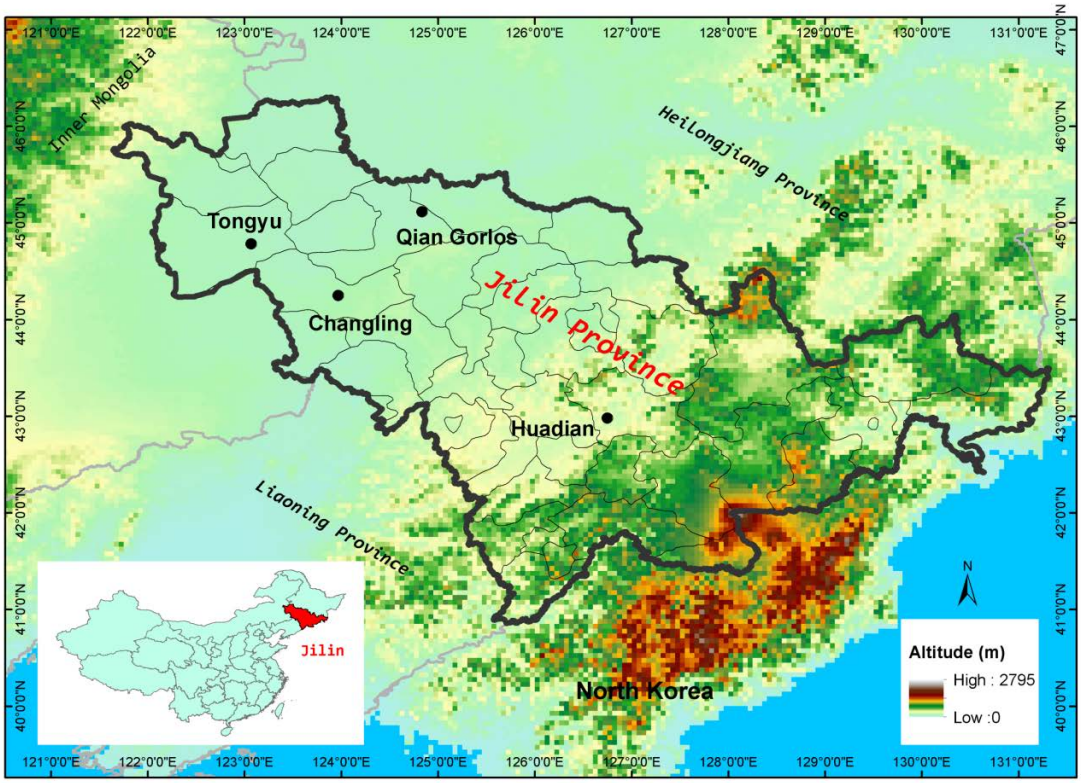

Figure 3-3 The location of study area and observation sites

For a temporal dimension test, I first chose suitable sites using the following criteria: 1) they are identified as irrigation areas on FAO/UF MAP, which shows the fraction of 5’ × 5’ cells equipped for irrigation as of the year 2000 (Siebert et al. 2005b). 2) The irrigation percentage at a given site should be consistent with the classification indicated on the GAIM and GMRCA generated by the IWMI (http://www.iwmigiam.org). For example, if the irrigation percentage of a site is equal to or greater than 50, but the IWMI map indicated the site is rainfed, then the site will be excluded. In contrast, if the irrigation percentage of a site is smaller than 50 and the IWMI map indicated the site is rainfed, then the site will be included. 3) The sites must be located on cultivated land. I excluded sites located in urban and residential areas by intensively reviewing the validated National Land Cover Dataset (NLCD) of China (Liu et al. 2005b) and Google Earth, and finally determined four sites from a total of 28 in Jilin Province (Figure 3-3 and Table 3-3). Over the course of this study the two sites with a relatively high irrigation percentage are denoted as HIP, and the other two with a relatively low irrigation percentage as LIP.

Although there are only four sites, the data quality is reliable because in the early 1990s, as well as during the period 2001–2002 and in 2004, the National Meteorological Center made three separate quality control audits on historical meteorological observations including a homogeneity and internal consistency review, climate extremes evaluation, http://d.wanfangdata.com.cn/Periodical_qxkj200801022.aspx, and confidence interval control. The differences created by changes in station location and observation instruments were revised using QXT22-2004, a professional standard for the

meteorological field in China (China Meteorological Administration 2004). There are no extreme points and outliers in the data based on the box-plot examination (Figure 3-4). Moreover, considering that the autocorrelation of a time series could make the traditional statistical analysis invalid, I first tested the temporal autocorrelation of the mean, maximum and minimum air temperature for each month during the growing season (April–September). I tested the temporal autocorrelation of the average mean, maximum and minimum air temperature of the growing season by using the Durbin-Watson (DW) method(Durbin and Watson 1950), which includes three steps: first, using linear regression to fit the time series of the meteorological observations; then, constructing a series of residuals; and finally, calculating the DW values based on Equation 3-3.

$$d = \frac{\sum_{t=2}^{T}(e_t - e_{t-1})^2}{\sum_{t=1}^{T} e_t^2} \qquad \textbf{Equation 3-3}$$

where e is the residual associated with the observation at time t, and d is the DW value. To test for autocorrelation at significance α, the test statistic d is compared to the lower and upper critical values (dL,α and dU,α), which is related to the level of significance (α), the number of observations, and the number of predictors in the regression equation. In this study, the number of observations was 53, the predictor was 1; thus, dL,α and dU,α are 1.356 and 1.428, respectively, under 0.01 significant level. If dU,α < d < 4-dU, there is no autocorrelation. If dL,α < d < dU,α or dL,α < (4 − d) < dU,α the test is inconclusive. From Figure 3-5, we can see that there is no autocorrelation between any of the time series observations, except the September

time series maximum air temperature of Tongyu, which is inconclusive. Overall, the time series data was considered to have had no autocorrelation.

Table 3-3 Information on the chosen observation sites

Site name	Altitude(m)	Latitude	Longitude	FAO/UF map (%)	IWMI map	UR(%)
Qian Gorlos	136.2	45.08	124.87	15.6	irrigation	27.0
Huadian	263.3	42.98	126.75	26.8	irrigation	42.9
Tongyu	149.5	44.78	123.07	7.4	Rainfed	31.5
Changling	188.9	44.25	123.97	6.7	Rainfed	17.4

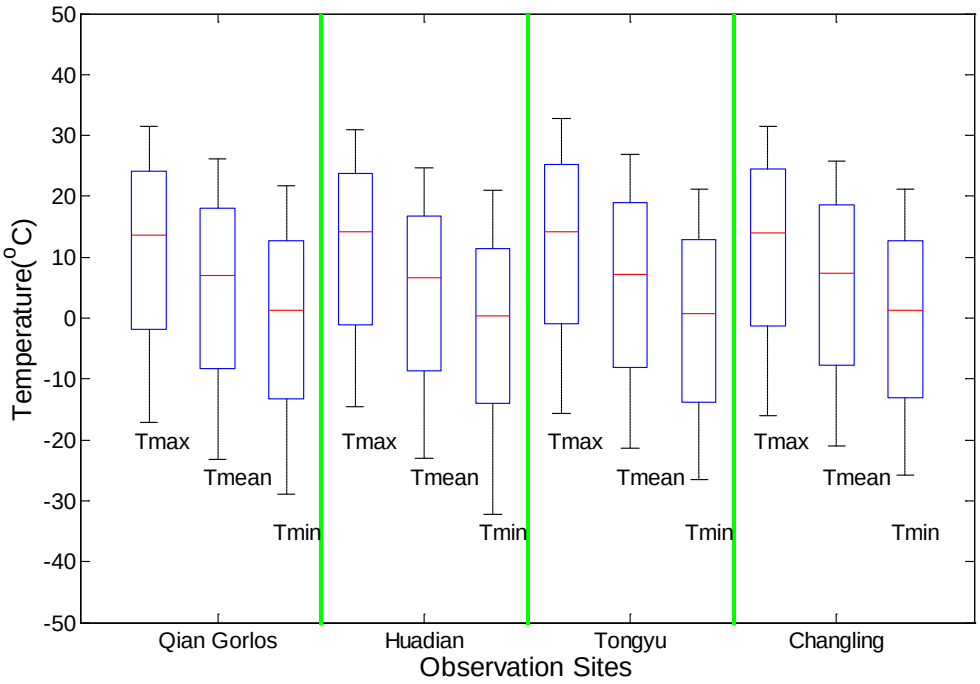

Figure 3-4 Box-plot examination for extreme points and outliers

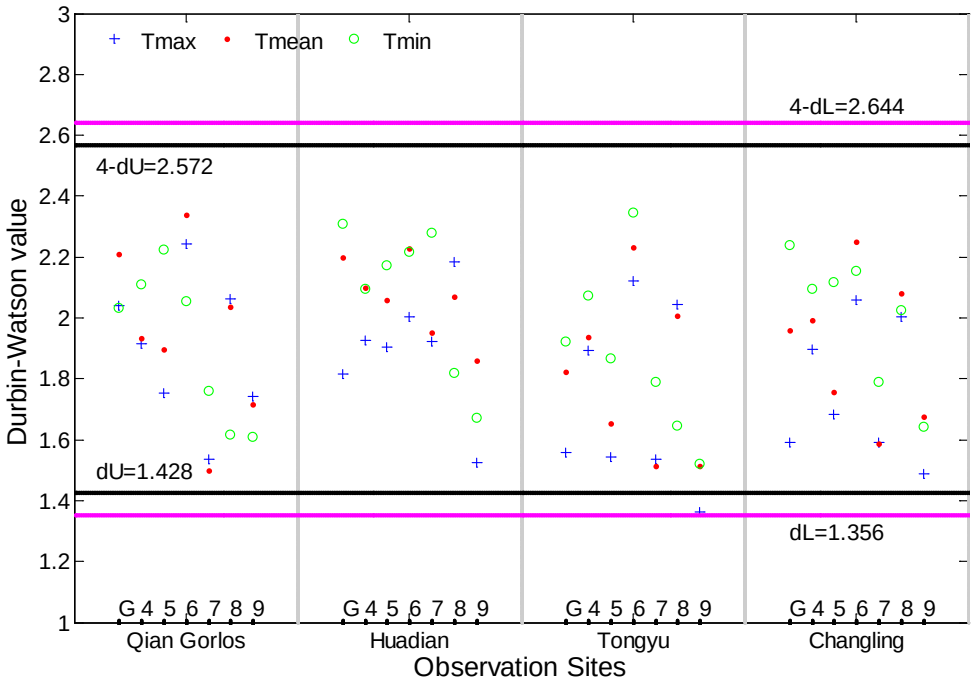

Figure 3-5 DW values of growing season time series mean, maximum, and minimum air temperature of 1956-2008, where G indicates the average air temperature of the growing season time series; 4-9 indicates the air temperature time series of April to September, respectively

I then conducted comparisons by subtracting the growing season mean maximum, minimum, and mean temperatures of HIP from the growing season mean maximum, minimum, and mean temperatures of LIP. I denote them as DTmax, DTmin, and DTmean, respectively. I also evaluated the significance of the temperature difference between the HIP and LIP locations by using an independent sample T-test and calculated the correlation of DTmax, DTmin, and DTmean with the EIA and CSA over the study period. Moreover, I calculated the standard precipitation index for a 12 month rainfall total(SPI12) for each selected observation site over the period 1956 to 2008 based on the code downloaded from http://www.drought.unl.edu/monitor/spi/program/spi_program.htm and then calculated the correlation of DTmax, DTmin, and DTmean with SPI12. The standardized precipitation index (SPI) is a tool for defining and monitoring drought. It

can be used to determine the rarity of a drought at a given time scale of interest for any rainfall station with historic data. SPI is between -3 and 3. A low SPI value indicates a low precipitation event (or drought), a high SPI value indicates a heavy precipitation event, and SPI around 0 indicates a normal precipitation event over the time period specified.

3.1.2.2 The spatial dimension test

For the spatial dimension test, I used a four-step process to compare the land surface parameters between cultivated areas featuring a high percentage of irrigated land, and those with a low irrigation percentage. Step 1: I re-projected NLCD onto a new map using a geographic projection, and then applied majority rules to coarsen the new map to a 0.05° spatial resolution; in which the new pixel class is dominant among the six land cover types within a 0.05° spatial extent. In this new map, if the new pixel class is cultivated land, I defined it as 1; otherwise I defined it as 0. This resulted in the creation of a binary map (1 cultivated land, 0 non-cultivated land). Step 2: I resized the 5' spatial resolution of the FAO/UF map to 0.05 degrees, and used the binary map derived from first step as a mask to exclude the non-cultivated areas from the FAO/UF map. I then divided the remaining pixels into 10 categories with a 10 percentage irrigation interval. The pixels with an irrigation percentage smaller than 10 were classified as "reference" areas (RA). The pixels with an irrigation percentage greater than 30 and 50 were denoted as "target1" and "target2" areas, respectively. Step 3: I re-projected the EASE-Grid global cylindrical projection of the AMSR-E soil moisture onto the geographic projection and resized it to a 0.05° spatial resolution. Step 4: I calculated the mean surface albedo, LST, SM, and ET, with the cloud-free dataset described above for "reference" areas target1 and target2.

I then subtracted the land surface parameters of the “reference” areas from target1 and target2, which are denoted as target1_RA and target2_RA. Lastly, these were compared.

3.1.3 Results and discussions

3.1.3.1 Results of temporal tests from meteorological observations

3.1.3.1.1 Temperature difference of HIP and LIP

The comparative results of HIP and LIP locations over the study period are shown in Figure 3-6. DTmax, DTmin, and DTmean are all negative, which indicates that the growing season mean maximum, minimum, and mean temperatures at HIP locations were lower than at LIP locations. The independent samples T-Test verifies that the differences in maximum and mean air temperature are significant at both the $\alpha = 0.05$ level and $a = 0.01$ level while the differences in minimum air temperature are significant only at the $\alpha = 0.05$ level. The magnitude of DTmax was almost twice that of DTmin for each examined period, and the linear regression coefficient of the DTmax time series was more than three times that of the DTmin time series. Hence, irrigation has more impact on the maximum temperature than the minimum temperature, which is similar to results from other studies (Adegoke et al. 2003; Kueppers et al. 2008; Lobell and Bonfils 2008). Considering the fact that urbanization has a much larger influence on minimum temperature (Kalnay and Cai 2003; Zhou et al. 2004), and the average urbanization ratio for HIP locations (35%) is even greater than that of LIP locations (24%), it is reasonable to assume that the temperature differences between the HIP and LIP sites are not caused by urbanization.

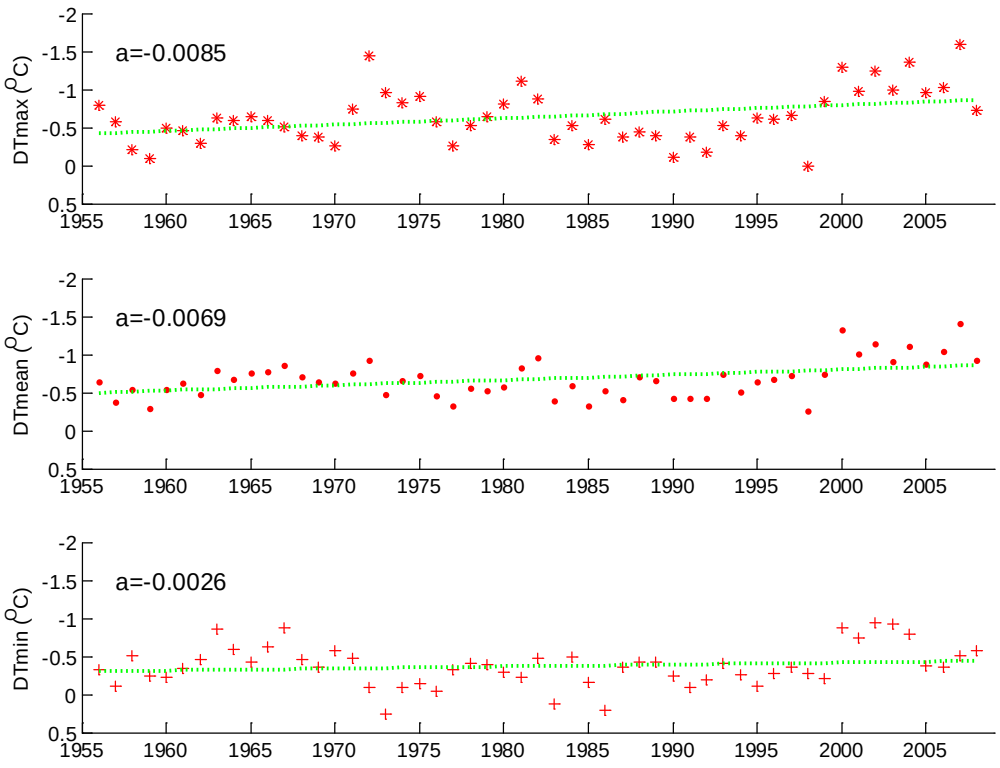

Figure 3-6 Temperature difference (a is the regression coefficient, DTmax, DTmin, and DTmean are daily maximum, minimum and mean temperature differences between highly and lightly irrigated area, respectively.)

3.1.3.1.2 The correlation between temperature difference and CSA/EIA

To measure the strength of the linear dependence between DTmin, DTmax, DTmean, and CSA/EIA, I first test to see if all these variables have a normal distribution based on the one-Sample Kolmogorov-Smirnov Test. The results show that all of the variables except CSA have a normal distribution. Therefore, I calculated the Spearman's rho instead of the Pearson correlation between them because Spearman's rho has no requirement on the distribution of the variable. Results are shown in Table 3-4. Based on the table, DTmax and DTmean are significantly correlated to both CSA and EIA, and DTmin is significantly correlated to CSA.

Table 3-4 Spearman correlation between DTmin, DTmax, DTmean and CSA/EIA

	DTmean	DTmax	DTmin
EIA	-.295(*)	-.329(*)	-0.057
CSA	-.517(**)	-.443(**)	-.451(**)

**Correlation is significant at the 0.01 level (2-tailed).
*Correlation is significant at the 0.05 level (2-tailed).

3.1.3.1.3 The correlation of Temperature difference between HIP and LIP with SPI12

I calculated the SPI12 for each selected observation site over the period 1956 to 2008 and show my results in Figure 3-7. The SPI12 of each observation site has a normal distribution based on the one-Sample Kolmogorov-Smirnov Test. Next, I calculated the Pearson correlation between SPI12 and DTmin, DTmax, and DTmean, and the results are shown in Table 3-5. Based on the table, we find that 1) DTmax and DTmean are significantly correlated to SPI12 of LIP sites; 2) the correlation between DTmax and SPI12 of LIP sites is more significant than the correlation between DTmin and SPI12 of LIP sites; 3) the correlation between temperature difference (DTmin, DTmax, and DTmean) and SPI12 of HIP sites is not statistically significant. These results indicate that the precipitation condition in the LIP sites has a strong relationship with the temperature difference between LIP and HIP. This is understandable because in China, the term “irrigated area” refers to land “where there are water sources or complete sets of irrigation facilities to lift and move adequate amounts of water for irrigation purposes under normal conditions,” and irrigated area statistics is an indication of “drought resistance capacity”. Moreover, the irrigation water in Jilin province mainly comes from underground water sources (Li et al. 2005). Therefore, a highly irrigated area is expected to have a higher resistance to precipitation change and drought than an area with low irrigation. Consequently, the

temperature difference between HIP and LIP is bigger in a drier year and is mainly caused by lower precipitation levels at the LIP sites.

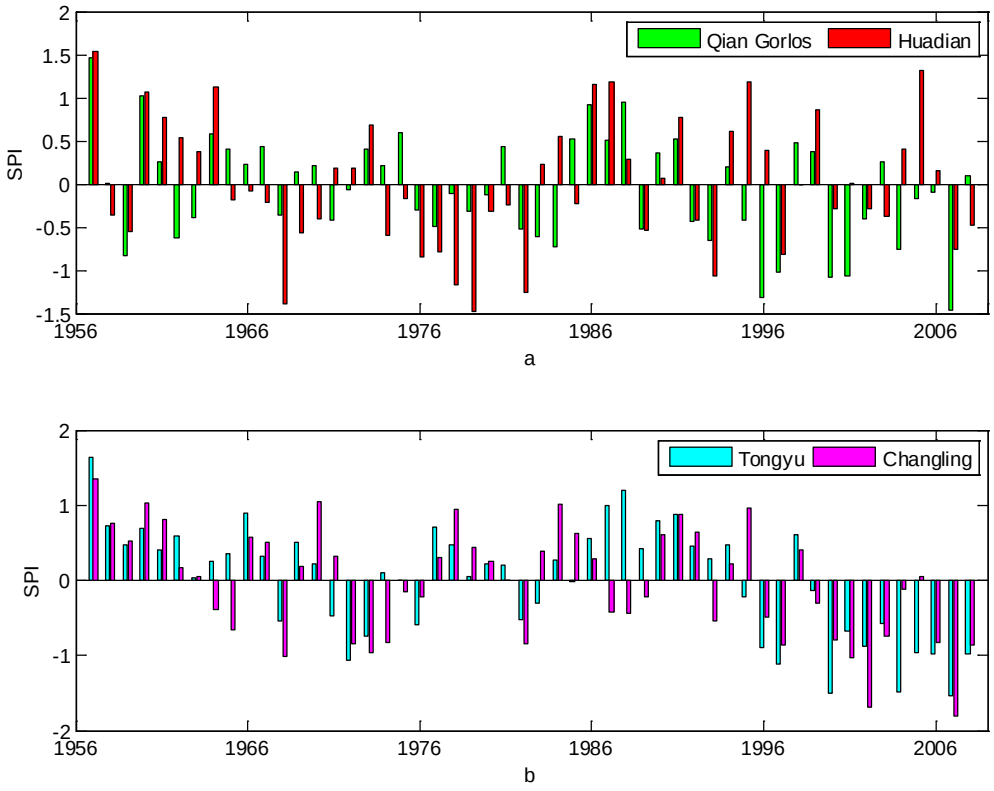

Figure 3-7 SPI12 of (a) 2 HIP sites and (b) 2 LIP sites

Table 3-5 **Pearson correlation between SPI12 and DTmin, DTmax, and DTmean**

	DTmean	DTmax	DTmin
SPI12 of Qian Gorlos	0.262	0.144	0.076
SPI12 of Huadian	0.115	0.082	0.045
Average SPI12 of 2 HIP sites	0.214	0.128	0.07
SPI12 of Tongyu	.609(**)	.574(**)	.312(*)
SPI12 of Changling	.559(**)	.556(**)	0.206
Average SPI12 of 2 LIP sites	.641(**)	.620(**)	.284(*)
Average SPI12 of 4 sites	.518(**)	.459(**)	0.216

**Correlation is significant at the 0.01 level (2-tailed).
*Correlation is significant at the 0.05 level (2-tailed).

3.1.3.2 Results of spatial tests from satellite observations

3.1.3.2.1 Land surface parameters of irrigated areas

The land surface parameters were extracted from satellite images and analyzed during the growing season from 2000 to 2008. The intra-annual variations of the land surface parameters within irrigated areas are shown in Figure 3-8 and Figure 3-9. Monthly ET rapidly increased since the crops were planted in April, and reached a plateau during July to August, before decreasing in harvest month (September). The average monthly ET of April, May, June, July, August, and September were 16.8W/m^2, 27.9W/m^2, 44.0W/m^2, 61.0W/m^2, 63.9W/m^2, and 36.4W/m^2, respectively. The lowest ET occurred in January and was only 0.2 percent of the average ET for August. The ET consumed in June, July, and August accounted for 62.7 percent of the total ET consumed in one year.

The average monthly soil moisture for 2003-2008 was highest in April, with an average 0.154 g/cm3, followed by the growing season of May, and highest in October during the non-growing season (although the rainfall was concentrated in summer.) The high soil moisture in April could be caused by irrigation before seeding used for crop sowing. The low soil moisture during June to September might have resulted from high ET.

From 2000-2008, the average monthly NDVI for April, May, June, July, August, and September were 0.23, 0.33, 0.61, 0.77, 0.79, and 0.69, respectively. With an average of 0.79, the highest average monthly NDVI occurred in August, which is the same as Piao's report (Piao et al. 2003). Spring corn, soybean and middle rice are in the grain filling period in the first 20 days of August, and get ripen in the last 10

days of August (see Table I). During the grain filling period, leaf chlorophyll content was almost the highest (Ciganda et al. 2009) which can contribute to the highest NDVI value. The NDVI is the average monthly value, the high NDVI during the first 20 days probably leads to a high average monthly NDVI.

In 2002-2008, the average monthly LST for April, May, June, July, August and September were 294.6K, 300.3K, 302.8K, 299.4K, 298.4K, and 296K respectively. The highest average monthly LST was in June.

The black sky albedos of NIR, shortwave, VIR broadband, are denoted as VIS-BB, SW-BB, NIR-BB, and have similar values with white sky albedo. Therefore, I only provide black sky albedo results in this study. VIS-BB, SW-BB, and NIR-BB albedos follow different trends during the growing season (Figure 3-9). NIR-BB albedo has an increasing-decreasing mode: increasing from 0.182 at DOY (day of year) 89 to 0.268 at DOY 209; then decreasing to 0.205 at the end of the growing season (DOY 289). The SW-BB albedo has a decreasing-increasing-stable mode: decreasing from 0.13 at DOY 89 to 0.124 at DOY 161; increasing to 0.154 at DOY 209; and then maintaining at approximately 0.148. The VIS-BB band has a decreasing-increasing mode: decreasing from 0.081 at DOY 89 to 0.036 at DOY 217, and then increasing to 0.084 at DOY 289.

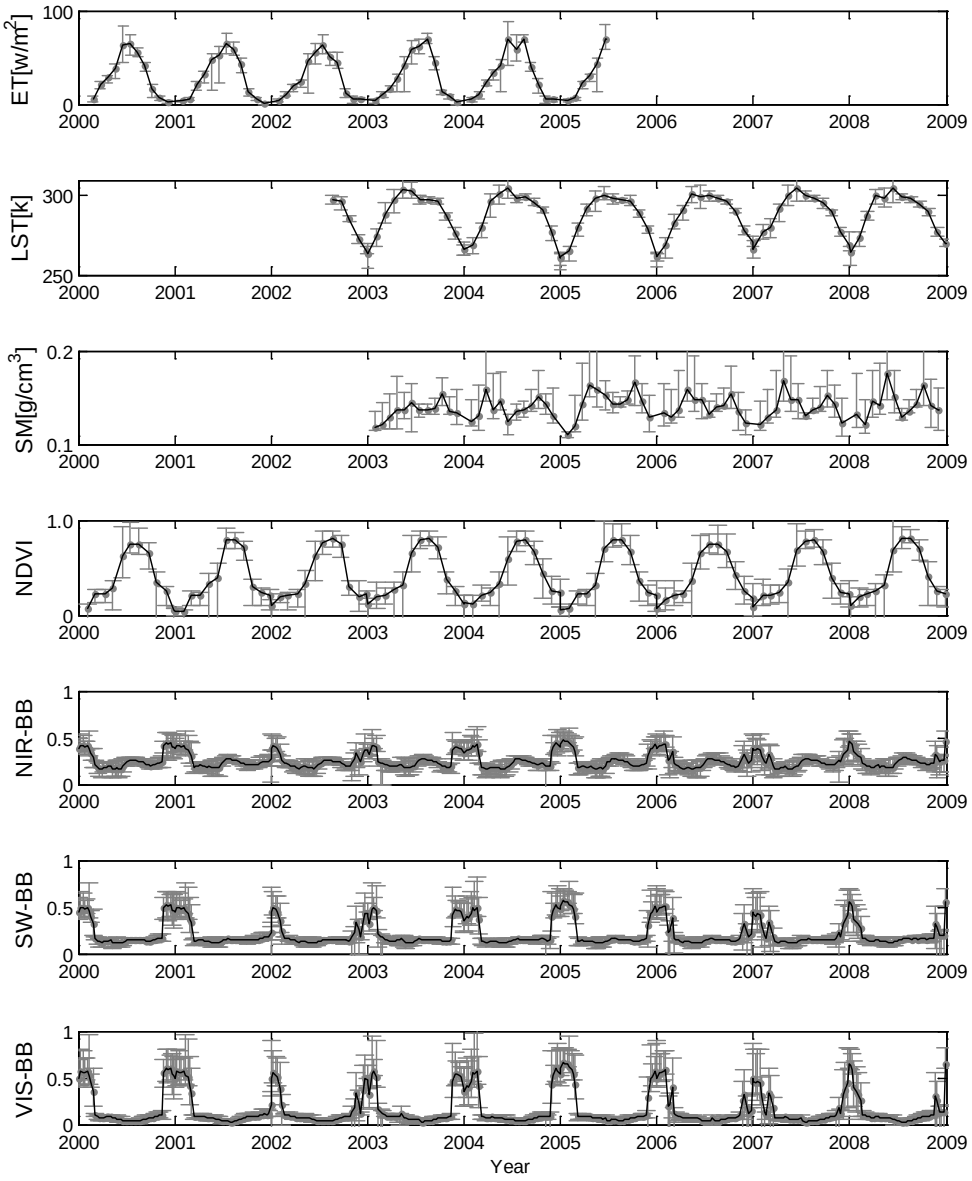

Figure 3-8 Time series ET, LST, SM, NDVI, VIS-BB, SW-BB, NIR-BB of target 2 during 2000-2008 (black and gray lines are mean and range of land surface parameter of target 2 in a given time, respectively. VIS-BB, SW-BB, NIR-BB are the black sky albedos of near-infrared, shortwave, visible broadband, respectively.)

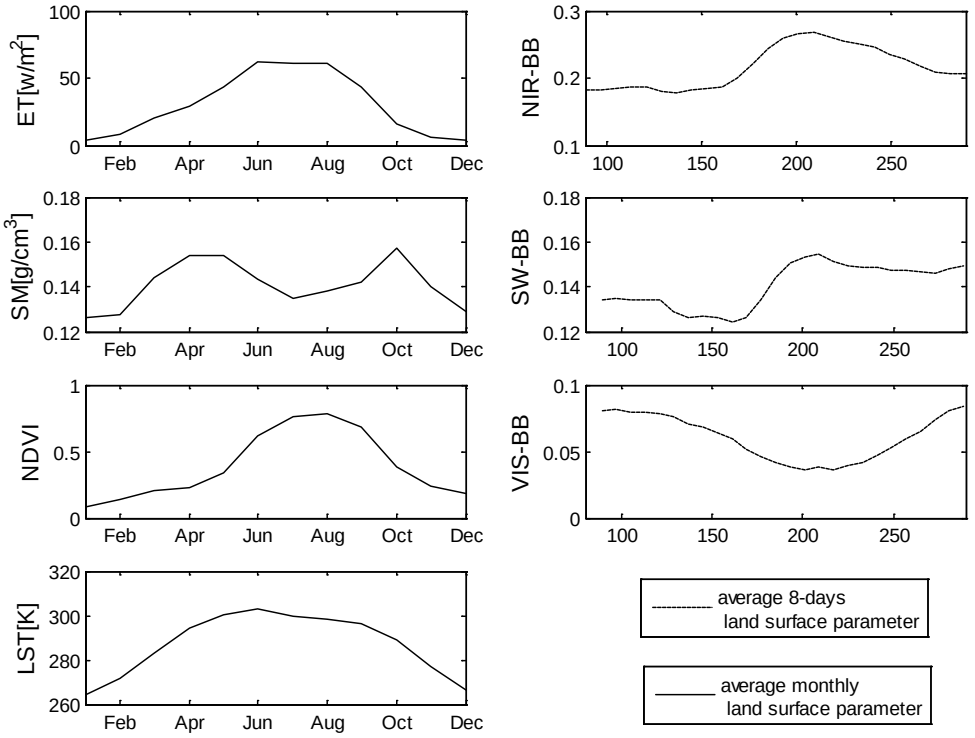

Figure 3-9 Average monthly ET, Soil moisture, NDVI, LST and 8-day NIR-BB SW-BB and VIS-BB of target **(**VIS-BB, SW-BB, NIR-BB are the black sky albedos of near-infrared, shortwave, visible broadband, respectively.**)**

3.1.3.2.2 Irrigation intensity impacts

To evaluate the land surface attributes under different irrigation intensities I determined land surface parameters by subtracting the land surface parameters of reference areas from target1 and target2 denoting them as target1_RA and target2_RA (Figure 3-10). First, target2_RA and target1_RA have similar attributes. The NDVI, ET, and soil moisture are positive, which means wetter soil, healthier crops, and more ET loss in highly irrigated areas versus areas with less irrigation. The VIS-BB, SW-BB, and NIR-BB albedos are negative because wetter soil in highly irrigated areas absorbs more shortwave radiation, causing the albedo to decrease. This provides more water for intense heat flux and less energy for heating the land surface,

resulting in lower LST. Second, during 2000-2008 the magnitudes of target2 _RA of NDVI, ET, soil moisture, LST, NIR_BB, SW_BB, and VIS_BB are all greater than the target1_RA. This indicates that the highly irrigated areas could have a much greater influence on land surface parameters. For example, in 2003 the target2_RA of NDVI, ET, soil moisture, LST, NIR-BB, SW-BB, and VIS-BB are 0.10, 4.53W/m^2, 0.01g/cm^3, -2.57, -0.03, -0.02, -0.03, which are 13.2, 17.9, 40.0, 22.3, 10.7, 12.0, and 13.5 percent greater than the target1_RA, respectively.

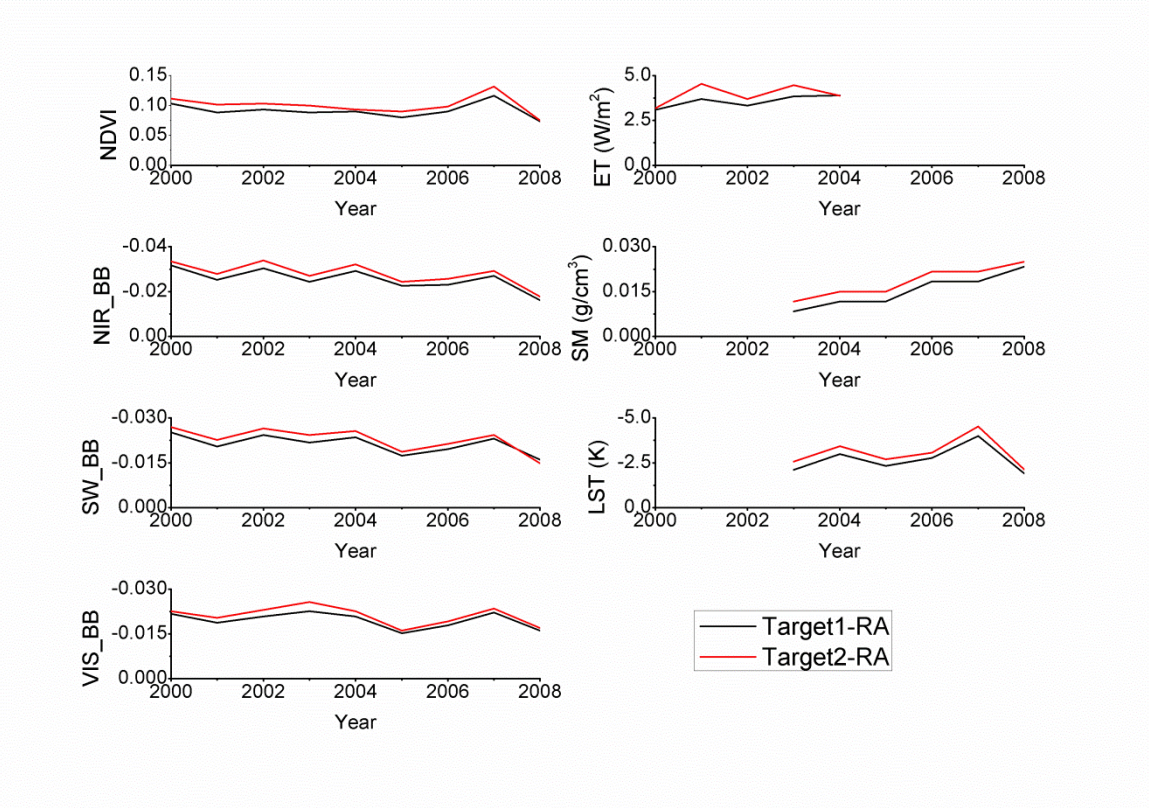

Figure 3-10 Comparison of land surface parameters between highly and lightly irrigated areas

3.1.4 Conclusion

In this study, I evaluated the impacts of agricultural irrigation on air temperature and land surface parameters during the growing season in Jilin Province, China. Results from both meteorological and satellite observations show an irrigation

cooling effect in Jilin Province. Consistent with other studies, irrigation in my case also displayed more of an impact on the maximum air temperature than on the minimum air temperature during the last 53 years. The magnitude of the difference in maximum air temperature was almost twice that of the difference in minimum air temperature, and the linear regression coefficient of the time series of the difference in maximum air temperature was greater than three times that of the minimum air temperature. This is because that evapotranspiration is increased by irrigation during daylight hours, reducing the energy for heating the land surface and causing lower LST (Boucher et al. 2004; Kueppers et al. 2007). At the same time, irrigation increases the near-surface water vapor, an important greenhouse gas, decreasing the shortwave radiation absorbed by the land surface, which also causes lower LST. However, at nighttime, water vapor can help hold the energy out of space, reducing the cooling effect. The temperature difference between HIP and LIP are statistically significant and highly correlated to EIA, CSA and as well as SPI12 of the LIP sites. Moreover, the temperature difference between HIP and LIP is bigger in a drier year.

Results from satellite observation show that the land surface parameters of irrigated areas had obvious intra-annual variations. Monthly ET rapidly increased since crops were planted in April, reached a plateau during June to August, and then decreased again in the harvest month (September). The highest average monthly soil moisture, LST, and NDVI was in April, June and August. Three broadband albedos follow different trends during the growing season, with an increasing-decreasing mode, decreasing-increasing-stable mode, and deceasing-increasing mode. Moreover,

highly irrigated areas always corresponded to a lower albedo and LST, and higher soil moisture, NDVI and ET over the study period of 2000-2008.

Overall, this study may provide some substantive evidence that a cooling effect from agricultural irrigation exists in China. However, this conclusion does not mitigate the potential of other factors to influence the air temperature of my study sites, since the climate system is so complex. No one single factor can be attributed to regional climate changes. More observations and evidence are needed in order to attain a greater understanding of the influence of irrigation on local climate in China.

Moreover, this study proved that satellite observations are sufficiently valid to determine the impact of irrigation on land surface parameters, and provide another viable method for understanding the impact of irrigation on local climate, especially in those regions where direct observations are limited or obscured by other factors, such as urbanization in China. Urbanization can change land surface parameters such as land surface temperature. The higher urbanization is corresponding to the higher land surface temperature (Wang et al. 2007). With the rapid urbanization, for example in China, most meteorological stations are becoming located within, or near cities (Zhou et al. 2004), which can impact the atmospheric signature of irrigation in two ways. First, the difference of irrigated and non-irrigated sites might be caused by different urbanization levels at these sites rather than by irrigation itself which exacerbates the difficulty in distinguishing the impacts of irrigation. Second, urbanization increases land surface temperature, while irrigation decreases land surface temperature. As a result, urbanization can weaken the impacts of irrigation.

3.2 Case study in North China

The first case study already proved that satellite observation can effectively assess the irrigation impact on land surface parameters and provide another valid method for determining the impact of irrigation on the local surface climate. However, the first case study covered only a small area, (Jilin Province, in China). Taking into account operational problems such as large gaps in data and lower quality due to cloud contamination in current satellite products, the applications of satellite products could be limited on a large scale. Therefore, the efficiency of satellite data to detect the impact of irrigation on land surface attributes needs to be validated over a large area.

Here, a similar method and data source that are described in the first case study were used to analyze the irrigation impact on land surface parameters in North China via a new irrigation map of China. The main objective of this study is to verify if satellite observations are capable of detecting the impact of irrigation on land surface parameters over a large area.

The study areas are 17 provinces in North China (Figure 3-11): Liaoning (LN), Jilin (JL), Heilongjiang (HLJ), Inner Mongolia (IN), Hebei (HEB), Henan (HEN), Shandong (SD), Jiangsu (JS), Anhui (AH), Shanxi (SX), Shaanxi (SAX), Gansu (GS), Qinghai (QH), Ningxia (NX) and Xinjiang (XJ), Beijing(BJ), and Tianjin (TJ). The background information for these provinces is summarized in Table 3-6. Based on the climate characteristics, geographical locations and planting structures of these provinces, the whole study area was further classified into three regions: Northeast (NE), Northwest (NW), and the North China Plain (NCP).

Table 3-6 Background information for studied areas (AT is the accumulated temperature steadily above 10 ℃, AAT is annual average temperature, ASH is annual sunlight hours, AR is annual rainfall, ASR is annual amount of solar radiation, FFS is frost-free days in one year)

Province	AT (℃)	AAT (℃)	ASH (H)	AR (MM)	ASR (MJ/M^2)	FFD (DAY)	SUMMER GRAINS	AUTUMN GRAINS
IM	2000-3200	0-8	2600-3400	50-450	5000-6700	50-150		Apr-Aug, Spring Corn, Spring Wheat
JL	2700-3200	2-6	2200-3000	400-900	4363-5276	130-150		Apr-Sep, Middle Rice, Spring wheat, Spring Corn
LN	2700-3700	7-11	2270-2990	440-1130	4187-8374	125-215		Apr-Sep, Middle Rice, Spring Corn
HlJ	2000-3000	-4-5	2300-2800	400-650	4600-5000	100-140		Apr-Sep, Middle Rice, Spring wheat, Spring Corn
NX	1900-3300	5-10	2200-3300	167-647	4932-6096	127-195		Apr-Sep, Middle Rice, Spring wheat, Spring Corn
QH	2914	-6-9	2328-3575	18-764	5880-7560	30-185		Apr-Aug, Spring Corn, Spring wheat
SX	2000-4600	-4-14	2200-2900	400-700	5000-6680	110-220	Sep-Next Jun, winter wheat	Apr-Oct, Spring Corn, Summer Corn, Cotton
SAX	1945-5000	9-16	1400-2900	340-1280	3768-5862	160-250	Sep-Next Jun, winter wheat	Apr-Oct, Spring Corn, Summer Corn, Cotton
GS	2804-4000	0-14	1700-3300	300-860	3517-4521	140-280	Sep-Next Jun, winter wheat	Apr-Aug, Spring Corn, Spring wheat
XJ	4162-5501	-4-14	2600-3400	25-200	5000-6500	140-220	Sep-Next Jun, winter wheat	Apr-Oct, Spring wheat, Spring Corn, Summer Corn, Cotton
HEB	2100-5200	2-14	2400-3100	350-815	4854-5981	80-205	Oct-Next Jun, winter wheat	Apr-Oct, Spring Corn, Summer Corn, Cotton, Middle rice
SD	3800-4600	11-14	2300-2900	550-950	4810-5400	180-220	Oct-Next Jun, winter wheat	Apr-Oct, Summer Corn, Cotton, Later rice
HEN	4200-4900	12-16	2000-2600	500-900	5000-5850	190-230	Oct-Next May, winter wheat	Apr-Oct, Summer Corn, Cotton
JS	4400-5100	13-16	2000-2600	870-1100	4564-4982	207-258	Oct-Next May, winter wheat, Spring corn	Apr-Oct, Middle Rice, Cotton
AH	4600-5300	14-17	1800-2500	770-1700	4396-5443	200-250	Oct-Next May, winter wheat, Early rice	Apr-Sep, Middle rice
BJ	4000	10-12	2000-2800	600-700	4689-5694	180~200	Oct-Next Jun, winter wheat	Apr-Oct, Spring Corn, Summer Corn, Middle Rice
TJ	2000-4200	11-13	2500-2900	550 - 680	3758-5932	196~246	Oct-Next Jun, winter wheat	Apr-Oct, Spring Corn, Summer Corn, Middle Rice

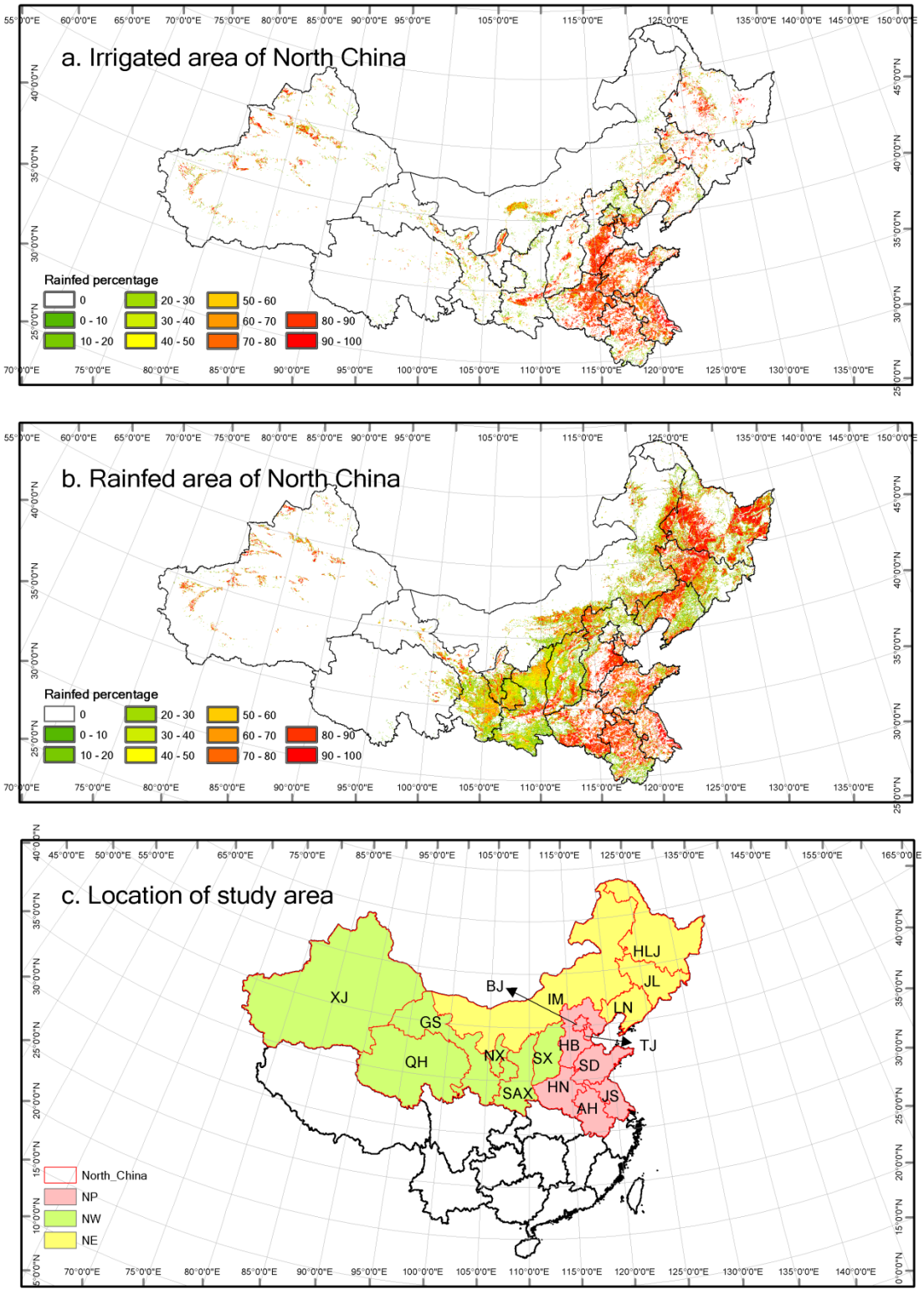

Figure 3-11 Study areas

3.2.1 Data

The land surface biogeophysical parameters used in this study include the albedo, land surface temperature (LST), normalized difference vegetation index (NDVI), and evapotranspiration (ET). The albedo is from the moderate-resolution imaging spectroradiometer (MODIS) albedo product MCD43C3, which has a 16-day temporal resolution and 0.05° spatial resolution. The LST is from the MODIS/Aqua Land Surface Temperature/Emissivity Monthly L3 Global 0.05° CMG (MYD11C3) products. NDVI is from the MODIS Vegetation Indices 16-Day L3 Global 0.05° CMG (MOD13C1) product. The temporal coverage of MCD43C3 and MOD13C1 is from 02/24/2000-current, and the temporal coverage of MYD11C3 is 08/01/2002-current.The final time periods used in this study are 2000-2010 for of NDVI and albedo, and 2003-2010 for LST . Similar to the first case study, ET was calculated using statistical equations (Wang and Liang 2008). The new irrigation map with 1 km resolution is from the section 4.

Other data sets used in this study include the irrigation map of China and a rainfed map of China produced in chapter 2 and the intensively validated National Land Cover Dataset (NLCD) of China mentioned above.

3.2.2 Methodology

In order to simplify the method, this study only focused on the period of April to October which is the most common growing season (GS) in North China. The specific starting and ending days of the year (DOY) for GS (Table 3-7) depend on the data source. For example, for the monthly MODIS LST with a spatial resolution of 0.05°, the data for April are recorded from DOY 91 in a normal year and DOY 92 in a

leap year; however, for the 8-day albedo with a resolution of 0.05°, DOY 97 is the closest date to April 1st that contains albedo data.

Table 3-7 Time periods used in this study for different MODIS products (DOY: Day of year)

MODIS Data	JJA	GS
8-day albedo (MCD43C3)	DOY 153- 241	DOY 97 - 305
monthly LST (MYD11C3)	DOY 152/153 -213/214	DOY 91/92 - 274/275
monthly NDVI (MOD13C1)	DOY 152/153 - 213/214	DOY 91/92 - 274/275

The methodology include the following steps: First, the NLCD was re-projected onto a new map using a geographic projection, and then applied majority rules to coarsen the new map to a 0.05° spatial resolution, in which the new pixel class is dominant among the six land cover types within a 0.05° spatial extent. In this new map, if the new pixel class is comprised of cultivated land, it was defined as 1; otherwise it was defined as 0. This resulted in the creation of a binary map (1; cultivated land, 0; non-cultivated land).

Second, the irrigation map and rainfed map mentioned above were re-projected and resized to 0.05 degrees, and then I used the binary map derived from first step as a mask to exclude the non-cultivated areas from the maps.

Third, for better understanding of the impact of irrigation on land parameters, the analyses were carried in the whole of North China as well as three sub-regions, namely, Northeast China, Northwest China, and the North China Plain. All the irrigation agriculture pixels for North China were extracted and defined as two areas of interest: high irrigation areas (e.g. irrigation percentage $\geq$ 50%) and low irrigation areas (e.g. irrigation percentage <50%) based on the difference in irrigation percentage. Rainfed areas where the crop percentage in a pixel is larger than 50 (thereafter, simply called them as rainfed areas) were also extracted. Considering that

the magnitude of irrigation impacts on land surface parameters could be different because of the differences in altitude and regional climate of different irrigated pixels, the mean value of each land surface parameter for high irrigation areas, low irrigation areas and rained areas during the growing season were first calculated province by province. Then, for each land surface parameter, this study averaged the mean values of 17 provinces, over the whole study area, averaged the mean value of each land surface parameter of 4 provinces (Liaoning, Jilin, Heilongjiang, and Inner Mongolia) for the NE, 6 provinces (Shanxi, Shaanxi, Gansu, Qinghai, Ningxia and Xinjiang) for the NW, and 7 provinces (Hebei, Henan, Shandong, Jiangsu, Anhui, Beijing, and Tianjin) for the NCP to get the final mean land surface parameter value, and then analyzed the differences in land surface parameters between high irrigation areas and low irrigation areas(/rainfed areas).

3.2.3 Results and discussions

In order to detect the impact of irrigation on land surface parameters over a large area, this study analyzed the differences between highly irrigated area and lightly irrigated/rainfed area in 17 provinces located in North China during both growing season and summer time. Results are shown in Figure 3-12, Table 3-8,Table 3-9 and Table 3-10. Generally, highly irrigated areas show the higher nighttime LST, NDVI, and ET, and lower daytime LST and albedo than both lightly irrigated areas (Table 3-8) and rainfed areas (Table4). Theoretically, excessive ET from irrigated agricultural land causes a change in the land surface energy distribution, which cools the land surface and near-surface air temperature during the day. ET also increases the atmospheric water vapor, which is the most dominant greenhouse gas with a significant and positive feedback on our climate system. At nighttime, more water

vapor in the atmosphere can increase the near-surface temperature. Meanwhile, irrigation increases soil moisture. The specific heat of water is higher than that of the land surface; hence, more moisture in the soil can reduce the cooling process of the land surface at nighttime. Soil moisture can also modify the radioactive properties of the soil, such as decreasing its albedo. In addition, irrigation assists crop growth in dry areas or increases in food production. Thus, crops within areas that include irrigation facilities have a greater ability to resist dry climate conditions, and are expected to be healthier in dry areas. Correspondingly, the NDVI values of areas with irrigated facilities are expected to be higher than those of non-irrigated areas in dry areas. In sum, results of this study are generally consistent to theoretical expectations.

The mean differences of land surface parameters between highly irrigated area and lightly irrigated areas (rainfed areas) are higher during summer time than during whole growing season. For all the parameters (daytime and nighttime, LST, and NDVI), the differences between the highly irrigated areas and the rainfed areas are larger than the differences between the high and the low irrigation areas (Table 3-8 and Table 3-9). Among three sub-regions, the differences between highly irrigated area and lightly irrigated/rainfed areas are largest in Northwest China although the North China Plain (NCP) is the most heavily irrigated area in China. One possible reason is that the effects of irrigation are more obvious in dry climate conditions such as those in the NW which is the driest area of China. The magnitudes of the irrigation effects are influenced by many factors: the acreage of the irrigated area, the absolute irrigation water consumption, the ratio of irrigation water consumption to total water consumption (irrigation and precipitation), and so on. A fully irrigated pixel might

accept less water in wet areas than in dry areas. The extra water from irrigation would amplify the impact caused by differences in the water condition between highly and lightly irrigated areas (or irrigated and non-irrigated areas) much more easily in a dry climate than in a wet climate. The previous modeling study also reported that irrigation has more impact in dry areas than wet areas when same amounts of irrigation water are used (Sacks et al. 2009).

Given that highly and lightly irrigated areas were compared in this study, a different choice of threshold for defining them might affect the results. Besides the threshold of irrigation percentages of 50, another different threshold (irrigation percentages of 30) was also used to define highly and lightly irrigated areas. The results from the two different thresholds were quite similar in terms of this study (Table 3-10).

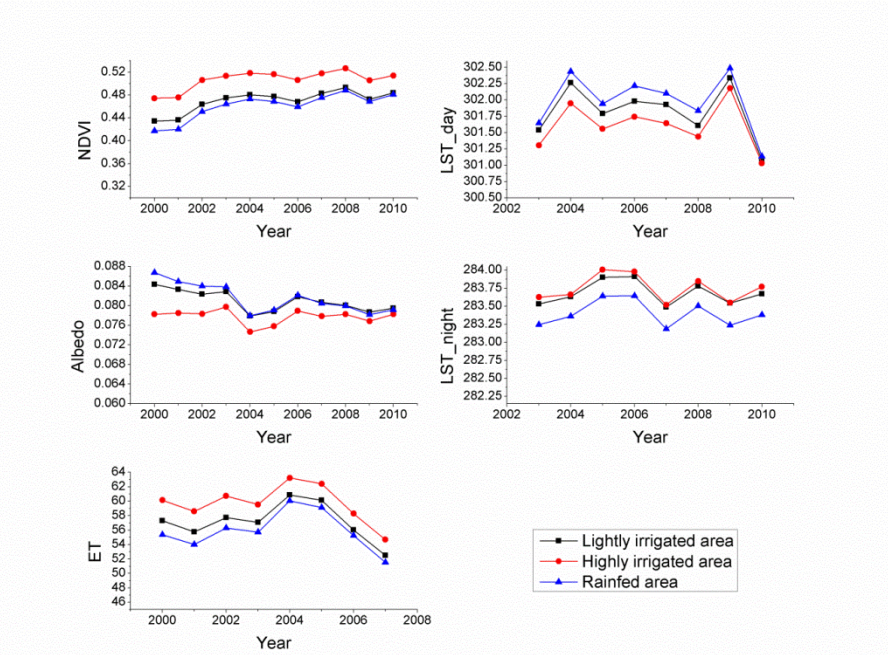

Figure 3-12 The mean of land surface parameters of rainfed areas and highly and lowly irrigated areas in North China during growing season (here, highly and lightly irrigated areas are separated by a threshold of irrigation percentages of 50)

Table 3-8 The mean differences of land surface parameters between highly and lowly irrigated areas in north China and three sub-regions during both growing season and summer (June-July-August, JJA)

	GS				JJA			
	North China	NE	NCP	NW	North China	NE	NCP	NW
LST_Day	-0.209	-0.322	0.079	-0.471*	-0.401***	-0.624	0.189	-0.939***
LST_Night	0.062	0.177	-0.068	0.138	0.156	0.206	0.068	0.225
NDVI	0.037***	0.017**	0.028** *	0.061***	0.052***	0.045***	0.021 *	0.092***
Vis_Albedo	-0.003***	0.002**	0.001	0.008***	-0.004***	0.004***	0.002	0.011***
ET	2.532*	0.039	1.769	5.083***	3.278	1.565	0.412	7.764***

T-test for equality of means of highly and lightly irrigated areas by independent samples tests (here, highly and lightly irrigated area are separated by a threshold of irrigation percentages of 50)
* p<0.1
*** p<0.05
*** p<0.01

Table 3-9 The mean differences of land surface parameters between highly irrigated areas and rainfed areas in north China and three sub-regions during both growing season and summer (June-July-August, JJA)

	GS				JJA			
	North China	NE	NCP	NW	North China	NE	NCP	NW
LST_Day	-0.368*	-0.317	-0.247	-0.544*	-0.601***	-0.602	-0.181	-1.092***
LST_Night	0.345***	0.460***	0.087	0.570***	0.398*	0.423	0.143	0.462
NDVI	0.046***	0.017**	0.039***	0.074***	0.062***	0.040**	0.032**	0.113***
Albedo	-0.004***	-0.002	-0.002**	-0.007***	-0.005***	-0.003***	-0.001	-0.010***
ET	3.778**	0.575	2.998	6.824***	5.189**	2.582	2.264	10.340***

T-test for equality of means of highly irrigated areas and rainfed area by independent samples tests (here, highly irrigated areas are areas with irrigation percentages in a pixel bigger than 50)
* p<0.1
*** p<0.05
*** p<0.01

Table 3-10 Mean land surface parameters during growing season over the studied periods in North China

Areas	NDVI	VIS_albedo	LST_Day (K)	LST_Night (K)	ET(W/m^2)
Irrigation Percentage <50	0.470	0.081	301.815	283.683	57.167
Irrigation Percentage >50	0.507	0.078	301.606	283.745	59.699
Irrigation Percentage <30	0.466	0.081	301.841	283.664	56.897
Irrigation Percentage >30	0.496	0.079	301.668	283.743	58.990
Rainfed area	0.461	0.081	301.137	283.379	55.921

3.2.4 Conclusion

In previous studies, a number of authors indicated that regional impacts of irrigation were as large as those from changes in land cover (Puma and Cook 2010; Sacks et al. 2009). Furthermore, some authors suggested that irrigation might mask the warming signal caused by an increase in greenhouse gases to some degree (Kueppers et al. 2007). Most of these studies are based on modeling research with irrigation maps. This raises a number of questions. Does irrigation really have such large effects on land surface parameters and near-surface systems? Do observations support the conclusions from modeling studies? In the future, a comprehensive method for evaluating the impact of irrigation needs to be developed, in which evidence from both observational studies (remote sensing and meteorological measurements) and modeling studies can validate one another. Satellite observation is a potential tool for studying the impact of irrigation because it can provide land parameter information on a large scale; however, the efficiency of satellite data in detecting the impact of irrigation on land surface attributes on a large scale has not been explored in previous studies.

In this study, the impacts of irrigation on land surface parameters in North China were analyzed by using a new irrigation map of China. Theoretically, irrigation can increase ET, NDVI, and nighttime LST, as well as decrease albedo and daytime LST. Overall, my results show that ET, NDVI, and nighttime LST are greater in highly irrigated areas than in lightly irrigated/ rainfed areas, whereas the albedo and daytime LST are lower in highly irrigated areas than in lightly irrigated/rainfed areas

in my study area. The consistency of results from this study to theoretical expectation indicates that satellite observation is a promising tool for studying the impact of irrigation on a large scale although additional similar examination need to be done in other irrigated areas.

Chapter 4 Modeling the irrigation impact over China

China experienced both large landscape changes and extensive irrigation growth in the past several decades. From the 1980s to 2000, the cropland increased by 3.0 million ha, woodland decreased by 2.9 million ha, grassland decreased by 0.4 Million ha, and built-up increased by 1.8 million ha (Liu et al. 2005c) in China. China has the second largest irrigation area (53.8 million ha), following India (57.3 Million ha), in the world (Siebert et al. 2005b). More than 45% of China's crop land will be irrigated in 2050 (Wu et al. 2010). Total irrigated area in China increased almost monotonically from 15.0 million ha to 58.5 million ha and agricultural water withdrawal increased from 100.1 billion m^3 to 366.4 billion m^3 between 1949 and 2008 (Wu et al. 2010). Therefore, both land cover change and land management (irrigation) may have contributed to the formation of the current climate system and could continue to influence our future climate system.

The following questions are worthy of exploration in order to improve our understanding about how human activities affect climate and to guide policies aimed at mitigating or adapting to climate change in China: 1) Is the impact of irrigation on climate comparable to the impact of land cover change on climate in China? 2) Did irrigation significantly impact the climate in China in the past? 3) How will irrigation impact the future climate in China? To answer those questions, I simulated both the irrigation impacts and land cover change impacts on the climate in China in one past time period (1978-2004) and two future time periods (2050 and 2100) via a land surface model, and then compared the differences among those simulations.

Here, I will introduce my modeling method and data in section 4.1. Section 4.2 presents the results and a discussion, and section 2.5 summarizes conclusion. Three manuscripts about the work in this chapter have been prepared; two were submitted (Zhu et al. 2011a, c) and another one is in preparation (Zhu et al. 2011b).

4.1 Method and data

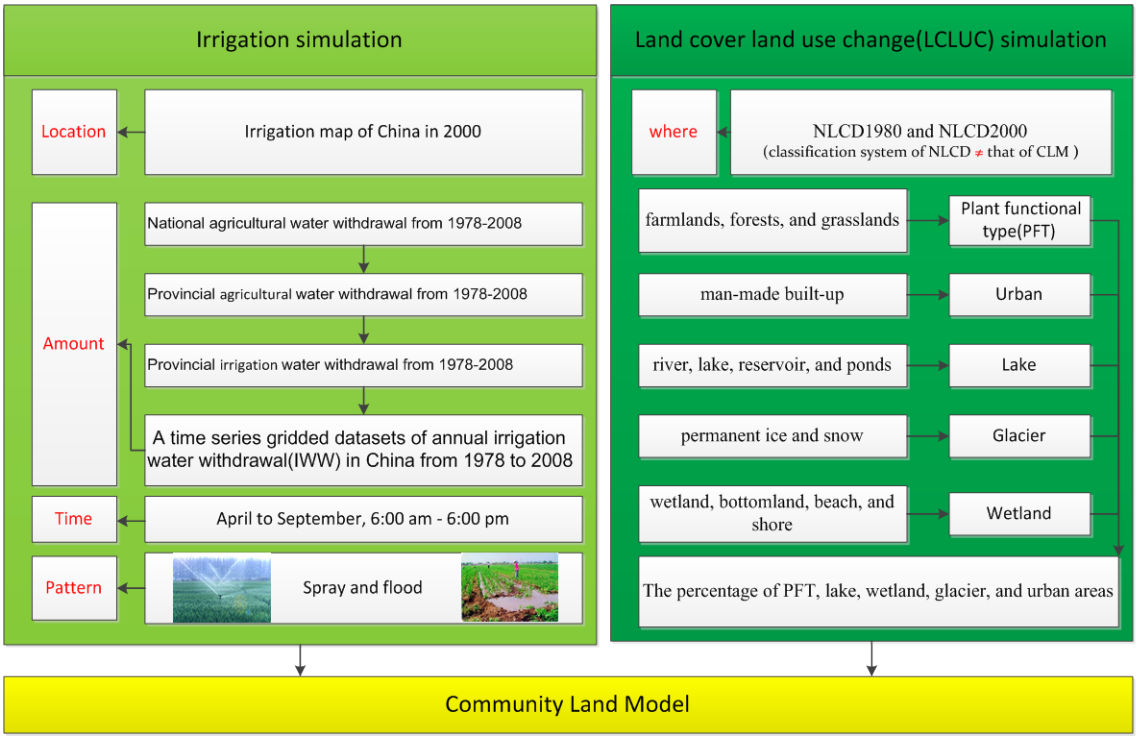

Figure 4-1 Flowchart of the modeling method

Figure 4-1 shows my main procedure for the modeling study, in which I simulated both the irrigation impact and land use land cover change (LULUC) impact. Both of them used the Community Land Model as a tool. For the irrigation simulation, four questions need to be considered: where to irrigate, how much to irrigate, when and how to irrigate (e.g., rain, spray, drip; and rate). In my simulation, I used the irrigation map which I made in Chapter 2 to control the irrigated grid and used a time series gridded datasets of annual irrigation water withdrawal in China

from 1978 to 2008 to control irrigation amount. I also built an irrigation module in the community land model to control the irrigation rate and time. For the LCLUC impact, two high-resolution National Land-Use/Land-Cover datasets of China (NLCD1980 and NLCD2000) were reconstructed and used as land surface input to run CLM. More details are described in the following subsections.

4.1.1 Community land model

The land surface model used in this study is version 4.0 of the Community Land Model (CLM4.0, hereafter simply referred to as CLM). In the CLM, land surface heterogeneity in a grid cell is represented by a sub-grid hierarchy. The first sub-grid hierarchy is the land unit. There are five different land units in the CLM: glacier, lake, wetland, urban, and vegetated. The second sub-grid hierarchy is the column. Soil and snow state variables can only be changed at the column level. In the current default configuration of version 4.0, the urban land unit has five columns, and each of the other land units has one column. The third sub-grid hierarchy incorporates plant functional type (PFT) and bare ground. There are 16 PFTs in the CLM: temperate needleleaf evergreen tree (NET Temperate), boreal needleleaf evergreen tree (NET Boreal), boreal needleleaf deciduous tree (NDT Boreal), tropical broadleaf evergreen tree (BET Tropical), temperate broadleaf evergreen tree (BET Temperate), tropical broadleaf deciduous tree (BDT Tropical), temperate Broadleaf deciduous (BDT Temperate), boreal broadleaf deciduous tree (BDT Boreal), temperate broadleaf evergreen shrub (BES Temperate), temperate broadleaf deciduous shrub (BDS Temperate), boreal broadleaf deciduous shrub (BDS Boreal), C3 arctic grass, C3 grass, C4 grass, crop1, and crop2. The same atmospheric forcing is used to force all sub-grid units within one grid cell. Biogeophysical and biochemical processes are

simulated for each sub-grid landunit, column, and PFT independently. The surface variables and fluxes output from the model are obtained by averaging the sub-grid quantities weighted by their fractional areas.

4.1.2 Land surface data

In order to simulate the impact of land cover change on the local climate over China, two high-resolution National Land-Use/Land-Cover datasets of China (NLCD1980 and NLCD2000) were used. Both of these were produced by the Chinese Academy of Sciences using visual interpretation and digitization of TM images at the scale of 1:100,000 (Liu et al. 2005c). These two datasets are reported to have high accuracy and have been used by many previous studies (Liu et al. 2002). It is reported that the average interpretation accuracy is 92.9% for land cover classification and 97.6% for land-cover change detection (Liu et al. 2005c). These two maps have the same hierarchical classification system of 6 classes and 25 sub-classes (Table 4-1). More details about these classes can be found in reference(Liu et al. 2005a).

Table 4-1 Classification system of National Land-Use/Land-Cover datasets of China

Class	Subclass
Farmland	Paddy, Dry farming
Forest	Forest, Shrub, Woods, others
Grassland	Dense grass, Moderate grass, Spare grass
Man-made Built-up	City built-up, Rural settlements, Others
Water body	River, Lake, Reservoir and ponds, Permanent ice and snow, Beach and Shore, Bottomland
Unused	Wetland, Sand Gobi, Salina, Bare Soil, Bare Rock, Others

The surface data for running the CLM require percentages of glacier, lake, wetland, urban, and each PFT. Because the classification system of NLCD is not directly compatible with the surface data of the CLM, I reconstructed the NLCD maps to correspond to the CLM surface data as follows. First, farmlands, forests, and grasslands of the NLCD maps were combined together as PFTs of the CLM surface data. The crop, grass, and tree types were distinguished and the time course of leaf area index (LAI) for them were prescribed with the help of the present day PFT dataset of the CLM downloaded from the public subversion input data repository at http://www.cesm.ucar.edu/models/cesm1.0/. The present day PFT dataset of the CLM was produced by Lawrence and Chase (2007). Second, the man-made built-up category of the NLCD was assigned to the urban class of the CLM surface data. Urban properties such as building height, street width, heat capacity, and thermal conductivity were selected from the present day CLM urban dataset produced by (Jackson et al. 2010). Third, the river, lake, reservoir, and ponds categories of the NLCD were assigned to the lake class of the CLM surface data. Fourth, the permanent ice and snow categories of the NLCD were assigned to the glacier class of the CLM surface data. Fifth, the wetland, bottomland, beach, and shore categories of the NLCD were assigned to the wetland class of the CLM surface data. Finally, the sand, Gobi, Salina, bare soil, and bare rock categories of the NLCD were assigned to the bare ground class of the CLM surface data. Subsequently, the percentages of lake, wetland, glacier, urban, and each PFT are calculated by aggregating the redefined NLCD 1-km grid to a CLM 0.5° grid. The percentage of lake, wetland, glacier, and urban areas are calculated with respect to the entire grid cell. The percentage of each

PFT is with regard to the vegetated portion of the grid cell and the sum of the PFTs is 100%. The above steps were carried out for both the NLCD1980 and the NLCD2000. The land surface datasets produced are referred to as CLM_NLCD1980 and CLM_NLCD2000, hereafter.

4.1.3 Irrigation map

The irrigation map of China from Chapter 2 was used to indicate where irrigation happened in my simulation. The new irrigation map was produced by allocating the statistics of irrigation areas from geopolitical units to individual pixels via an irrigation spatial allocation model. In the irrigation spatial allocation model, three irrigation potential indices were developed based on an assumption that the productivity of crops remains high and stable for a long time series in the irrigated area compared with rainfed crops in a given land unit. A land unit refers to land with certain characteristics such as productivity, irrigation requirements, and climate conditions. Then, an automated classification routine was used, in which the pixel with the highest irrigation potential within the crop grids is identified as an irrigated pixel. The irrigation percentage in the irrigated pixel equals the crop percentage of this pixel, obtained from China's NLCD. The cumulative area covered by irrigated pixels was then calculated. This cumulative area was compared with the target number of hectares provided by the census of irrigated area given in the statistics yearbook. If the total area of the selected pixels was less than the target area, then the pixel with the next highest irrigation potential was selected. These steps were repeated until the target area for the province was exceeded.

4.1.4 Irrigation water withdrawals in the past

There are two types of data sources for irrigation water withdrawal in China. One source is the estimates obtained from modeling studies (Doll and Siebert 2002; Thomas 2008; Yang et al. 2010); the other source is the official statistical data collected by the Ministry of Water Resources of China. Irrigation modeling can simulate the irrigation requirement for optimal crop growth; however, the estimated irrigation amount may drift away from the actual amount owing to two reasons. First, water crises are more serious in the current era than at any other time because of the rapid population increase, continuous economic growth, and extended drought disasters. Farmers are more likely to use supplemental rather than full irrigation in order to increase grain yield under great water stress. In other words, the irrigation requirement is more likely to be higher than the real irrigation water quota. Second, agricultural water is consumed not only by field crops but is also wasted in the process of delivery from water source to the fields. In many countries, especially in poor developing countries, the inadequately maintained irrigation infrastructures, backward water management systems, and deficient agriculture investments contribute to lower the water use efficiency. As a result, more water is consumed than the actual water required for growing healthy crops. Conversely, official statistical data of agricultural water withdrawal might be more relevant to the actual water consumption in the agriculture sector. However, agricultural water withdrawal is always reported on the basis of geopolitical units or river basins, without detailed distribution information.

In this study, I developed a time series gridded dataset of annual irrigation water withdrawal in China from 1978 to 2008 by using the historical agricultural

water withdrawal data and the irrigation maps of China around 2000 and used this dataset to control the irrigation amount in irrigation simulations.

Generally, my method is a serial of downscaling processes: downscaling national agricultural water withdrawal (AWW) to provincial AWW, downscaling provincial AWW to water consumption of irrigated dryland and paddy filed in a given province, and calculating the AWW per square kilometer (km^2) of irrigated dryland and irrigated paddy field in this province. Finally, the AWW of a given pixel equals to AWW of irrigated dryland within this pixel plus AWW of irrigated paddy field within this pixel. Besides the previous process, a conversion from agricultural water withdrawal to irrigation water withdrawal is also needed. More details are described below.

First, national agricultural water withdrawal data from 1997 to 2008 were taken from the China Statistical Yearbook of 1998 to 2009 and those of 1978, 1980, 1985, 1990, 1993, and 1995 were from reference (Wang et al. 2010). The missing national agricultural water withdrawal data were filled by applying linear interpolation with the following equation:

$$AWW_j = \left(\frac{AWW_p - AWW_o}{EIA_p - EIA_o} \right) \times (EIA_j - EIA_o) + AWW_o \qquad \text{Equation 4-1}$$

where AWW_j is the calculated agricultural water withdrawal (m^3) of China in year *j*; EIA_j is the effective irrigated area (Kha) of China in year *j*; *AWWp* and *AWWo* are the reported agricultural water withdrawal of China in years *p* and *o*, respectively; and EIA_p and EIA_o are the effective irrigated area of China in years *p*

and *o*, respectively. *p* and *o* are the nearest year with available data before and after year *j*, respectively. EIA refers to land "where there are water sources or complete sets of irrigation facilities to lift and move adequate amounts of water for irrigation purposes under normal conditions," and irrigated area statistics are an indication of "drought resistance capacity" (China Statistical Yearbook 2008). In China, irrigated areas are reported on the basis of census data. Conventional local-level Bureau of Statistics reports include irrigation statistics at the village level, which is then aggregated to higher levels such as county, city, province, and national levels. The National Bureau of Statistics regularly releases data on national and provincial irrigated areas in its Statistics Yearbook.

Second, the provincial agricultural water withdrawal after 2001 is reported in China Statistical Yearbook and the provincial agricultural water withdrawal before 2002 was derived by downscaling the nation AWW via the following formulas:

$$AWW_{i,j} = AWW_j \times R_i = AWW_j \times \frac{mean(GIQ_{i,2002-2008}) \times EIA_{i,j}}{\sum_{i=1}^{n} (mean(GIQ_{i,2002-2008}) \times EIA_{i,j})} \quad \text{Equation 4-2}$$

Where $AWW_{i,j}$ and $EIA_{i,j}$ are agricultural water withdrawal (m^3) and effective irrigated area (k ha) of province *i* in year *j*, respectively. AWW_j is the agricultural water withdrawal of China (m^3) in year *j* (data are taken from the National Statistical Yearbook for most years or calculated from the first step in the missing years). R_i is the ratio of the AWW of province *i* to the national AWW; it is decided by two factors: the Gross Irrigation Quota (GIQ) and EIA. GIQ is defined as the ratio of the agricultural irrigation water quantity to the effective irrigation area (Wu et al. 2010).

The annual provincial agricultural water withdrawal information since 2002 has been reported in the China Statistical Yearbook. The China Statistical Yearbook also lists the effective irrigation area for each province. Therefore, I can calculate the GIQ for each province *i* from 2002 to 2008, and further calculate the mean GIQ of each province *i* during 2002 to 2008 (denoted as $mean(GIQ_{i,2002-2008})$, shown in Table 4-2). Variable *i* goes from 1 to *n*, where n is the number of provinces, excluding Hong Kong, Macao, and Taiwan due to lack of available EIA for them in the China Statistics Yearbook. It should be noted that *n* changed to 31 after 1997 when Chongqing separated from the Sichuan province, and it was 30 during 1987–1996 and 29 during 1978–1986 because no data for that period was available from Hainan province. *j* covers the period from 1978 to 2008.

Table 4-2 The mean GIQ of each province during 2002 to 2008

Province	mean GIQ (mm)	Province	mean GIQ (mm)	Province	mean GIQ (mm)
Beijing	625	Anhui	363	Chongqing	317
Tianjin	351	Fujian	1089	Sichuan	479
Hebei	335	Jiangxi	724	Guizhou	696
Shanxi	294	Shandong	338	Yunnan	730
Inner Mongolia	544	Henan	257	Tibet	1726
Liaoning	578	Hubei	652	Shaanxi	412
Jilin	442	Hunan	753	Gansu	919
Heilongjiang	776	Guangdong	1686	Qinghai	1117
Shanghai	687	Guangxi	1402	Ningxia	1615
Jiangsu	703	Hainan	1965	Xinjiang	1436
Zhejiang	755				

Third, I calculated the total irrigation water withdrawal of each province via Equation 4-3.

$$Irr_{i,j} = r_i \times AWW_{i,j} \quad \textbf{Equation 4-3}$$

where $Irr_{i,j}$ is the irrigation water withdrawal(m^3) of province *i* in year *j*. r_i is the ratio of irrigation water withdrawal of farmland to agricultural water withdrawal in province *i*. The r_i is colleted from different sources and shown in Table 4-3.

Table 4-3 The ratio of irrigation water withdrawal to agricultural water withdrawal of each province

Num	Province	Ratio	Source
1	Beijing	0.79	(Song et al. 2010)
2	Tianjin	0.99	Tianjin Water Resources Bulletin 2001
3	Hebei	0.96	Thematic Database for Human-Earth System available at http://www.data.ac.cn/
4	Shanxi	0.96	Thematic Database for Human-Earth System available at http://www.data.ac.cn/
5	Inner Mongolia	0.95	Thematic Database for Human-Earth System available at http://www.data.ac.cn/
6	Liaoning	0.98	Thematic Database for Human-Earth System available at http://www.data.ac.cn/
7	Jilin	0.95	Thematic Database for Human-Earth System available at http://www.data.ac.cn/
8	Heilongjiang	0.92	Thematic Database for Human-Earth System available at http://www.data.ac.cn/
9	Shanghai	0.92	(Wang et al. 2010)
10	Jiangsu	0.94	Thematic Database for Human-Earth System available at http://www.data.ac.cn/
11	Zhejiang	0.92	(Wang et al. 2010)
12	Anhui	0.95	Thematic Database for Human-Earth System available at http://www.data.ac.cn/
13	Fujian	0.92	(Wang et al. 2010)
14	Jiangxi	0.92	(Wang et al. 2010)
15	Shandong	0.95	Thematic Database for Human-Earth System available at http://www.data.ac.cn/
16	Henan	0.93	Thematic Database for Human-Earth System available at http://www.data.ac.cn/
17	Hubei	0.92	(Wang et al. 2010)
18	Hunan	0.97	Hunan Water Resources Bulletin 2007
19	Guangdong	0.83	China Water Resources (http://www.cws.net.cn/cwsnet/gazette/zhujiang/2004/4.html)

20	Guangxi	0.94	Guangxi Water Resources (http://www.gxwater.gov.cn/szbg.asp?blx=xnr&nd=1998&bt=%D3%C3%CB%AE%C1%BF)
21	Hainan	0.77	Hainan Water Resources Bulletin 2008
22	Chongqing	0.92	Chongqin Water Resources Bulletin 2001
23	Sichuan	0.96	(He and Lu 2007)
24	Guizhou	0.95	Guizhou Water Resources Bulletin 2001
25	Yunnan	0.97	Yunnan Water Resources Bulletin 2000
26	Tibet	0.61	(Wa 2009)
27	Shaanxi	0.92	Thematic Database for Human-Earth System available at http://www.data.ac.cn/
28	Gansu	0.95	Thematic Database for Human-Earth System available at http://www.data.ac.cn/
29	Qinghai	0.83	Qinghai Water Resources Bulletin 2007
30	Ningxia	0.92	Thematic Database for Human-Earth System available at http://www.data.ac.cn/
31	Xinjiang	0.77	Xinjiang Water Resources Bulletin 2001

Fourth, I calculated the irrigation water withdrawal per square kilometer (km^2) of irrigated dryland ($Irr\_dryland_{i,j}$, unit: m) and irrigated paddy filed ($Irr\_paddy_{i,j}$, unit: m) in a given province and a given year via Equation 4-4 and Equation 4-5.

$$Irr\_paddy_{i,j} = Irr_{i,j} \times \frac{NIR\_paddy_i}{NIR\_paddy_i \times S\_paddy_{i,j} + NIR\_dryland_i \times S\_dryland_{i,j}} \quad \textbf{Equation 4-4}$$

$$Irr\_dryland_{i,j} = Irr_{i,j} \times \frac{NIR\_dryland_i}{NIR\_paddy_i \times S\_paddy_{i,j} + NIR\_dryland_i \times S\_dryland_{i,j}} \quad \textbf{Equation 4-5}$$

where $S\_Paddy_{i,j}$ and $S\_Dryland_{i,j}$ are the area (km^2) of irrigated paddy field and irrigated dryland of province *i* in year *j*, respectively. Since it is impossible to obtain the time series values of $S\_Paddy_{i,j}$ and $S\_Dryland_{i,j}$, the values of $S\_Paddy_{i,j}$ and $S\_Dryland_{i,j}$ in 2000 are used in each year. The values of $S\_Paddy_{i,j}$ and

$S\_Dryland_{i,j}$ in 2000 can be derived from the irrigation map of China for 2000. $NIR\_paddy_{i,j}$ and $NIR\_dryland_{i,j}$ are the estimated net irrigation requirements (mm) of paddy filed and dryland in province *i*, which are derived by referencing to (Liu et al. 2009) and shown in Table 4-4. Liu et al. (2009) divided China into 216 subregions based on differences in climate conditions and water sources, chose a typical meteorological station for each subregion, and collected the daily meteorological observations including precipitation, mean air temperature, maximum air temperature, minimum air temperature, wind speed, relative humidity, and sunshine hours from 1970 to 2000. They then calculated the net irrigation requirement by subtracting effective precipitation from the irrigation requirement during crop growing season in each subregion. The crop irrigation requirement was calculated using the Penman-Monteith method. They reported the average net irrigation requirements (NIR) of the main crops (including corn, wheat, rice etc.) in different areas of China during 1970–2000. Because wheat and corn are planted in dryland and rice is planted is paddy field, in this study, I summed up the NIR of wheat (spring wheat, winter wheat) and corn (spring corn, summer corn) estimated by Liu et al. (2009) to get the NIR of dryland (NIR_dryland), and summed up the NIR of rice (including early rice, middle rice and late rice) estimated by Liu et al. (2009) to get the NIR of paddy field for each province.

Table 4-4 Mean net irrigation requirements for dryland and paddy field in different provinces of China from 1970-2000

Province	$NIR\_dryland_i$	$NIR\_paddy\ field_i$	Province	$NIR\_dryland_i$	$NIR\_paddy\ field_i$
Beijing	375	475	Hubei	100	460
Tianjin	375	475	Hunan	100	460
Hebei	375	475	Guangdong	100	460

Shanxi	730	550	Guangxi	100	460
Inner Mongolia	755	675	Hainan	100	460
Liaoning	115	265	Chongqing	225	150
Jilin	115	265	Sichuan	285	150
Heilongjiang	115	265	Guizhou	190	300
Shanghai	100	285	Yunnan	190	300
Jiangsu	250	285	Tibet	350	-
Zhejiang	100	750	Shaanxi	445	550
Anhui	250	750	Gansu	730	550
Fujian	100	630	Qinghai	350	-
Jiangxi	100	460	Ningxia	755	675
Shandong	375	475	Xinjiang	785	750
Henan	375	475			

Finally, the irrigation water withdrawal of each irrigated pixel can be calculated via the following equation.

$$Irr_{k,j} = [Irr\_paddy_{i,j} \times Perc\_paddy_{k,j} + Irr\_dryland_{i,j} \times Perc\_Dryland_{k,j}] \times 10^6 \quad \text{Equation 4- 6}$$

$Prec\_Paddy_{k,j}$ and $Perc\_Dryland_{k,j}$ are the irrigation percentages of the paddy fields and dryland at pixel *k* in year *j*. The pixel size is 1 km^2. Again, because it is impossible to obtain the time series values of $Prec\_Paddy_{k,j}$ and $Perc\_Dryland_{k,j}$ the values of $Prec\_Paddy_{k,j}$ and $Perc\_Dryland_{k,j}$ in 2000 derived from the irrigation map of China for 2000 are used in each year. $Irr_{k,j}$ is the total irrigation withdrawal(m^3) at pixel *k* in year *j*.

4.1.5 Irrigation water withdrawals in the future

To estimate the irrigation water withdrawals in the future, I first estimated the ratio of the net irrigation requirement (IR) in the past to the net IR in the future, and then multiplied the ratio by mean irrigation water withdrawal in the past estimated in section 4.1.4.

The net irrigation requirement per unit during the growing season was computed as the difference between crop-specific potential evapotranspiration (PET) and effective precipitation (P_{eff}) (FAO 1992). PET is calculated using the Hargreaves and Samani function (Hargreaves and Samani 1982).

$$PET = 0.0135 \times (T + 17.8) \times RSDS / \lambda \quad \text{Equation 4-7}$$

$$NIR = Kc \times PET - P_{eff} \quad \text{if } Kc \times PET > P_{eff} \quad \text{Equation 4- 8}$$

$$NIR = 0 \quad \text{otherwise} \quad \text{Equation 4- 9}$$

$$P_{eff} = P_r(4.17 - 0.2P_r) / 4.17 \quad \text{For } P_r < 8.3 \text{ mm/d} \quad \text{Equation 4- 10}$$

$$P_{eff} = 4.17 + 0.1P_r \quad \text{For } P_r \geq 8.3 \text{ mm/d} \quad \text{Equation 4- 11}$$

Where PET is potential evapotranspiration (mm/d), T is air temperature (ºC) , λ is latent heat of vaporization (2.45 MJ/kg), RSDS is downwelling shortwave radiation (MJ/[m2•d]), P_r is the daily total precipitation (mm/d), P_{eff} is the fraction of P_r available to the crop and called effective precipitation (mm/d), and *Kc* is crop coefficient (dimensionless), which is a function of the crop type and the day of the growing season (Table 4-5). Three main crops (wheat, corn, and rice) were selected for estimating NIRs in China. Paddy rice includes early, middle, and late rice, grown mainly in the Yangtze River Valley, southern China, and on the Yunnan-Guizhou Plateau;wheat includes spring and winter wheat, planted mainly on the North China Plain; and corn includes spring and summer corn, planted mainly in the northeastern, northern, and southwestern provinces. According to the China Statistical Yearbook 2009, the total sown area was 156.3 million ha, and the sown area of grain crops was 106.8 million ha in 2008. The sown areas of rice, wheat, and corn took up 77.5% of the sown area of grain crops. Rice, wheat, and corn outputs accounted for 36.2%, 21.3%, and 31.4% of the total output of grain (528.7 million tons), respectively. The cropping systems, planting dates, and harvest dates for each of these crops in each

province have been reported online by the Chinese government since 2000 (http://www.zzys.gov.cn/; accessed September 12, 2011). The planting and harvest dates of each crop during the past decade are quite stable. The average planting dates and harvest dates of rice, wheat, and corn from 2000 to 2008 were calculated for each province and are shown in Table 4-6.

Table 4-5 Length of crop stages as a fraction of the whole growing period for initial (*L_ini*), crop development (*L_dev*), mid-season (*L_mid*), and late season (*L_late*) and crop coefficients for initial period (*kc_ini*), mid-season (*kc_mid*) and end of season (*kc_end*) (Siebert and Döll 2008)

crop	Length of crop development stage				Crop coefficients		
	L_ini	*L_dev*	*L_mid*	*L_late*	K_c*_ini*	K_c*_mid*	K_c*_ini*
wheat	0.15	0.25	0.40	0.20	0.40	1.15	0.30
Crop	0.17	0.28	0.33	0.22	0.30	1.20	0.40
Rice	0.17	0.18	0.44	0.21	1.05	1.20	0.75

Table 4-6 The growing season of main crops in each province of China

	Growing season				
Area	Wheat	Corn	Early rice	Middle rice	Late rice
Beijing	Sep 21-next Jun 10	Jun 11 - Sep 10		Apr 11 - Sep 10	
Tianjin	Sep 21-next Jun 11	Jun 11 - Sep 10		Apr 11 - Sep 10	
Hebei	Sep 21-next Jun 12	Jun 11 - Sep 10		Apr 11 - Sep 10	
Shanxi	Sep 21 - next Jun 10	Apr 21 - Aug 20			
Inner Mongolia		Mar 21 - Aug 31			
Liaoning		Apr 11 - Sep 10		Apr 11 - Sep 10	
Jilin		Apr 11 - Sep 11		Apr 11 - Sep 10	
Heilongjiang		Apr 11 - Sep 12		Apr 11 - Sep 10	
Shanghai				Apr 21 - Sep 20	
Jiangsu	Oct 1 - next May 10			Apr 11 - Sep 20	
Zhejiang			Mar 21 - Jul 10	May 21 - Sep 30	Jun 11 - Oct 10
Anhui	Oct 21 - next May 10		Apr 1- Jul 10	Apr 11 - Aug 31	Jun 11 - Oct 10
Fujian			Mar 1 - Jul 10	Apr 11 - Sep 10	Jun 11 - Oct 20

Jiangxi		Feb 21 - Jun 20	Mar 21 - Jul 10		Jun 11 - Oct 10
Shandong	Oct 1 - next May 10	Jun 11 - Sep 10		Apr 21 - Sep 10	
Henan	Oct 1 - next May 10	Jun 1 - Aug 31		Apr 11 - Sep 10	
Hubei		Mar 21 - Jul 10		Apr 11 - Aug 31	
Hunan		Feb 21 - Jun 20	Mar 21 - Jul 10		Jun 1 - Sep 30
Guangdong			Feb 11 - Jul 10		Jul 1 -Oct 20
Guangxi			Mar 1 - Jul 10		Jun 21 - Oct 20
Hainan			Jan 1 - May 20		Jun 11 - Oct 10
Chongqing	Oct 21 - next Apr 10			Mar 11 - Aug 21	
Sichuan	Oct 21 - next Apr 20	May 21 - Aug 10		Mar 11 - Aug 20	
Guizhou					
Yunnan		May 1 - Aug 10		Mar 21 - Aug 31	
Tibet	Oct 11 - next Jul 10				
Shaanxi	Sep 11 - next May 20	Jun 1 - Sep 10		Apr 1 - Sep 10	
Gansu	Sep 11 - next Jun 10	Apr 21 - Aug 10			
Qinghai	Mar 21 - next Aug 10				
Ningxia		Apr 1 - Aug 20		Apr 11 - Sep 10	
Xinjiang	Sep 21 - next Jun 10	Jun 11 - Sep 10			

The NIR in the past was calculated during 1961-2000, and NIR in the future was calculated during two future time periods: 2046-2065 and 2081-2100. Daily precipitation (Pr), downwelling shortwave radiation (RSDS), and mean temperature (T) during 1961-2000 are from the Climate of the 20th Century (20C3m) Experiment of IPCC 4. The Pr, RSDS, and T during 2 future time periods (2046-2065 and 2081-2100) are from 3 IPCC 4 scenarios (B1, A1B, and A2). Scenario A1 assumes that economic growth occurs rapidly in the future with the introduction of new and more efficient technologies and that the global population will peak in the middle of the

21st century. A1 is divided into 3 groups (A1FI, A1T, and A1B) based on the alternative directions of technological change. A1FI refers to fossil intensive, A1T refers to non-fossil energy resources, and A1B is a balance of all sources. Scenario B1 assumes a convergent world. Similar to A1, it assumes that the global population will peak in the middle of the 21st century but that the economic structure changes rapidly to a service and information economy. Scenario A2 describes a very heterogeneous world. Under this scenario, population growth is high, and economic development and technological change are slow (Pachauri and Reisinger 2007). All data were downloaded from the WCRP CMIP3 multi-model database (https://esg.llnl.gov:8443/home/publicHomePage.do). A total of 24 models are included in IPCC 4. This study uses the results from 8 of those models (Table 4-7). All 8 models provide daily data over the same time periods and are interpolated to 0.5º latitude/longitude because the data from different models have different spatial resolutions.

Table 4-7 Climate change models used in this study

Num	Model name	Short name	Country	Resolution (degree)
1	cccma_cgcm3_1	CGMR	Canada	3.75×3.71
2	cnrm_cm3	CNCM3	France	2.81×2.79
3	csiro_mk3_0	CSMK30	Australia	1.88×1.87
4	csiro_mk3_5	CSMK35	Australia	1.88×1.87
5	gfdl_cm2_0	GFCM20	USA	2.50×2.00
6	gfdl_cm2_1	GFCM21	USA	2.50×2.00
7	miroc3_2_medres	MIMR	Japan	2.81×2.79
8	mri_cgcm2_3_2a	MRCGCM	Japan	2.81×2.79

4.1.6 Irrigation modeling

I used the irrigation map, described above, to prescribe the locations and used the irrigation water withdrawal maps to decide annual amounts of irrigation in the model. I assumed that irrigation occurs during April to September and from 6:00 am to 6:00 pm. Then, when April began, the irrigation crop column is irrigated at the following rate:

$$R_i = \frac{W_{ann,i}}{183 \times 12 \times 60} \times T_s \qquad \textbf{Equation 4-12}$$

Where R*i* is the irrigation rate over the crop soil column in grid cell *i* (mm/s), $W_{ann,i}$ is the annual irrigation amount in grid cell *i* from irrigation water data set (mm/year), Ts is the simulated time step in CLM (3 hours in default configuration of CLM). The total days from April to September are 183; the total irrigation hours in each day are 12; and there are 60 total minutes in each hour. Irrigation only happened over irrigated crop soil column. This means I didn't irrigate a grid cell without crop or a grid with crop but without irrigation. Irrigation water was used by two different ways: one applied water above a canopy to simulate spray irrigation (IRRc), and another one applied water directly on the ground to simulate flood irrigation (IRRg).

4.1.7 Future forcing data

Forcing data in offline CLM requires incident solar, precipitation, surface pressure, temperature, wind speed, and specific humidity. Among 8 models used in estimating irrigation water requirement in the future, cnrm_cm_3 has the most 3-hourly atmosphere data including incident solar, precipitation, surface pressure and temperature. Thus, the atmosphere data from cnrm_cm_3 is finally used in this study. However, cnrm_cm_3 just has daily data for wind speed and specific humidity.

Therefore, the time resolution of the wind speed and specific humidity are daily rather than 3-hourly in my future forcing data. All data mentioned above covers two years: 2050 and 2100.

The aerosol deposition is also required for offline CLM. They include hydrophilic BC wet deposition, hydrophilic BC dry deposition, hydrophobic BC dry deposition, DSTX01 dry deposition flux at bottom, DSTX01 wet deposition flux at bottom, DSTX02 dry deposition flux at bottom, DSTX02 wet deposition flux at bottom, DSTX03 dry deposition flux at bottom, DSTX03 wet deposition flux at bottom, DSTX04 dry deposition flux at bottom, DSTX04 wet deposition flux at bottom, hydrophilic OC wet deposition, hydrophilic OC dry deposition, and hydrophobic OC dry deposition. In this study, the aerosol depositions in 2050 and 2100 were extracted from Representative Concentration Pathway (RCP4.5), which can be accessed from the public subversion input data repository at http://www.cesm.ucar.edu/models/cesm1.0/.

In terms of the IPCC4.0 report (available at http://www.ipcc.ch/ipccreports/tar/wg1/531.htm), the CO2 abundances of ISAM model under Scenario B1, A1B and A2 were defined as 488 ppm, 532 ppm, and 532 ppm in 2050, and 549 ppm, 717 ppm and 856 ppm in 2100, respectively. The CO2 abundances of Bern-CC model under Scenario B1, A1B and A2 were defined as 482 ppm, 522 ppm, and 522 ppm in 2050, and 540 ppm, 703 ppm, and 863 ppm, respectively. In this study, referring to CO2 abundances of ISAM model and Bern-CC model, the CO2 abundances under Scenario B1, A1B and A2 were defined as

485ppm, 527ppm, and 527ppm in 2050, and 544.5, 846, and 710 ppm in 2100, respectively.

4.1.8 Experiments

28 experiments were conducted in this study to evaluate the irrigation impact. Those experiments can be divided into two groups in terms of the different aims of the experiments. The experiments in the first group try to answer the following questions: 1) what are the irrigation impacts over China in the past? 2) Do different irrigation patterns (spay irrigation and flood irrigation) have different impacts? 3) Is the impact of irrigation is comparable to that of LCLUC on near surface climate over China in the past? The experiments in the second group try to explore the irrigation impacts over China in the future. Meanwhile, group two tries to explore the LCLUC impact in the future by assuming that the LCLUC occurred during 1980 to 2000 will happen again in the future, and then compare the irrigation impact and LCLUC impact to see if their relationship will be comparable or incomparable in the future. Overall, the experiments in the first group focus on contemporary simulations, while the experiments in the second group focus on the future simulations. The land cover status, forcing data and irrigation information about those experiments can be found in Table 4-8. Their specific details are explained below.

The first group (Group I) includes four experiments: LCLUC_1980, LCLUC_2000, IRRc_2000 and IRRg_2000. LCLUC_1980 and LCLUC_2000 were used as control tests, while IRRc_2000 and IRRg_2000 were performed to investigate irrigation impact on local climate over China. The comparisons between LCLUC_1980 and LCLUC_2000 (named as Dif_LCLUC thereafter) are used to

analyze the land cover land use change (LCLUC) impact on local climate over China in the past. The comparisons between IRRc_2000 and IRRg_2000 are used to analyze the differences of irrigation impact caused by different irrigation patterns. The comparisons between LCLUC_2000 and IRRc_2000/ IRRg_2000 are used to analyze the irrigation impact on local climate over China in the past.

The Second group (Group II) includes 6 subgroups and each subgroup has 4 experiments. The 4 experiments in each subgroup are quite similar, but for different future times (2050 or 2100) and for different scenarios (A1B, A2 or B1). Thus, I take the experiments in first subgroup (Group II-1) as examples to explain my experiment design. In Group II-1, there are four experiments: two irrigation simulations (IRRc_B1_2050 and IRRg_B1_2050), and two LCLUC simulations (LCLUC1980_B1_2050 and LCLUC2000_B1_2050). The comparisons between LCLUC1980_B1_2050 and LCLUC2000_B1_2050 are used to analyze LCLUC impact on local climate over China around 2050 under scenario B1. The comparisons between IRRc_B1_2050 and IRRg_B1_2050 are used to analyze the difference of irrigation impact caused by different irrigation patterns around 2050 under scenario B1. The comparisons between LCLUC2000_B1_2050 and IRRc_B1_2050/ IRRg_B1_2050 are used to analyze the irrigation impact on local climate over China around 2050 under scenario B1.

Table 4-8 Experiments designed for this study

Group	Experiment	Spin-up Land surface status	Irrigation simulation	Climate forcing
I	LCLUC_1980	1980	No	Qian
	LCLUC_2000	2000	No	Qian
	IRRc_2000	2000	Spray irrigation	Qian
	IRRg_2000	2000	Flood irrigation	Qian
II-1	LCLUC1980_ B1_2050	1980	No	Scenario B1 2050
	LCLUC2000_ B1_2050	2000	No	Scenario B1 2050
	IRRc_B1_2050	2000	Spray irrigation	Scenario B1 2050
	IRRg_B1_2050	2000	Flood irrigation	Scenario B1 2050
II-2	LCLUC1980_A1B_2050	1980	No	Scenario A1B 2050
	LCLUC2000_A1B_2050	2000	No	Scenario A1B 2050
	IRRc_A1B_2050	2000	Spray irrigation	Scenario A1B 2050
	IRRg_ A1B_2050	2000	Flood irrigation	Scenario A1B 2050
II-3	LCLUC1980_A2_2050	1980	No	Scenario A2 2050
	LCLUC2000_A2_2050	2000	No	Scenario A2 2050
	IRRc_A2_2050	2000	Spray irrigation	Scenario A2 2050
	IRRg_ A2_2050	2000	Flood irrigation	Scenario A2 2050
II-4	LCLUC1980_ B1_2100	1980	No	Scenario B1 2100
	LCLUC2000_ B1_2100	2000	No	Scenario B1 2100
	IRRc_B1_2100	2000	Spray irrigation	Scenario B1 2100
	IRRg_B1_2100	2000	Flood irrigation	Scenario B1 2100
II-5	LCLUC1980_A1B_2100	1980	No	Scenario A1B 2100
	LCLUC2000_A1B_2100	2000	No	Scenario A1B 2100
	IRRc_A1B_2100	2000	Spray irrigation	Scenario A1B 2100
	IRRg_ A1B_2100	2000	Flood irrigation	Scenario A1B 2100
II-6	LCLUC1980_A2_2100	1980	No	Scenario A2 2100
	LCLUC2000_A2_2100	2000	No	Scenario A2 2100
	IRRc_A2_2100	2000	Spray irrigation	Scenario A2 2100
	IRRg_ A2_2100	2000	Flood irrigation	Scenario A2 2100

All of the experiments run the CLM at approximately 0.5° resolution (0.47° × 0.63°) and in offline mode but with different forcing data. In the first group, all

experiments were run with the standard forcing provided by the model from 1978 to 2004. The standard forcing is a 57-year (1948–2004) dataset produced by Qian et al. (2006) and has a 3-hourly temporal resolution. The other experiments from the second seventh groups were run with the future forcing data mentioned above in subsection 4.1.7. Before carrying out the experiments, the initial conditions for each experiment were taken from a 285-year spin-up with CLM Carbon-Nitrogen Model to ensure a near-equilibrium initial state. Except the LCLUC_1980 in which initial data were derived by spinning up the CLM Carbon-Nitrogen Model with land surface data from 1980, all other experiments' initial data were derived by spinning up the CLM Carbon-Nitrogen Model with land surface data from 2000.

4.2 Results and discussions

4.2.1 Irrigation water

In this study, I developed a time series gridded datasets of annual irrigation water withdrawal in China from 1978 to 2008. Figure 4-2shows the mean irrigation water withdrawal during 1978 to 2008. Table 4-9, Table 4-10 and Table 4-11 show the provincial AWW during 1978 to 2008. In irrigation simulations IRRc_2000 and IRRg_2000, the gridded datasets of annual irrigation water withdrawal in China just from 1978 to 2004 were used because the standard forcing of CLM produced by Qian et al. (2006) is ended in 2004. Table 4-12 reports the irrigation amounts used to force irrigation simulations.

Table 4-9 Agricultural water withdrawal during 1978 to 1987

Provinces	Agricultural water withdrawal ($10^8 m^3$)									
	1978	1979	1980	1981	1982	1983	1984	1985	1986	1987
Beijing	27.7	28.3	26.2	26.0	25.5	26.2	26.0	25.3	25.1	25.2
Tianjin	16.9	17.8	16.4	16.2	15.8	15.6	15.4	14.7	14.2	14.3
Hebei	159.0	163.3	149.7	144.9	143.6	146.1	145.8	143.2	141.9	144.1
Shanxi	41.6	43.8	40.5	39.7	38.9	39.5	39.4	38.0	36.9	37.8
Inner Mongolia	46.7	85.4	74.1	68.8	67.2	67.7	64.8	62.8	65.2	67.4
Liaoning	84.3	61.7	54.2	50.6	50.3	47.7	48.8	50.1	50.3	53.0
Jilin	50.3	33.5	39.9	40.1	39.0	38.6	38.2	36.8	37.8	39.7
Heilongjiang	64.9	62.3	64.2	66.1	62.9	60.3	58.7	63.1	66.6	71.0
Shanghai	31.6	31.9	29.6	29.1	28.7	29.0	28.5	27.5	26.8	26.8
Jiangsu	295.4	314.5	296.1	296.2	294.2	299.7	307.0	301.8	296.4	295.1
Zhejiang	147.3	152.4	142.1	140.2	138.7	140.4	140.2	138.1	134.7	134.8
Anhui	112.8	121.4	109.2	105.9	101.1	98.6	95.2	91.5	90.5	93.4
Fujian	121.8	127.1	118.4	111.0	106.5	108.8	106.3	102.6	118.6	119.8
Jiangxi	154.0	159.2	149.2	147.5	138.5	159.4	159.3	157.0	156.5	157.4
Shandong	193.4	197.7	183.8	182.7	182.4	187.0	186.9	184.7	183.1	180.7
Henan	124.0	124.1	112.1	106.1	101.0	100.6	102.3	98.1	98.4	99.7
Hubei	199.0	203.8	188.7	188.5	186.2	185.4	182.9	178.9	175.0	172.0
Hunan	250.5	244.8	224.5	221.6	215.0	254.7	253.8	249.3	248.7	239.5
Guangdong	467.6	481.6	438.5	426.5	415.7	420.3	405.4	391.1	384.4	373.2
Guangxi	267.3	272.1	247.9	241.6	237.3	240.0	235.5	226.2	225.6	229.9
Hainan	-	-	-	-	-	-	-	-	-	-
Chongqing	-	-	-	-	-	-	-	-	-	-
Sichuan	167.8	176.0	166.4	165.1	163.4	166.1	160.9	148.5	145.1	146.1
Guizhou	44.9	43.4	39.2	38.2	36.7	38.4	35.1	39.9	44.1	44.7
Yunnan	85.3	88.2	82.3	81.8	81.2	85.3	85.2	84.3	84.1	84.8
Tibet	35.2	35.0	31.6	30.7	28.6	25.5	23.4	27.5	25.0	26.7
Shaanxi	64.8	67.7	63.5	62.8	61.9	62.3	59.0	58.1	61.1	61.9
Gansu	101.6	103.3	96.8	95.1	93.7	94.8	94.6	91.4	90.4	91.5
Qinghai	22.2	22.8	22.0	21.7	21.3	21.4	21.5	21.4	21.8	22.0
Ningxia	48.7	50.2	46.3	44.9	45.2	46.0	46.2	46.1	47.3	48.8
Xinjiang	485.2	497.1	462.6	461.9	451.4	461.6	460.8	447.6	463.4	469.7

Table 4-10 Agricultural water withdrawal during 1988 to 1997

Provinces	Agricultural water withdrawal ($10^8 m^3$)									
	1988	1989	1990	1991	1992	1993	1994	1995	1996	1997
Beijing	25.3	25.3	24.9	23.1	22.6	23.3	22.9	23.9	23.8	23.3
Tianjin	14.4	14.4	14.4	13.8	13.8	14.4	14.5	14.7	14.5	14.4
Hebei	145.4	147.8	149.4	146.0	148.1	155.9	157.6	160.4	167.7	168.5
Shanxi	38.6	39.3	39.5	38.4	38.9	40.9	41.4	41.9	41.8	36.2
Inner Mongolia	70.2	75.2	80.8	99.4	104.6	112.8	113.3	114.5	118.6	124.8
Liaoning	52.7	52.6	72.7	71.4	74.7	80.0	81.2	82.4	83.6	85.9
Jilin	40.9	44.3	46.3	46.3	45.8	47.5	47.7	47.4	48.7	55.4
Heilongjiang	68.6	72.3	99.3	98.3	101.7	106.8	93.5	100.6	122.1	145.1
Shanghai	26.6	26.4	26.1	24.8	24.5	24.3	23.7	23.4	23.1	22.5
Jiangsu	293.9	297.5	331.3	306.9	307.3	318.1	317.1	319.3	317.9	313.9
Zhejiang	133.9	134.0	132.4	126.4	125.2	129.4	128.0	126.2	125.7	123.4
Anhui	96.1	100.2	113.5	111.9	113.9	121.1	124.0	126.2	127.1	128.8
Fujian	120.3	118.0	120.7	116.0	116.5	121.8	121.4	120.8	120.0	118.3
Jiangxi	157.3	158.4	157.8	151.7	152.2	159.7	156.2	161.3	161.1	160.1
Shandong	174.7	176.4	179.1	174.5	176.1	185.0	186.3	186.8	186.9	186.3
Henan	103.2	105.8	108.3	107.1	110.1	117.7	119.9	123.2	126.9	129.6
Hubei	169.4	171.7	179.9	174.9	174.1	175.9	173.2	168.0	183.2	163.2
Hunan	240.1	241.3	239.2	228.8	228.8	238.5	239.5	239.2	236.6	234.6
Guangdong	338.9	342.2	341.2	413.5	406.7	299.2	293.2	297.4	295.8	297.4
Guangxi	224.2	223.5	248.0	240.5	240.5	248.3	247.7	244.6	242.9	242.9
Hainan	31.5	32.8	33.3	52.0	52.4	40.7	40.4	41.9	40.5	51.9
Chongqing	-	-	-	-	-	-	-	-	-	18.8
Sichuan	147.3	148.8	148.5	142.9	143.7	150.9	152.1	153.2	153.7	131.3
Guizhou	45.3	45.8	45.5	44.8	46.2	49.2	50.1	50.5	50.7	51.1
Yunnan	86.3	89.2	91.3	89.6	91.4	97.6	102.3	108.2	110.4	112.2
Tibet	24.9	25.0	25.9	26.5	26.9	28.8	39.3	33.1	30.0	31.4
Shaanxi	61.1	61.3	61.8	59.9	60.9	64.3	64.8	65.4	62.5	62.0
Gansu	92.2	92.7	93.2	96.3	98.7	97.8	99.7	97.2	101.7	102.1
Qinghai	21.8	22.4	22.7	28.5	29.4	23.3	23.3	23.4	23.2	26.6
Ningxia	49.3	49.9	49.9	58.7	60.2	52.6	52.9	53.2	53.5	71.4
Xinjiang	474.6	469.2	487.1	462.4	463.1	477.6	477.0	473.2	480.7	486.3

Table 4-11 Agricultural water withdrawal during 1998 to 2008

Provinces	Agricultural water withdrawal ($10^8 m^3$)										
	1998	1999	2000	2001	2002	2003	2004	2005	2006	2007	2008
Beijing	22.3	22.6	22.1	21.9	15.5	12.9	13.0	12.7	12.0	11.7	11.4
Tianjin	13.6	13.5	13.4	13.5	10.7	11.2	12.0	13.6	13.4	13.8	13.0
Hebei	162.2	166.8	162.1	162.9	161.4	149.6	147.1	150.2	152.6	151.6	143.2
Shanxi	34.7	36.0	35.1	35.2	35.5	33.3	32.9	32.7	34.2	34.3	32.9
Inner Mongolia	124.1	137.0	139.2	145.8	158.8	146.1	149.4	143.9	142.2	141.8	134.1
Liaoning	85.1	89.9	89.9	92.9	83.2	83.5	85.7	87.2	91.5	91.7	90.9
Jilin	61.0	64.0	62.7	66.2	83.6	67.5	66.4	66.4	70.4	67.5	69.3
Heilongjiang	155.4	170.8	170.2	175.8	174.8	171.4	186.3	192.1	208.3	214.8	218.2
Shanghai	21.0	21.2	21.2	20.9	12.0	16.3	18.8	18.5	18.4	16.2	16.7
Jiangsu	299.0	306.0	296.0	297.2	289.2	223.1	288.5	263.8	270.7	268.5	287.3
Zhejiang	115.4	118.5	114.3	114.6	118.1	110.2	107.3	106.7	101.1	100.2	98.7
Anhui	124.2	128.2	125.3	127.0	127.9	93.8	121.7	113.6	136.4	120.6	151.9
Fujian	112.1	113.7	110.5	111.3	111.5	101.0	104.2	101.5	98.0	100.9	99.3
Jiangxi	151.5	154.2	148.7	148.9	136.8	104.1	128.5	134.6	132.9	151.4	148.9
Shandong	178.3	181.9	176.0	177.2	188.3	157.0	154.3	156.3	169.4	159.7	157.6
Henan	128.0	133.8	131.1	132.8	145.7	113.3	124.5	114.5	140.2	120.1	133.5
Hubei	155.5	155.6	145.8	143.3	136.1	136.2	131.7	142.1	143.0	132.6	142.8
Hunan	222.2	216.4	217.6	218.5	205.9	209.4	202.3	201.3	198.4	193.9	193.2
Guangdong	279.4	285.9	269.0	264.5	250.4	242.6	240.3	230.7	226.9	224.8	227.7
Guangxi	227.1	232.1	227.2	230.9	225.9	205.4	210.1	225.4	222.3	208.4	202.9
Hainan	38.3	37.8	38.1	38.5	35.8	35.7	37.9	35.1	36.7	35.8	35.6
Chongqing	21.5	22.0	21.4	21.7	20.7	20.7	20.3	21.4	18.1	18.7	18.9
Sichuan	126.3	130.3	127.6	131.5	122.3	121.7	121.2	121.8	121.2	118.7	113.6
Guizhou	49.0	50.2	49.1	49.8	51.3	52.2	51.9	50.5	54.3	48.7	51.6
Yunnan	108.7	112.3	110.6	112.7	110.7	109.6	109.7	108.4	105.6	105.9	105.1
Tibet	28.6	29.2	29.2	28.9	27.3	22.6	25.7	30.3	31.8	33.4	33.9
Shaanxi	59.2	60.4	58.2	58.7	54.6	50.7	49.7	52.2	56.8	55.5	57.7
Gansu	97.7	100.1	97.3	97.9	97.3	96.4	96.7	95.0	94.3	96.1	96.9
Qinghai	23.1	23.7	25.5	25.2	20.4	21.7	21.8	21.1	21.8	20.5	22.4
Ningxia	69.0	62.2	69.5	71.0	76.0	58.4	68.6	72.3	71.7	64.8	68.0
Xinjiang	472.7	493.0	479.6	488.5	448.9	454.9	457.0	464.4	470.0	476.8	486.2

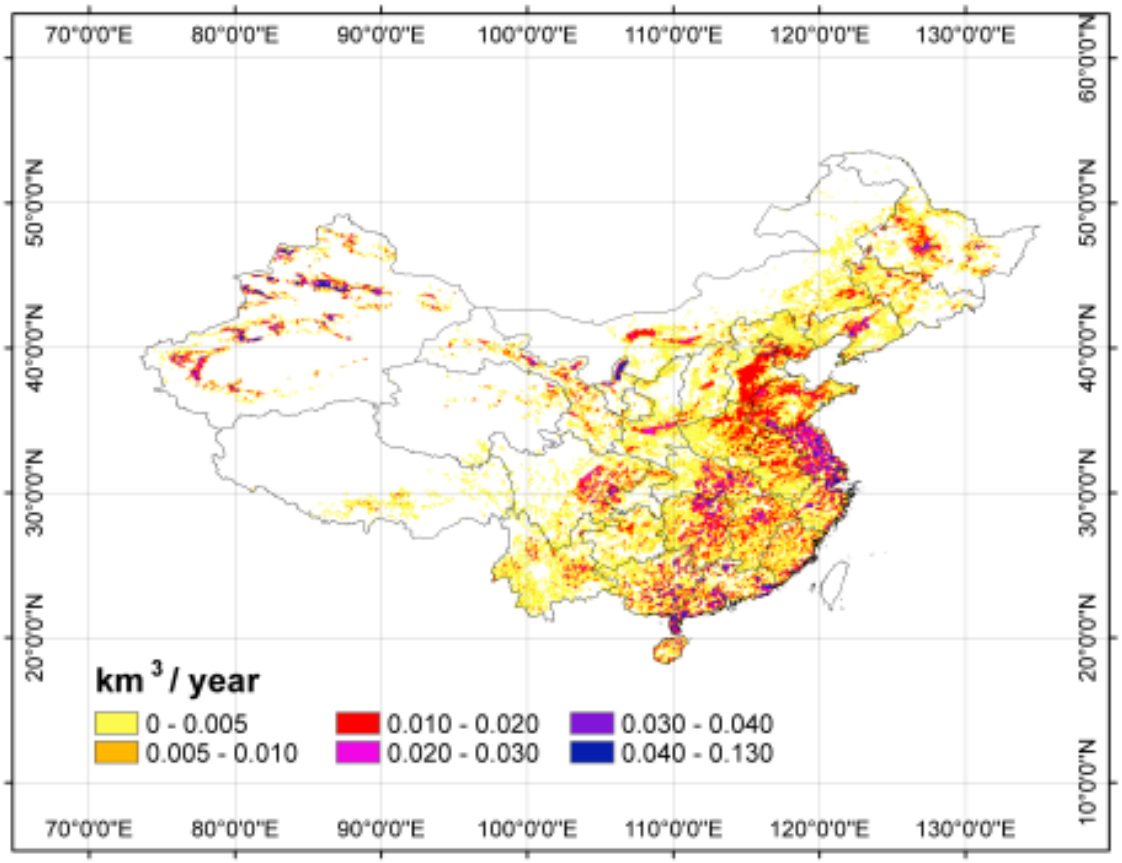

Figure 4-2 The mean irrigation water withdrawal during 1978 to 2008

Table 4-12 The irrigation amounts used to force irrigation simulations

Year	IR(10^8m^3)	Year	IR (10^8m^3)	Year	IR(10^8m^3)
1978	3534.414	1989	3256.633	2000	3431.709
1979	3621.295	1990	3405.354	2001	3470.791
1980	3356.866	1991	3409.821	2002	3397.083
1981	3299.365	1992	3432.798	2003	3114.134
1982	3228.649	1993	3448.936	2004	3255.368
1983	3317.202	1994	3447.990	2050_A1B	3676.661
1984	3282.436	1995	3465.269	2050_A2	3616.330
1985	3206.524	1996	3516.774	2050_B1	3594.180
1986	3216.582	1997	3552.316	2100_A1B	3788.030
1987	3226.833	1998	3415.680	2100_A2	3911.737
1988	3223.760	1999	3508.179	2100_B1	3628.531

4.2.2 Irrigation impact in the past

The differences of 2-m air daily mean temperature (Tmean), 2-m air daily minimum temperature (Tmin), 2-m air daily maximum temperature (Tmax), ground temperature(TG), specific humidity (Q2M), relative humidity (RH2M), wind speed (WS), sensible heat flux (FSH), latent heat flux (FLH) and ground heat flux (FGR) between two irrigation simulations by the CLM are statistically significant in terms of this study (Table 4-13). However, the differences between two irrigation simulations and control tests are quite similar. Therefore, just the simulation results of spray irrigation are reported in the following texts in order to avoid redundancy and repetition. The simulation results of flood irrigation simulation can be found in Table 4-13 and Table 4-14.

Nationally, spray irrigation simulated by the CLM led to an increase in annual FLH of7.074 W/m^2, and a decrease in annual FSH of 4.760 W/m^2. When only considering the irrigated grids, the decrease in FLH is around 1.5 times as much as the decrease in FLH averaged over the whole of China. The greater FLH decrease in North China led to the bigger temperature changes in North China as compared to South China. Irrigation has especially, impacted more impact in North China Plain, Xinjiang Province, Hetao of Yellow River, Hexi Corridor, Weihe Basin of Shaanxi Province, and Fenhe Basin of Shanxi Province (Figure 4-3 and Figure 4-4).

Table 4-13 Annual mean differences between different simulations, averaged over the whole of China, only irrigated area in China (IA), irrigated area in North China (IA_North), and irrigated area in South China (IA_South)

		Tmean(k)	Tmin(k)	Tmax(k)	TG(k)	Q2M(g/kg)	RH2M(%)	WS(m/s)	FSH(W/m^2)	FLH(W/m^2)	FGR(W/m^2)
China	Dif_LCLUC	0.086***	0.110***	0.071***	0.158***	-0.027***	-0.646***	-0.017***	3.096***	-1.916***	-0.699***
	IRRc_IRRg	-0.019***	-0.012***	0.001***	-0.022***	0.031***	0.305***	-0.009***	-0.672***	1.034***	0.005***
	IRRc_NIRR	-0.045***	0.022***	-0.079***	-0.232***	0.102***	0.822***	-0.017***	-4.760***	7.074***	-0.078***
	IRRg_NIRR	-0.026***	0.034***	-0.080***	-0.210***	0.070***	0.517***	-0.008***	-4.088***	6.041***	-0.082***
IA	Dif_LCLUC	0.119***	0.152***	0.104***	0.227***	-0.039***	-0.928***	-0.023***	4.363***	-2.868***	-0.925***
	IRRc_IRRg	-0.028***	-0.018***	0.001***	-0.033***	0.047***	0.453***	-0.013***	-0.999***	1.536***	0.007***
	IRRc_NIRR	-0.066***	0.032***	-0.117***	-0.344***	0.151***	1.222***	-0.025***	-7.073***	10.512***	-0.115***
	IRRg_NIRR	-0.038***	0.051***	-0.119***	-0.312***	0.104***	0.768***	-0.012***	-6.074***	8.976***	-0.122***
IA_North	Dif_LCLUC	0.185***	0.234***	0.132***	0.400***	-0.057***	-1.431***	-0.014***	6.115***	-3.109***	-1.650***
	IRRc_IRRg	-0.034***	-0.020***	0.005***	-0.028***	0.065***	0.626***	-0.014***	-0.494***	0.934***	0.007***
	IRRc_NIRR	-0.106***	0.067***	-0.210***	-0.595***	0.255***	2.043***	-0.038***	-11.622***	17.362***	-0.163***
	IRRg_NIRR	-0.073***	0.087***	-0.215***	-0.567***	0.190***	1.417***	-0.025***	-11.128***	16.429***	-0.170***
IA_South	Dif_LCLUC	0.054***	0.073***	0.086***	0.042***	-0.023***	-0.439***	-0.040***	2.875***	-3.093***	-0.141***
	IRRc_IRRg	-0.026***	-0.020***	-0.004***	-0.045***	0.031***	0.311***	-0.015***	-1.856***	2.622***	0.008***
	IRRc_NIRR	-0.026***	-0.008***	-0.017***	-0.078***	0.042***	0.367***	-0.013***	-2.400***	3.448***	-0.075***
	IRRg_NIRR	0.000	0.012***	-0.013***	-0.033***	0.011***	0.056***	0.002***	-0.544***	0.826***	-0.083***

Note:

Dif_LCLUC is the difference between LCLUC_2000 and LCLUC_1980 and calculated by LCLUC_2000 minus LCLUC_1980.

IRRC_IRRG is the difference between IRRc_2000 and IRRg_2000 and calculated by IRRc_2000 minus IRRg_2000.

IRRc_NIRR is the difference between IRRc_2000 and LCLUC_2000 and calculated by IRRc_2000 minus LCLUC_2000.

IRRg_NIRR is the difference between IRRg_2000 and LCLUC_2000 and calculated by IRRg_2000 minus LCLUC_2000.

*** indicates that the difference is significant at 0.001 level.

** indicates that the difference is significant at 0.01 level.

Table 4-14 Comparison between the magnitude of impacts of irrigation and those of land cover change

		Tmean(k)	Tmin(k)	Tmax(k)	TG(k)	Q2M(g/kg)	RH2M(%)	WS(m/s)	FSH(W/m^2)	FLH(W/m^2)	FGR(W/m^2)
China	LCLUC_IRRcNIRR	0.041***	0.089***	-0.008**	-0.073***	-0.075***	-0.176***	0.000	-1.664***	-5.158***	0.621***
	LCLUC_IRRgNIRR	0.060***	0.076***	-0.009**	-0.051***	-0.043***	0.129***	0.009*	-0.992***	-4.124***	0.617***
IA	LCLUC_IRRcNIRR	0.053***	0.120***	-0.013**	-0.117***	-0.112***	-0.294***	-0.002	-2.710***	-7.644***	0.809***
	LCLUC_IRRgNIRR	0.081***	0.102***	-0.015**	-0.085***	-0.065***	0.160***	0.011***	-1.711***	-6.108***	0.803***
IA_North	LCLUC_IRRcNIRR	0.079***	0.167***	-0.078***	-0.195***	-0.198***	-0.612***	-0.024***	-5.507***	-14.254***	1.487***
	LCLUC_IRRgNIRR	0.113***	0.147***	-0.083***	-0.167***	-0.133***	0.014	-0.011***	-5.013***	-13.320***	1.480***
IA_South	LCLUC_IRRcNIRR	0.029***	0.065***	0.069***	-0.036***	-0.019***	0.072***	0.027***	0.475***	-0.355**	0.067***
	LCLUC_IRRgNIRR	0.054***	0.061***	0.073***	0.008	0.012***	0.383***	0.039***	2.331***	2.267***	0.059***

Note:

The values in this table are the magnitudes of the impacts of land cover change minus the magnitudes of the impacts of irrigation.

LCLUC_IRRcNIRR is calculated by the modulus of Dif_LCLUC minus the modulus of IRRc_NIRR.

LCLUC_IRRgNIRR is calculated by the modulus of Dif_LCLUC minus the modulus of IRRg_NIRR.

*** indicates that the magnitude difference between the impacts of irrigation and those of land cover change is significant at 0.001 level.

**indicates that the magnitude difference between the impacts of irrigation and those of land cover change is significant at 0.01 level.

*indicates that the magnitude difference between the impacts of irrigation and those of land cover change is significant at 0.05 level

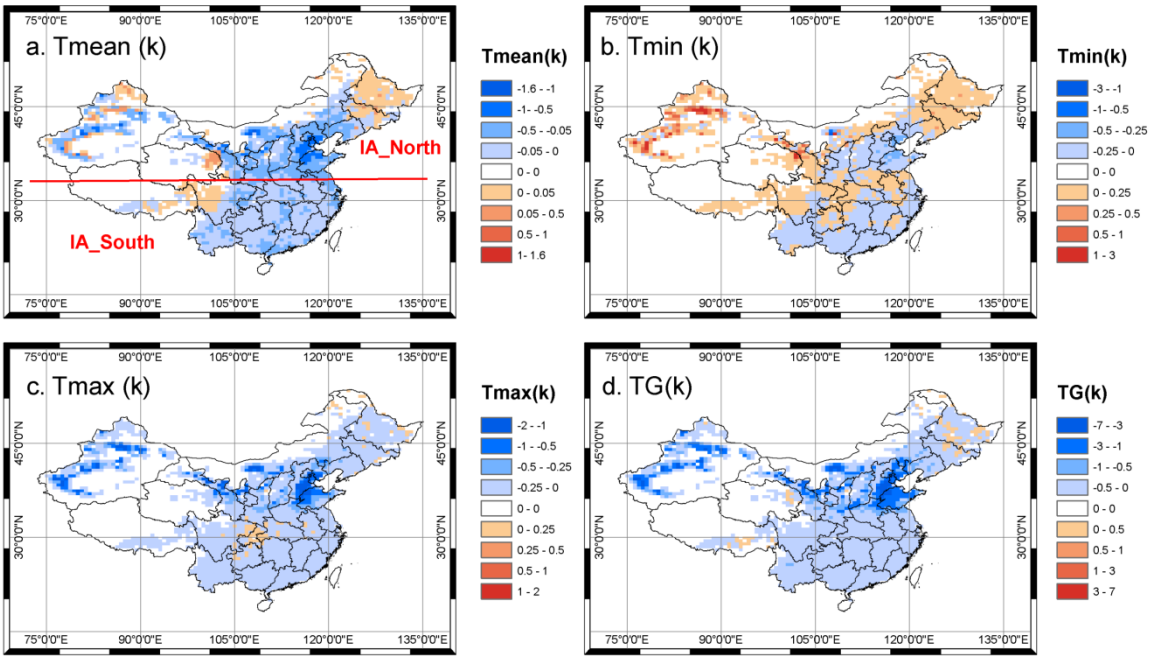

Figure 4-3 The Tmean, Tmin, Tmax and TG difference between IRRc _2000 and NIRR_2000 (IA_North refers to irrigated areas located in North China and IA_South refers to irrigated areas located in South China)

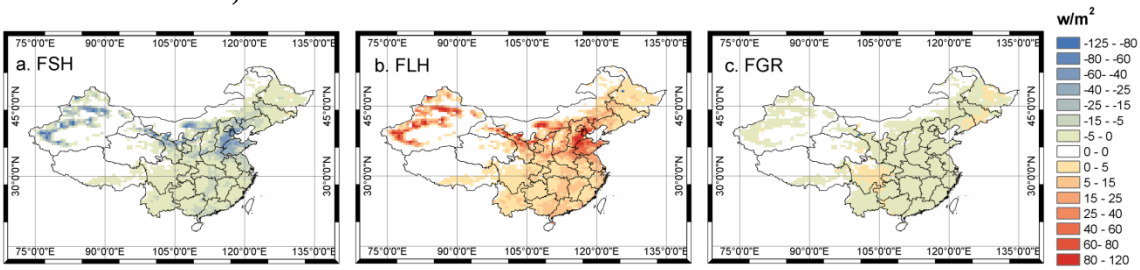

Figure 4-4 The FSH, FLH, and FGR difference between IRRc _2000 and NIRR_2000

Temporally, FLH increased throughout the whole year due to the irrigation and the biggest increase of FLH was in the summer (JJA). Correspondingly, Tmax decreased throughout the whole year and the biggest decrease of Tmax was in the summer (JJA) (Figure 4-5). Tmin decreased in the summer (JJA) and increased in other seasons in the irrigation simulation. The biggest Tmin increase was in winter (DJF). The impact of irrigation on daily Tmean depends more on its impact on Tmin in winter time (DJF) and depends more on Tmax in other seasons. As a result, daily Tmean increased in winter time and decreased in other seasons. Finally, irrigation led to a decrease in annual Tmean (Table 4-13).

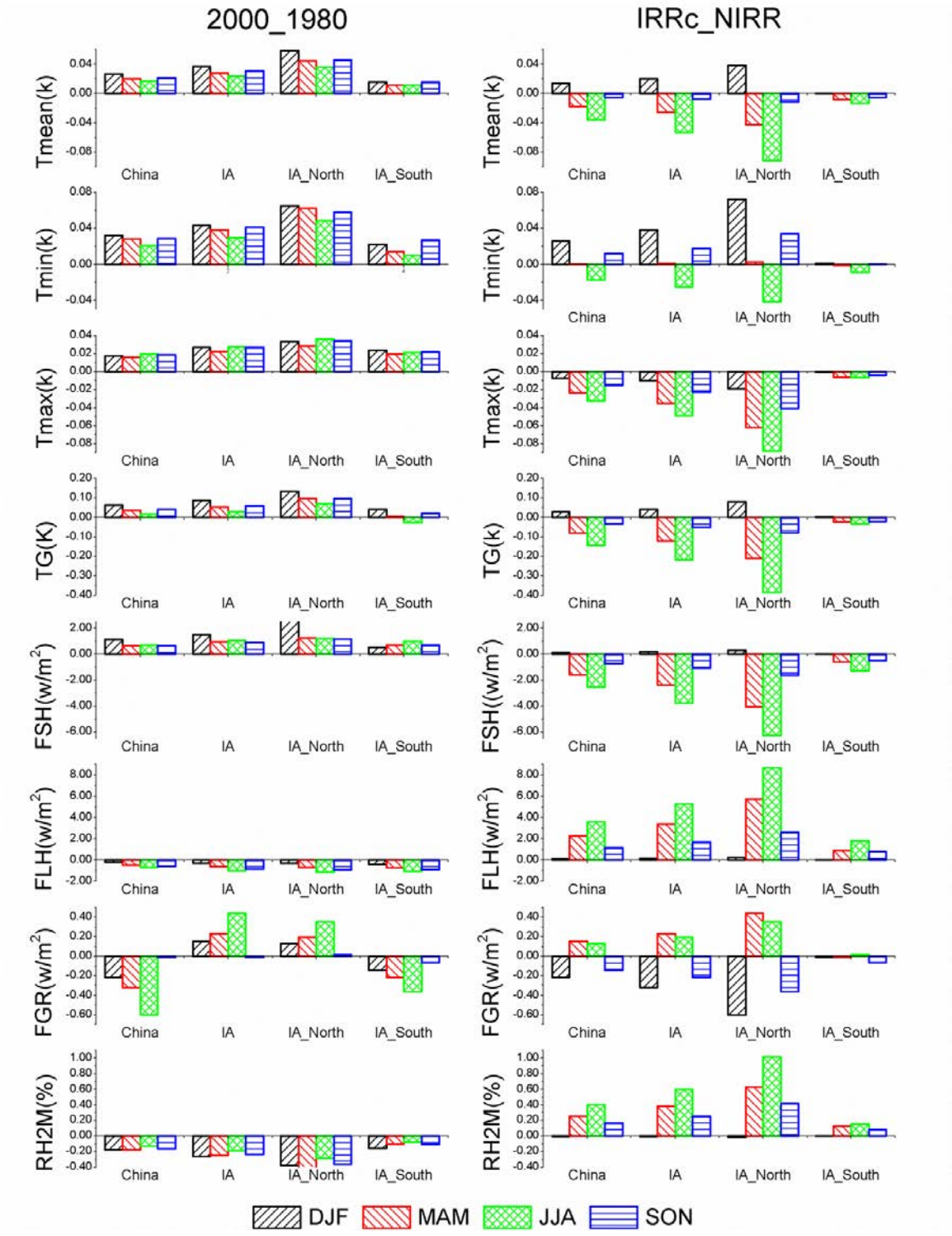

Figure 4-5 Comparison of the mean seasonal difference between LCLUC_1980 and LCLUC_2000 , and between IRRc_2000 and LCLUC_2000

Irrigation shows a greater impact on Tmax than Tmin, which is consistent with previous studies (Sacks et al. 2009). Moreover, the irrigation impact on Tmin is more complicated than the impact on Tmax. The Tmax decrease due to irrigation occurred almost over all China, while Tmin increased in northeast, southwest and northwest China and decreased in the North China Plain and in southeast China (Figure 4-3). Nationally, irrigation led to increases in Tmin of 0.022 K in the spay irrigation simulation and 0.034 K in the flood irrigation simulation. But in the south irrigated area, irrigation led to a decrease in Tmin of 0.008 K in the spray irrigation simulation and to an increase in Tmin of 0.012 K in the flood irrigation simulation.

Theoretically, excessive ET from irrigated agricultural land causes a change in the land surface energy distribution, which cools the land surface and near-surface air temperature during the day. Tmax always happens during daytime. Therefore, irrigation decreases Tmax. ET also increases the atmospheric water vapor, which is the most dominant greenhouse gas with a significant and positive feedback on our climate system. At nighttime, more water vapor in the atmosphere can increase the near-surface temperature. Meanwhile, irrigation increases soil moisture. The specific heat of water is higher than that of the land surface; hence, more moisture in the soil can reduce the cooling process of the land surface at nighttime. Tmin usually happens at nighttime, and there is a little ET generation at nighttime because of low temperature. Therefore, Tmin is more expected to increase because the warming effect from the increased water vapor offsets the cooling effect from the increased soil moisture.

Comparing the impacts of irrigation with those of land cover change can indicate how changes in land management compare to changes in land cover in terms of their effects on climate. So, in this study, we also simulated LCLUC impact on climate over China. The difference between the two LCLUC simulations shows nationally FLH decreased 1.916 W/m^2 and FSH increased 3.096 W/m^2 (Table 4-13) when transferring land surface status from 1980 to 2000. Nationally, the annual mean Tmean, Tmin, and Tmax increased 0.086K, 0.110K, and 0.071K respectively due to LCLUC.

Nationally, land cover change had more impact on Tmean, Tmin, FGR, and WS, and less impact on Tmax, TG, Q2M, RH2M, FSH, and FLH than irrigation (Table 4-14). The differences between the impacts of irrigation and those of land cover change are more obvious in irrigated areas of North China. For example, the Tmean differences between LCLUC simulation and irrigation simulation averaged over the irrigated areas of North China (0.079 k and 0.113 K, respectively) are around 1.9 times as much as those averaged over whole China(0.041K and0.060K, respectively) (Table 4-13).

The directions of the impacts of irrigation, and those of land cover change are opposite in most of cases (Table 4-13). Irrigation significantly increased Q2M, RH2M, and FLH while land cover change significantly decreased them. Irrigation significantly decreased Tmean, Tmax, TG, and FSH while land cover change significantly increased them. Nationally, both irrigation and land cover change increased Tmin, and decreased WS and FGR.

To investigate whether changes in land management are comparable to changes in land cover in terms of their effects on climate in China, I compared the impacts of irrigation with those of land cover change by a paired-t test. Results are also shown in Table 4-14. Here, one point which should be mentioned is that, in paired t-test, I compared the magnitude of the impacts of irrigation with those of land cover change because the directions of their impacts are opposite in most of cases. Therefore, before making the paired-t test, I first calculated the absolute values of the impacts of irrigation and those of land cover change. From Table 4-14, we can see LCLUC has more impact on Tmean, Tmin, and FGR, and less impact on Tmax, TG, Q2M, RH2M, FSH, and FLH. The difference in magnitude between LCLUC simulations and irrigation simulations pass paired t-test at 0.001 level in almost all cases, which suggest that changes in land management are incomparable to changes in land cover in terms of their effects on climate in China. This finding is different from the previous study by Sacks et al. (2009).This maybe because I used the offline CLM while Sacks et al coupled the CLM with the CAM. Sacks et al. (2009) suggested that more irrigation cooling effect was due to non-local processes such as changes in cloud cover, rather than changes in ET. The offline mode in this study cannot reflect the indirect cooling effect such as cooling from an increase in cloud-reflected solar radiation, and may cause an underestimate of the irrigation impact in this study. However, this study suggests that changes in land management are not comparable to changes in land cover when only considering their effects on climate due to the changes in heat flux partition in China.

Considering the magnitude of irrigation and land cover change impact on Tmax and Tmean are significantly different and the direction of their impacts are opposite. Therefore, the irrigation may mask the greenhouse gases impact on Tmax and Tmean in the past. In contrast, the irrigation may have enhanced the warming effect of greenhouse gases on Tmin to some degree in the past because both land cover change and irrigation increased Tmin.

4.2.3 Irrigation impact in the future

The results for future simulations are shown in Table 4-15 to Table 4-21. Similar to the results reported in 4.2.2, the differences between two irrigation simulations by CLM under future scenarios are also statistically significant according to this study. Spray irrigation shows more impact on FSH and FLH, and less impact on FGR than flood irrigation. In spray irrigation simulations, the irrigation shows similar impacts on heat flux in irrigation areas located in South China and in irrigation areas located in North China. However,in flood irrigation simulations, the irrigation shows more impacts on heat flux in irrigation areas located in North China than those located in South China. For example, nationally, spray irrigation simulated by the CLM leads to an increase in annual FLH of 1.721 W/m^2, a decrease in annual FSH of 1.162 W/m^2 and a decrease in annual FGR of 0.061 W/m^2 in 2050 under scenarios A1B(Table 4-15). Flood irrigation simulated by the CLM leads to an increase in annual FLH of 0.529 W/m^2, a decrease in annual FSH of 0.402 W/m^2 and a decrease in annual FGR of 0.067 W/m^2 in 2050 under scenarios A1B. When only considering the irrigated grids, the changes in FLH and FSH are around 1.5 times as much as the changes in FLH and FSH averaged over the whole of China in the spray irrigation simulation. In spray irrigation simulation, the decrease in FLH (2.701

W/m^2) in irrigation areas of South China is as much as that (2.815 W/m^2) in irrigation areas of North China, but in flood irrigation, the decrease in FLH (1.354 W/m^2) in irrigation areas of North China is 7 times as much as that (0.183) in irrigation areas of South China.

Table 4-15 Annual mean differences between different simulations, averaged over the whole of China, only irrigated area in China (IA), irrigated area in North China (IA_North), and irrigated area in South China (IA_South) under scenario A1B in 2050

		Tmean(k)	Tmin(k)	Tmax(k)	TG(k)	Q2M(g/kg)	RH2M (%)	WS(m/s)	FSH(W/m^2)	FLH(W/m^2)	FGR(W/m^2)
China	Dif_LCLUC_2050A1B	0.083***	0.100***	0.131***	0.157***	-0.035***	-0.717***	-0.001***	2.927***	-2.428***	-0.686***
	IRRc_IRRg_2050A1B	-0.019***	-0.007***	-0.011***	-0.023***	0.047***	0.396***	-0.007***	-0.760***	1.192***	0.006***
	IRRc_NIRR_2050A1B	-0.001***	0.031***	-0.022***	-0.012***	0.063***	0.437***	-0.004***	-1.162***	1.721***	-0.061***
	IRRg_NIRR_2050A1B	0.018***	0.038***	-0.012***	0.012***	0.015***	0.041***	0.003***	-0.402***	0.529***	-0.067***
IA	Dif_LCLUC_2050A1B	0.112***	0.133***	0.188***	0.219***	-0.052***	-1.005***	-0.001***	4.109***	-3.500***	-0.913***
	IRRc_IRRg_2050A1B	-0.028***	-0.010***	-0.016***	-0.035***	0.070***	0.589***	-0.010***	-1.130***	1.772***	0.009***
	IRRc_NIRR_2050A1B	-0.002***	0.046***	-0.033***	-0.018***	0.093***	0.650***	-0.006***	-1.727***	2.558***	-0.090***
	IRRg_NIRR_2050A1B	0.027***	0.056***	-0.018***	0.017***	0.023***	0.061***	0.005***	-0.597***	0.786***	-0.099***
IA_North	Dif_LCLUC_2050A1B	0.221***	0.244***	0.216***	0.457***	-0.057***	-1.659***	0.015***	6.033***	-4.793***	-1.561***
	IRRc_IRRg_2050A1B	-0.027***	-0.009***	-0.011***	-0.030***	0.078***	0.684***	-0.009***	-0.866***	1.461***	0.009***
	IRRc_NIRR_2050A1B	0.015***	0.082***	-0.041***	-0.009***	0.115***	0.801***	-0.002***	-1.918***	2.815***	-0.094***
	IRRg_NIRR_2050A1B	0.042***	0.091***	-0.030***	0.021***	0.037***	0.117***	0.007***	-1.052***	1.354***	-0.103***
IA_South	Dif_LCLUC_2050A1B	-0.012***	0.011***	0.187***	-0.055***	-0.055***	-0.329***	-0.023***	2.344***	-2.454***	-0.229***
	IRRc_IRRg_2050A1B	-0.035***	-0.014***	-0.025***	-0.047***	0.073***	0.574***	-0.014***	-1.693***	2.518***	0.011***
	IRRc_NIRR_2050A1B	-0.025***	0.006***	-0.030***	-0.031***	0.081***	0.574***	-0.012***	-1.802***	2.701***	-0.103***
	IRRg_NIRR_2050A1B	0.011***	0.020***	-0.005***	0.016***	0.008***	0.000	0.003***	-0.109***	0.183***	-0.114***

Note:

Dif_LCLUC_2050A1B is the difference between LCLUC2000_A1B_2050 and LCLUC1980_A1B_2050 and calculated by LCLUC2000_A1B_2050 minus LCLUC1980_A1B_2050.

IRRc_IRRg_2050A1B is the difference between IRRc_A1B_2050 and IRRg_A1B_2050 and calculated by IRRc_A1B_2050 minus IRRg_A1B_2050.

IRRc_NIRR_2050A1B is the difference between IRRc_A1B_2050 and LCLUC2000_A1B_2050 and calculated by IRRc_A1B_2050 minus LCLUC2000_ A1B_2050.

IRRc_NIRR_2050A1B is the difference between IRRg_A1B_2050 and LCLUC2000_ A1B_2050 and calculated by IRRg_A1B_2050 minus LCLUC2000_ A1B_2050.

*** indicates that the difference is significant at 0.001 level.

Table 4-16 Annual mean differences between different simulations, averaged over the whole of China, only irrigated area in China (IA), irrigated area in North China (IA_North), and irrigated area in South China (IA_South) under scenario A2 in 2050

		Tmean(k)	Tmin(k)	Tmax(k)	TG(k)	Q2M(g/kg)	RH2M (%)	WS(m/s)	FSH(W/m^2)	FLH(W/m^2)	FGR(W/m^2)
China	Dif_LCLUC_2050A2	0.022***	0.066***	0.041***	0.063***	0.015***	-0.164***	-0.018***	-4.297***	6.483***	-0.799***
	IRRc_IRRg_2050A2	-0.013***	-0.002**	-0.009***	-0.016***	0.036***	0.312***	-0.007***	-0.729***	1.140***	0.005***
	IRRc_NIRR_2050A2	0.002**	0.031***	-0.022***	-0.016***	0.053***	0.359***	-0.004***	-1.256***	1.847***	-0.051***
	IRRc_NIRR_2050A2	0.015***	0.033***	-0.013***	0.000	0.017***	0.046***	0.003***	-0.527***	0.707***	-0.056***
IA	Dif_LCLUC_2050A2	0.040***	0.091***	0.082***	0.104***	0.011***	-0.326***	-0.022***	-4.657***	7.418***	-1.034***
	IRRc_IRRg_2050A2	-0.019***	-0.003**	-0.013***	-0.024***	0.053***	0.464***	-0.011***	-1.084***	1.694***	0.007***
	IRRc_NIRR_2050A2	0.003**	0.046***	-0.033***	-0.024***	0.078***	0.533***	-0.006***	-1.867***	2.745***	-0.076***
	IRRc_NIRR_2050A2	0.022***	0.049***	-0.019***	0.000	0.025***	0.069***	0.004***	-0.783***	1.051***	-0.083***
IA_North	Dif_LCLUC_2050A2	0.156***	0.190***	0.169***	0.367***	0.011***	-0.971***	0.001***	0.640***	2.751***	-1.749***
	IRRc_IRRg_2050A2	-0.019***	-0.003	-0.008***	-0.020***	0.066***	0.586***	-0.009***	-0.812***	1.381***	0.008***
	IRRc_NIRR_2050A2	0.015***	0.078***	-0.041***	-0.030***	0.111***	0.728***	-0.003***	-2.220***	3.281***	-0.086***
	IRRc_NIRR_2050A2	0.034***	0.080***	-0.033***	-0.011***	0.044***	0.141***	0.006***	-1.408***	1.901***	-0.094***
IA_South	Dif_LCLUC_2050A2	-0.105***	-0.022***	-0.018***	-0.224***	0.013***	0.465***	-0.057***	-12.538***	14.989***	-0.286***
	IRRc_IRRg_2050A2	-0.023***	-0.005***	-0.023***	-0.033***	0.045***	0.391***	-0.015***	-1.648***	2.429***	0.007***
	IRRc_NIRR_2050A2	-0.013***	0.013***	-0.028***	-0.020***	0.050***	0.376***	-0.011***	-1.753***	2.556***	-0.077***
	IRRc_NIRR_2050A2	0.010***	0.018***	-0.006***	0.013***	0.005***	-0.014***	0.003***	-0.106***	0.127***	-0.084***

Note:

Dif_LCLUC_2050A2 is the difference between LCLUC2000_A2_2050 and LCLUC1980_A2_2050 and calculated by LCLUC2000_A2_2050 minus LCLUC1980_A2_2050.

IRRc_IRRg_2050A2 is the difference between IRRc_A2_2050 and IRRg_A2_2050 and calculated by IRRc_A2_2050 minus IRRg_A2_2050.

IRRc_NIRR_2050A2 is the difference between IRRc_A2_2050 and LCLUC2000_ A2_2050 and calculated by IRRc_A2_2050 minus LCLUC2000_ A2_2050.

IRRc_NIRR_2050A2 is the difference between IRRg_A2_2050 and LCLUC2000_ A2_2050 and calculated by IRRg_A2_2050 minus LCLUC2000_ A2_2050.

*** indicates that the difference is significant at 0.001 level.

** indicates that the difference is significant at 0.01 level.

Table 4-17 Annual mean differences between different simulations, averaged over the whole of China, only irrigated area in China (IA), irrigated area in North China (IA_North), and irrigated area in South China (IA_South) under scenario B1 in 2050

		Tmean(k)	Tmin(k)	Tmax(k)	TG(k)	Q2M(g/kg)	RH2M(%)	WS(m/s)	FSH(W/m^2)	FLH(W/m^2)	FGR(W/m^2)
China	Dif_LCLUC_2050B1	0.082***	0.103***	0.133***	0.137***	-0.031***	-0.721***	-0.00009**	3.080***	-2.250***	-0.780***
	IRRc_IRRg_2050 B1	-0.017***	-0.005***	-0.010***	-0.019***	0.045***	0.383***	-0.007***	-0.747***	1.167***	0.007***
	IRRc_NIRR_2050 B1	0.002	0.057***	-0.045***	-0.056***	0.083***	0.590***	-0.004***	-2.311***	3.326***	-0.061***
	IRRc_NIRR_2050 B1	0.019***	0.062***	-0.036***	-0.037***	0.038***	0.207***	0.002***	-1.564***	2.159***	-0.068***
IA	Dif_LCLUC_2050B1	0.115***	0.145***	0.190***	0.200***	-0.046***	-1.008***	0.0002***	4.328***	-3.206***	-1.048***
	IRRc_IRRg_2050 B1	-0.025***	-0.007***	-0.014***	-0.029***	0.067***	0.568***	-0.010***	-1.110***	1.733***	0.010***
	IRRc_NIRR_2050 B1	0.003***	0.085***	-0.067***	-0.084***	0.124***	0.876***	-0.006***	-3.434***	4.942***	-0.090***
	IRRc_NIRR_2050 B1	0.028***	0.091***	-0.053***	-0.055***	0.057***	0.308***	0.004***	-2.324***	3.208***	-0.101***
IA_North	Dif_LCLUC_2050B1	0.225***	0.257***	0.226***	0.438***	-0.045***	-1.639***	0.018***	6.336***	-4.211***	-1.784***
	IRRc_IRRg_2050 B1	-0.023***	-0.006***	-0.009***	-0.026***	0.074***	0.648***	-0.008***	-0.890***	1.467***	0.012***
	IRRc_NIRR_2050 B1	0.020***	0.143***	-0.099***	-0.129***	0.171***	1.205***	-0.004***	-4.886***	7.014***	-0.105***
	IRRc_NIRR_2050 B1	0.043***	0.149***	-0.089***	-0.103***	0.096***	0.557***	0.004***	-3.996***	5.546***	-0.117***
IA_South	Dif_LCLUC_2050B1	-0.010***	0.023***	0.177***	-0.077***	-0.055***	-0.364***	-0.023***	2.495***	-2.485***	-0.273***
	IRRc_IRRg_2050 B1	-0.031***	-0.009***	-0.024***	-0.038***	0.071***	0.571***	-0.014***	-1.611***	2.413***	0.010***
	IRRc_NIRR_2050 B1	-0.019***	0.024***	-0.039***	-0.040***	0.086***	0.608***	-0.011***	-2.165***	3.139***	-0.088***
	IRRc_NIRR_2050 B1	0.012***	0.033***	-0.015***v	-0.002***	0.014***	0.037***	0.003***	-0.553***	0.726***	-0.098***

Note:

Dif_LCLUC_2050B1 is the difference between LCLUC2000_B1_2050 and LCLUC1980_B1_2050 and calculated by LCLUC2000_B1_2050 minus LCLUC1980_B1_2050.

IRRc_IRRg_2050B1 is the difference between IRRc_B1_2050 and IRRg_B1_2050 and calculated by IRRc_B1_2050 minus IRRg_B1_2050.

IRRc_NIRR_2050B1 is the difference between IRRc_B1_2050 and LCLUC2000_ B1_2050 and calculated by IRRc_B1_2050 minus LCLUC2000_ B1_2050.

IRRc_NIRR_2050B1 is the difference between IRRg_B1_2050 and LCLUC2000_ B1_2050 and calculated by IRRg_B1_2050 minus LCLUC2000_ B1_2050.

*** indicates that the difference is significant at 0.001 level.

** indicates that the difference is significant at 0.01 level.

Table 4-18 Annual mean differences between different simulations, averaged over whole China, only irrigated area in China (IA), irrigated area in North China (IA_North), and irrigated area in South China (IA_South) under scenario A1B in 2100

		Tmean(k)	Tmin(k)	Tmax(k)	TG(k)	Q2M(g/kg)	RH2M(%)	WS(m/s)	FSH(W/m^2)	FLH(W/m^2)	FGR(W/m^2)
China	Dif_LCLUC_2100A1B	0.092***	0.115***	0.143***	0.169***	-0.044***	-0.798***	0.0004***	3.193***	-2.679***	-0.656***
	IRRc_IRRg_2100A1B	-0.021***	-0.005***	-0.010***	-0.021***	0.062***	0.450***	-0.008***	-0.893***	1.423***	0.009***
	IRRc_NIRR_2100A1B	-0.018***	0.028***	-0.038***	-0.085***	0.109***	0.639***	-0.011***	-2.304***	3.439***	-0.068***
	IRRg_NIRR_2100A1B	0.003***	0.033***	-0.028***	-0.064***	0.047***	0.190***	-0.003***	-1.411***	2.016***	-0.076***
IA	Dif_LCLUC_2100A1B	0.127***	0.159***	0.205***	0.241***	-0.065***	-1.131***	0.001***	4.466***	-3.863***	-0.877***
	IRRc_IRRg_2100A1B	-0.031***	-0.007***	-0.015***	-0.031***	0.092***	0.668***	-0.012***	-1.327***	2.114***	0.013***
	IRRc_NIRR_2100A1B	-0.027***	0.042***	-0.056***	-0.126***	0.162***	0.950***	-0.017***	-3.424***	5.110***	-0.100***
	IRRg_NIRR_2100A1B	0.004***	0.049***	-0.041***	-0.095***	0.069***	0.282***	-0.004***	-2.097***	2.996***	-0.113***
IA_North	Dif_LCLUC_2100A1B	0.235***	0.268***	0.224***	0.470***	-0.065***	-1.700***	0.017***	6.230***	-4.843***	-1.512***
	IRRc_IRRg_2100A1B	-0.024***	-0.004**	-0.010***	-0.020***	0.092***	0.685***	-0.010***	-0.934***	1.615***	0.016***
	IRRc_NIRR_2100A1B	-0.024***	0.067***	-0.078***	-0.193***	0.208***	1.187***	-0.019***	-4.489***	6.708***	-0.105***
	IRRg_NIRR_2100A1B	0.000	0.070***	-0.069***	-0.172***	0.116***	0.502***	-0.009***	-3.555***	5.093***	-0.121***
IA_South	Dif_LCLUC_2100A1B	0.010***	0.046***	0.218***	-0.017***	-0.078***	-0.592***	-0.020***	2.979***	-3.297***	-0.204***
	IRRc_IRRg_2100A1B	-0.045***	-0.013***	-0.025***	-0.051***	0.110***	0.772***	-0.018***	-2.098***	3.173***	0.011***
	IRRc_NIRR_2100A1B	-0.035***	0.017***	-0.038***	-0.061***	0.131***	0.817***	-0.017***	-2.665***	3.964***	-0.113***
	IRRg_NIRR_2100A1B	0.010***	0.029***	-0.013***	-0.010***	0.021***	0.045***	0.001***	-0.568***	0.791***	-0.124***

Note:

Dif_LCLUC_2100A1B is the difference between LCLUC2000_A1B_2100 and LCLUC1980_A1B_2100 and calculated by LCLUC2000_A1B_2100 minus LCLUC1980_A1B_2100.

IRRc_IRRg_2100A1B is the difference between IRRc_A1B_2100 and IRRg_A1B_2100 and calculated by IRRc_A1B_2100 minus IRRg_A1B_2100.

IRRc_NIRR_2100A1B is the difference between IRRc_A1B_2100 and LCLUC2000_A1B_2100 and calculated by IRRc_A1B_2100 minus LCLUC2000_ A1B_2100.

IRRc_NIRR_2100A1B is the difference between IRRg_A1B_2100 and LCLUC2000_ A1B_2100 and calculated by IRRg_A1B_2100 minus LCLUC2000_ A1B_2100.

*** indicates that the difference is significant at 0.001 level.

** indicates that the difference is significant at 0.01 level.

Table 4-19 Annual mean differences between different simulations, averaged over whole China, only irrigated area in China (IA), irrigated area in North China (IA_North), and irrigated area in South China (IA_South) under scenario A2 in 2100

		Tmean(k)	Tmin(k)	Tmax(k)	TG(k)	Q2M(g/kg)	RH2M (%)	WS(m/s)	FSH(W/m^2)	FLH(W/m^2)	FGR(W/m^2)
China	Dif_LCLUC_2100A2	0.085***	0.097***	0.134***	0.155***	-0.033***	-0.695***	-0.001***	2.996***	-2.707***	-0.606***
	IRRc_IRRg_2100A2	-0.018***	-0.005***	-0.013***	-0.027***	0.041***	0.307***	-0.009***	-1.076***	1.612***	0.004***
	IRRc_NIRR_2100A2	-0.009***	0.019***	-0.023***	-0.031***	0.059***	0.373***	-0.007***	-1.465***	2.179***	-0.058***
	IRRg_NIRR_2100A2	0.009***	0.023***	-0.010***	-0.004***	0.018***	0.066***	0.002***	-0.388***	0.567***	-0.062***
IA	Dif_LCLUC_2100A2	0.114***	0.128***	0.191***	0.215***	-0.049***	-0.971***	-0.002***	4.184***	-3.873***	-0.805***
	IRRc_IRRg_2100A2	-0.027***	-0.007***	-0.019***	-0.041***	0.061***	0.456***	-0.013***	-1.599***	2.395***	0.006***
	IRRc_NIRR_2100A2	-0.013***	0.028***	-0.034***	-0.046***	0.088***	0.554***	-0.010***	-2.177***	3.238***	-0.086***
	IRRg_NIRR_2100A2	0.014***	0.035***	-0.015***	-0.006***	0.027***	0.098***	0.003***	-0.577***	0.843***	-0.092***
IA_North	Dif_LCLUC_2100A2	0.205***	0.219***	0.209***	0.414***	-0.041***	-1.406***	0.014***	5.802***	-4.917***	-1.397***
	IRRc_IRRg_2100A2	-0.021***	-0.004***	-0.014***	-0.031***	0.062***	0.470***	-0.010***	-1.170***	1.840***	0.003***
	IRRc_NIRR_2100A2	0.000	0.051***	-0.039***	-0.047***	0.107***	0.644***	-0.006***	-2.153***	3.242***	-0.087***
	IRRg_NIRR_2100A2	0.021***	0.055***	-0.025***	-0.016***	0.045***	0.174***	0.004***	-0.984***	1.402***	-0.090***
IA_South	Dif_LCLUC_2100A2	0.015***	0.033***	0.202***	-0.007***	-0.070***	-0.580***	-0.023***	2.838***	-3.226***	-0.175***
	IRRc_IRRg_2100A2	-0.040***	-0.012***	-0.029***	-0.061***	0.071***	0.524***	-0.019***	-2.470***	3.582***	0.010***
	IRRc_NIRR_2100A2	-0.033***	0.002*	-0.035***	-0.055***	0.079***	0.540***	-0.017***	-2.620***	3.845***	-0.101***
	IRRg_NIRR_2100A2	0.007***	0.015***	-0.006***	0.006**	0.008***	0.017***	0.002***	-0.149***	0.262***	-0.111***

Note:

Dif_LCLUC_2100A2 is the difference between LCLUC2000_A2_2100 and LCLUC1980_A2_2100 and calculated by LCLUC2000_A2_2100 minus LCLUC1980_A2_2100.

IRRc_IRRg_2100A2 is the difference between IRRc_A2_2100 and IRRg_A2_2100 and calculated by IRRc_A2_2100 minus IRRg_A2_2100.

IRRc_NIRR_2100A2 is the difference between IRRc_A2_2100 and LCLUC2000_A2_2100 and calculated by IRRc_A2_2100 minus LCLUC2000_ A2_2100.

IRRc_NIRR_2100A2 is the difference between IRRg_A2_2100 and LCLUC2000_ A2_2100 and calculated by IRRg_A2_2100 minus LCLUC2000_ A2_2100.

*** indicates that the difference is significant at 0.001 level.

** indicates that the difference is significant at 0.01 level.

* indicates that the difference is significant at 0.05 level.

Table 4-20 Annual mean differences between different simulations, averaged over whole China, only irrigated area in China (IA), irrigated area in North China (IA_North), and irrigated area in South China (IA_South) under scenario B1 in 2100

		Tmean(k)	Tmin(k)	Tmax(k)	TG(k)	Q2M(g/kg)	RH2M (%)	WS(m/s)	FSH(W/m^2)	FLH(W/m^2)	FGR(W/m^2)
China	Dif_LCLUC_2100B1	0.086***	0.103***	0.137***	0.154***	-0.028***	-0.667***	-0.002***	2.973***	-2.445***	-0.684***
	IRRc_IRRg_2100B1	-0.016***	-0.004***	-0.010***	-0.020***	0.044***	0.351***	-0.007***	-0.833***	1.278***	0.006***
	IRRc_NIRR_2100B1	0.000	0.033***	-0.025***	-0.023***	0.066***	0.425***	-0.004***	-1.420***	2.127***	-0.094***
	IRRg_NIRR_2100B1	0.015***	0.037***	-0.015***	-0.003**	0.022***	0.074***	0.003***	-0.588***	0.849***	-0.101***
IA	Dif_LCLUC_2100B1	0.117***	0.141***	0.196***	0.219***	-0.042***	-0.936***	-0.002***	4.181***	-3.509***	-0.912***
	IRRc_IRRg_2100B1	-0.023***	-0.006***	-0.015***	-0.029***	0.065***	0.521***	-0.011***	-1.238***	1.899***	0.010***
	IRRc_NIRR_2100B1	-0.001	0.050***	-0.038***	-0.034***	0.098***	0.631***	-0.006***	-2.111***	3.160***	-0.140***
	IRRg_NIRR_2100B1	0.022***	0.055***	-0.023***	-0.004***	0.033***	0.110***	0.005***	-0.873***	1.261***	-0.150***
IA_North	Dif_LCLUC_2100B1	0.219***	0.240***	0.228***	0.441***	-0.043***	-1.495***	0.013***	5.939***	-4.452***	-1.569***
	IRRc_IRRg_2100B1	-0.020***	-0.003***	-0.011***	-0.022***	0.076***	0.608***	-0.009***	-0.913***	1.525***	0.008***
	IRRc_NIRR_2100B1	0.014***	0.085***	-0.049***	-0.038***	0.130***	0.810***	-0.002***	-2.454***	3.715***	-0.166***
	IRRg_NIRR_2100B1	0.035***	0.089***	-0.039***	-0.017***	0.055***	0.201***	0.006***	-1.541***	2.189***	-0.175***
IA_South	Dif_LCLUC_2100B1	0.006***	0.038***	0.191***	-0.034***	-0.050***	-0.375***	-0.023***	2.650***	-2.927***	-0.215***
	IRRc_IRRg_2100B1	-0.031***	-0.009**	-0.024***	-0.045***	0.063***	0.505***	-0.015***	-1.900***	2.751***	0.013***
	IRRc_NIRR_2100B1	-0.021***	0.012***	-0.030***	-0.034***	0.074***	0.514***	-0.012***	-2.056***	3.025***	-0.133***
	IRRg_NIRR_2100B1	0.011***	0.021***	-0.006***	0.011***	0.011***	0.010***	0.004***	-0.155***	0.274***	-0.146***

Note:

Dif_LCLUC_2100B1 is the difference between LCLUC2000_B1_2100 and LCLUC1980_B1_2100 and calculated by LCLUC2000_B1_2100 minus LCLUC1980_B1_2100.

IRRc_IRRg_2100B1 is the difference between IRRc_B1_2100 and IRRg_B1_2100 and calculated by IRRc_B1_2100 minus IRRg_B1_2100.

IRRc_NIRR_2100B1 is the difference between IRRc_B1_2100 and LCLUC2000_B1_2100 and calculated by IRRc_B1_2100 minus LCLUC2000_ B1_2100.

IRRc_NIRR_2100B1 is the difference between IRRg_B1_2100 and LCLUC2000_ B1_2100 and calculated by IRRg_B1_2100 minus LCLUC2000_ B1_2100.

*** indicates that the difference is significant at 0.001 level.

Table 4-21 Comparison between the magnitude of impacts of irrigation and those of land cover change in two future time periods and under three future scenarios, averaged over whole China

	Tmean(k)	Tmin(k)	Tmax(k)	TG(k)	Q2M(g/kg)	RH2M(%)	WS(m/s)	FSH(W/m^2)	FLH(W/m^2)	FGR(W/m^2)
LCLUC_IRRcNIRR_2050A1B	0.082***	0.069***	0.108***	0.145***	-0.028***	0.279***	-0.003***	1.765***	0.707***	0.625***
LCLUC_IRRgNIRR_2050A1B	0.001***	0.031***	0.022***	0.012***	0.063***	0.437***	0.004***	1.162***	1.721***	0.061***
LCLUC_IRRcNIRR_2050A2	0.021***	0.035***	0.019***	0.047***	-0.037***	-0.195***	0.014***	3.040***	4.636***	0.748***
LCLUC_IRRgNIRR_2050A2	0.002***	0.031***	0.022***	0.016***	0.053***	0.359***	0.004***	1.256***	1.847***	0.051***
LCLUC_IRRcNIRR_2050B1	0.080***	0.046***	0.087***	0.080***	-0.053***	0.131***	-0.004***	0.769***	-1.076***	0.719***
LCLUC_IRRgNIRR_2050B1	0.002***	0.057***	0.045***	0.056***	0.083***	0.590***	0.004***	2.311***	3.326***	0.061***
LCLUC_IRRcNIRR_2100A1B	0.074***	0.087***	0.105***	0.085***	-0.065***	0.158***	-0.011***	0.888***	-0.760***	0.589***
LCLUC_IRRgNIRR_2100A1B	0.018***	0.028***	0.038***	0.085***	0.109***	0.639***	0.011***	2.304***	3.439***	0.068***
LCLUC_IRRcNIRR_2100A2	0.076***	0.078***	0.111***	0.123***	-0.026***	0.322***	-0.005***	1.531***	0.528***	0.548***
LCLUC_IRRgNIRR_2100A2	0.009***	0.019***	0.023***	0.031***	0.059***	0.373***	0.007***	1.465***	2.179***	0.058***
LCLUC_IRRcNIRR_2100B1	0.085***	0.070***	0.111***	0.131***	-0.038***	0.243***	-0.002***	1.553***	0.319***	0.590***
LCLUC_IRRgNIRR_2100B1	0.000***	0.033***	0.025***	0.023***	0.066***	0.425***	0.004***	1.420***	2.127***	0.094***

Note:
The values in this table are the magnitudes of the impacts of land cover change minus the magnitudes of the impacts of irrigation.
LCLUC_IRRcNIRR_2050A1B is calculated by the modulus of Dif_LCLUC_2050A1B minus the modulus of IRRc_NIRR_2050A1B.
LCLUC_IRRgNIRR_2050A1B is calculated by the modulus of Dif_LCLUC_2050A1B minus the modulus of IRRg_NIRR_2050A1B.
LCLUC_IRRcNIRR_2050A2 is calculated by the modulus of Dif_LCLUC_2050A2 minus the modulus of IRRc_NIRR_2050A2.
LCLUC_IRRgNIRR_2050A2 is calculated by the modulus of Dif_LCLUC_2050A2 minus the modulus of IRRg_NIRR_2050A2.
LCLUC_IRRcNIRR_2050B1 is calculated by the modulus of Dif_LCLUC_2050B1 minus the modulus of IRRc_NIRR_2050B1.
LCLUC_IRRgNIRR_2050B1 is calculated by the modulus of Dif_LCLUC_2050B1 minus the modulus of IRRg_NIRR_2050B1.
LCLUC_IRRcNIRR_2100A1B is calculated by the modulus of Dif_LCLUC_2100A1B minus the modulus of IRRc_NIRR_2100A1B.
LCLUC_IRRgNIRR_2100A1B is calculated by the modulus of Dif_LCLUC_2100A1B minus the modulus of IRRg_NIRR_2100A1B.
LCLUC_IRRcNIRR_2100A2 is calculated by the modulus of Dif_LCLUC_2100A2 minus the modulus of IRRc_NIRR_2100A2.
LCLUC_IRRgNIRR_2100A2 is calculated by the modulus of Dif_LCLUC_2100A2 minus the modulus of IRRg_NIRR_2100A2.
LCLUC_IRRcNIRR_2100B1 is calculated by the modulus of Dif_LCLUC_2100B1 minus the modulus of IRRc_NIRR_2100B1.
LCLUC_IRRgNIRR_2100B1 is calculated by the modulus of Dif_LCLUC_2100B1 minus the modulus of IRRg_NIRR_2050B1.
*** indicates that the magnitude difference between the impacts of irrigation and those of land cover change is significant at 0.001 level.

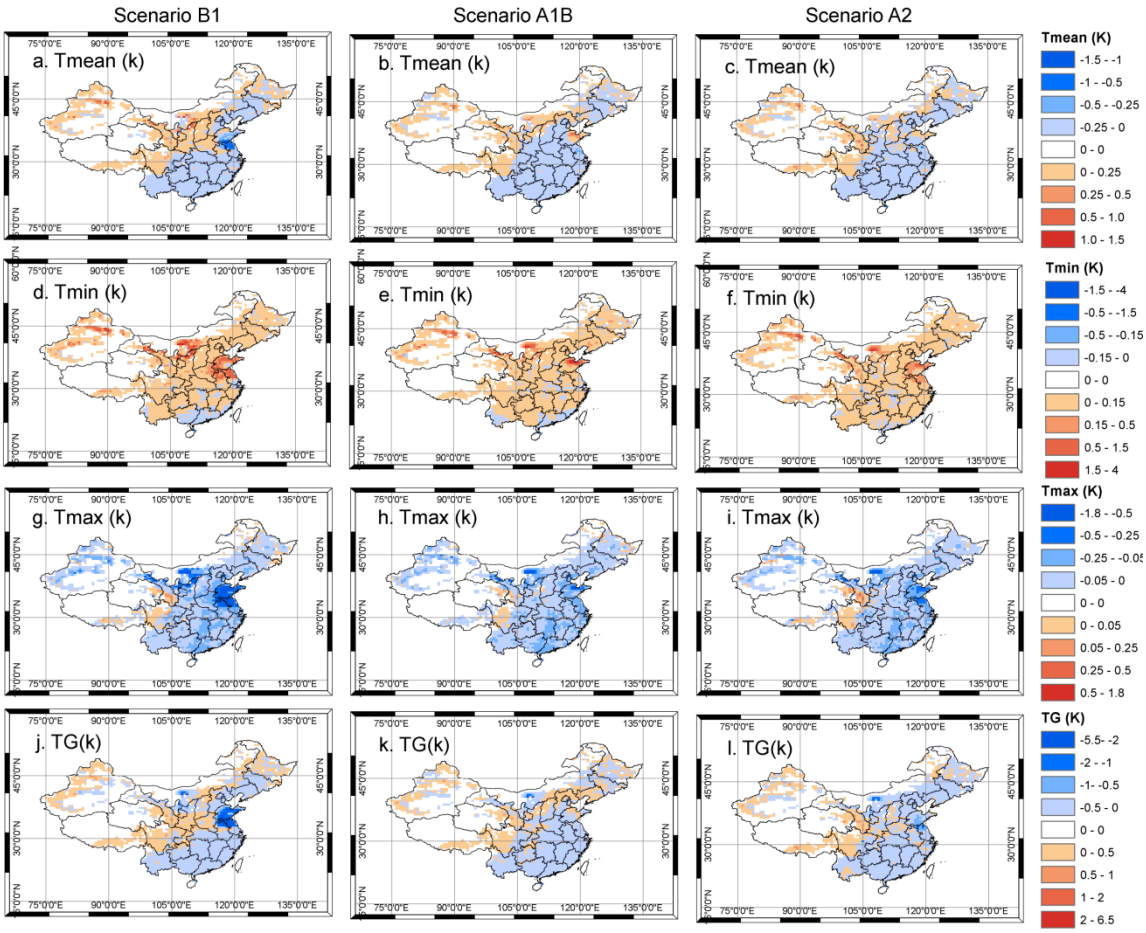

Figure 4-6 Spray irrigation impact on temperature in 2050 under three future scenarios

Temporally, Tmax decreases throughout the whole year and the biggest decrease of Tmax is in summer (JJA) in the future simulations (Figure 4-8). Tmin decreases in summer (JJA) and increases in other seasons in irrigation simulation in the future simulations. The biggest Tmin increase is in winter (DJF). The impact of irrigation on daily Tmean depends more on its impact on Tmax in summer time (JJA) and depends more on Tmin in other seasons. As a result, daily Tmean decreases in summer and increases in other seasons. Finally, irrigation leads to an increase in annual Tmean in most of cases in the future irrigation simulations (Table 4-15 to Table 4-20).

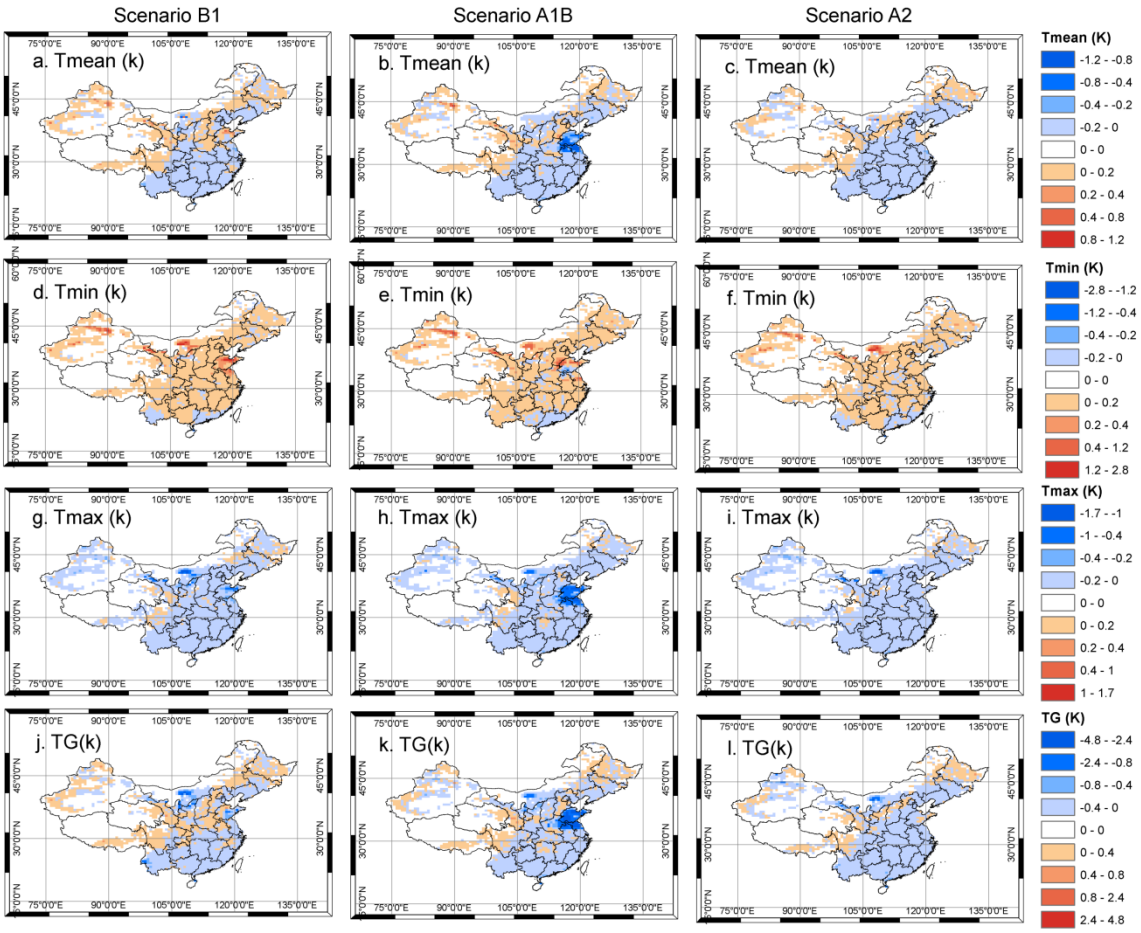

Figure 4-7 Spray irrigation impact on temperature in 2100 under three future scenarios

Generally, irrigation shows more impact on Tmin than Tmax with opposite direction under the future scenarios. For example, nationally, spray irrigation simulated by the CLM led to an increase in annual Tmin of 0.031K under scenario A1B, 0.031 under scenario A2, and 0.057 under scenario B1 and an decrease in annual Tmax of 0.022 under scenario A1B, 0.022 under scenario A2, and 0.045 under scenario B1 in 2050.

Comparing the impacts of irrigation with those of land cover change in the future simulations shows that land cover change has more impact on temperature than irrigation. For example, under scenario A1B in 2050, the difference between two LCLUC simulations shows, nationally, the annual mean Tmean, Tmin, and Tmax

increased 0.083K, 0.100K, and 0.131K due to LCLUC, respectively (Table 4-15). The Tmean change due to LCLUC is 83 times as much as the Tmean change due to spray irrigation (0.001 K). The Tmin change due to LCLUC is 3 times as much as the Tmin change due to spray irrigation (0.031 K). The Tmax change due to LCLUC is 6 times as much as the Tmax change due to spray irrigation (0.022 K). I also compared the magnitude of the impacts of irrigation with those of land cover change in the future simulations by t-test (Table 4-21) and results show that the impact of LCLUC on temperature are significantly higher than the impact of irrigation on temperature in the future. In other words, this study suggests that changes in land management are not comparable to changes in land cover over China in the future in terms of their impact on temperature.

Comparing irrigation simulations in the past (IRRc_2000 and IRRg_2000, Table 4-13) with those in the future (e.g. IRRc_A1B_2050 and IRRg_A1B_2050 etc., Table 4-15to Table 4-20), we can find the irrigation has less impact on Tmax and Tmean in the future. For example, nationally, spray irrigation leads to a decrease in Tmax of 0.022 K in IRRc_A1B_2050 experiment, which is as much as 28% of that (0.079 K) in IRRc_2000 experiment. Spray irrigation leads to a decrease in Tmean of 0.001 in IRRc_A1B_2050 experiment, which is as much as 2% of that (0.045 K) in IRRc_2000 experiment. The reduced impacts of irrigation on Tmax and Tmean in the future are caused by the reduced evaporative cooling effect. Nationally, the decreased wind speed and downward shortwave radiation projected in the future forcing data may contribute to the decrease of ET in the future simulations. Besides, in future scenarios, the increased precipitation in non-irrigated area reduce the difference of

water capability between irrigated and non-irrigated area and contribute the decreased difference of ET between irrigated and non-irrigated area.

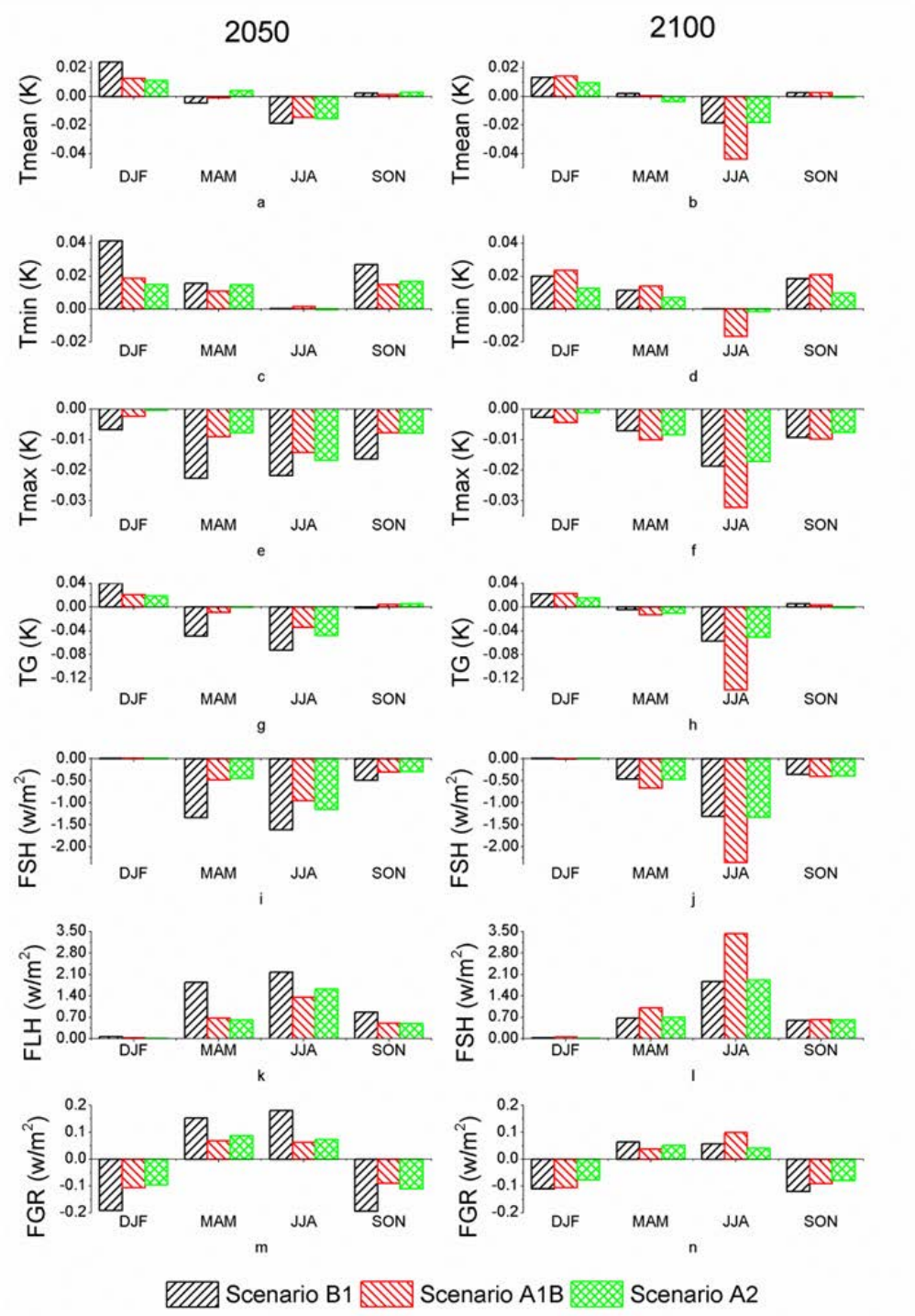

Figure 4-8 Mean irrigation impact during four seasons in 2050 and 2100 and under three scenarios

Comparing LCLUC simulations in the past (LCLUC_2000 and LCLUC_1980, Table 4-13) with those (e.g. LCLUC2000_A1B_2050 and LCLUC1980_A1B_2050 etc., Table 4-15 to Table 4-20) in the future, we can find the LCLUC generally has more impact on Tmax in the future. Nationally, LCLUC leads to an increase in Tmax of 0.131 K under scenario A1B, 0.041 K under scenario A2 and 0.133 K under scenario B1 in 2050, and leads to an increase in Tmax of 0.143 K under scenario A1B, 0.134 K under scenario A2 and 0.137 K in 2100. Transferring land status from 1980 to 2000 in the contemporary LCLUC simulation shows an increase in Tmax of 0.071K, averaged over the whole of china (Table 4-13).

4.3 Conclusions

In this study, I simulated both the irrigation impacts and land cover change impacts on climate in China in one past time period(1978-2004) and in two future time periods (2050 and 2100) via the Community Land Model. By comparing the differences among those simulations, I found that:

1) The irrigation pattern has a statistically significant different impact on local climate in terms of the magnitude of their impact.

2) Irrigation shows more impacts on Tmax than Tmin. Moreover, the irrigation impact on Tmin is more complicated than the impact on Tmax. Both contemporary and future irrigation simulations show, nationally, irrigation decreases Tmax but increases Tmin. Tmean is a combination of Tmax and Tmin. Tmean decreases in contemporary irrigation simulations but increases in most of cases in future irrigation simulations. In general, results from this study do not support the former argument that irrigation might mask the warming signal caused by an increase

in greenhouse gases. Furthermore, the irrigation impact on temperature is much less in the future than in the 20th Century because the evaporative cooling effect will decrease as a result of increased precipitation, decreased downward shortwave radiation and decreased wind speed in the future scenarios.

3) The irrigation and land cover change show statistically significant differences in terms of the magnitude of their impact on local climate in this study. Overall, LCLUC shows more impacts on climate in both contemporary and future simulations. Nationally, the differences of the impact magnitude between LCLUC and spray irrigation are -0.008K for Tmax, 0.089K for Tmin, and 0.04K for Tmean in 20^{th} Century, respectively. In the future scenarios, the differences of the impact magnitude between LCLUC and spray irrigation range from 0.019K to 0.111K for Tmax, from 0.035K to 0.087K for Tmin, and from 0.021K to 0.085K, respectively.

Chapter 5 Conclusions

Land cover and land use change can significantly influence the climate system by modulating surface-atmosphere exchanges. Land management, such as irrigation also has a profound influence on the climate system. Irrigation can alter the water and energy flux from ground surface to the atmosphere and further influence near surface climate. Considering its dramatic expansion during the last century, the widespread use of irrigation has had an ongoing impact on our climate system. However, until now, this relationship between increased irrigation and its effect on climate system change has not received the serious examination, and attention deserves.

In this dissertation, I used both observational and modeling methods to explore the impact of irrigation in China. The main goals are to explore what might have happened in the past, what will happen as a result of irrigation expansion in the future and what is the relationship between LCLUC impact and irrigation impact on near surface climate in China. To answer those questions, I undertook three tasks in this dissertation.

First, I developed a set of irrigation potential indices by using time series NDVI and precipitation data. Based on these indices, I further developed an irrigation spatial allocation model to allocate the statistics of irrigation from geopolitical units to individual pixels. Finally, I made an irrigation map of China in 2000 and three secondary products (irrigated dryland area, irrigated paddy field and rainfed area).

Second, I analyzed land surface parameters and near surface temperature observations in irrigated and non-irrigated agriculture areas in two study areas of

China. One is Jilin province in which both satellite and meteorological observations were used. Another much larger area is North China including 17 provinces where only satellite observations were used.

Third, I simulated the irrigation and LCLUC impacts over China in the past and also two future time periods (2050 and 2100) under three scenarios by the CLM and compared the impact of irrigation with that of LCLUC. Unlike irrigation simulations in previous studies, I developed a time series gridded datasets of annual irrigation water withdrawal in China from 1978 to 2008 by using the historical effective irrigated area and agricultural water withdrawal data, and used this dataset to control the irrigation amount.

The main findings and contributions of this dissertation are summarized in 5.1 and 5.2, respectively. Section 5.3 describes future research directions.

5.1 Main findings

Meteorological observations in Jilin Province show that the temperature differences between highly and lightly irrigated areas are statistically significant. The differences are highly correlated to the effective irrigation area (EIA), sown area of crops (CSA) and as well as the standard precipitation index for a 12 month rainfall total (SPI12) of the LIP sites. Moreover, the temperature difference between highly and lightly irrigated areas is larger in a drier year.

Results from satellite observation show that the land surface parameters of irrigated areas had obvious intra-annual variations. Highly irrigated areas corresponded to a lower albedo and daytime LST, and higher NDVI and ET. And the difference between highly and lightly irrigated areas is bigger in drier areas.

Consistent with other studies, irrigation from both observational and modeling studies in this dissertation also displayed a larger impact on the maximum air temperature than on the minimum air temperature. The irrigation impact on minimum air temperature/nighttime LST is more complicated. Both contemporary and future irrigation simulations show, nationally, that irrigation decreases Tmax but increases Tmin. Tmean decreases in contemporary irrigation simulations but increases in most of cases in future irrigation simulations. Irrigation impact on temperature is much less in the future than in the 20th Century. In general, results from this study do not support the former argument that irrigation might mask the warming signal caused by an increase in greenhouse gases. This study indicates that the irrigation pattern has a statistically significant different impact on local climate in terms of the magnitude of its impact. Besides, LCLUC shows a much greater impact on climate than irrigation in both contemporary and future simulations.

5.2 Main contributions

The irrigation map of China around 2000 produced in this dissertation is the first irrigation map which focuses only on China .The validation results show my new map has the highest overall accuracy, which indicates that my method is a promising tool for mapping irrigated areas. Besides, my method also has several advantages. First, its inputs are quite simple, and no training samples are needed. Second, my model is general and repeatable. Third, it can be used to map historically irrigated areas.

This dissertation is the first study which focuses solely on China, systematically using both satellite and meteorological observation and also a

modeling method. The studies in Jilin province and North China provide some substantive evidence that a cooling effect from agricultural irrigation exists in China. Moreover, this study proved that satellite observations are sufficiently valid to determine the impact of irrigation on land surface parameters, and provide another valuable method for understanding the impact of irrigation on local climate, especially in those regions where direct observations are limited or obscured by other factors, such as urbanization in China.

In this study, I developed time series gridded dataset of annual irrigation water withdrawal in China from 1978 to 2008 by using the historical effective irrigated area and agricultural water withdrawal data. These new maps are the first gridded datasets that portray a spatially explicit distribution of the actual water withdrawal for both irrigated paddy fields and drylands in China, with a higher resolution and covering a longer time period. The time series gridded datasets of annual irrigation water withdrawal in China from 1978 to 2008 can help accurately simulate the irrigation impact on the near surface climate in China. Furthermore, the new dataset can improve our ability to estimate the crop yield, water stress, drought resistance, and water use efficiency in China.

In previous studies, no one has simulated both land cover change impacts and land management (irrigation) impacts on local climate at the same time. So, results from direct comparisons between irrigation impact and LCLUC impact have not been reported yet. This study simulated both the irrigation impact and land cover change impact on climate in China in one previous time period (1978-2004) and two future

time periods (2050 and 2100) via the Community Land Model and compared the differences among those simulations.

5.3 Future directions

Both the observational and the modeling studies need information on the distribution of irrigated areas. To date, there are three irrigation maps covering mainland China: The FAO/ University of Frankfurt global map of irrigated areas with a fraction of 5 arc-minutes by 5 arc-minutes cells (Siebert et al. 2007) , the International Water Management Institute (IWMI)'s Global Map of Irrigated Area (Thenkabail et al. 2009) with a 10 km grid resolution, and the new irrigation map of China 2000 with a 1-km resolution developed in this study. Based on my validation, my map has the highest overall accuracy (68.40%), but the accuracy still has room for improvement. Errors in irrigation map certainly will lead to the uncertainty in irrigation simulations. Therefore, a highly accurate irrigation map is needed. Besides, more validation of the current irrigation map is also needed.

The study on the irrigation impact by meteorological observations in Jilin Province provides some substantive evidence that a cooling effect from agricultural irrigation exists in China. However, this conclusion does not mitigate the other factors that influence the air temperature of the study sites, since the climate system is so complex. No single factor can be attributed to regional climate changes. More observations and evidence are needed in order to attain a greater understanding of the influence of irrigation on local climate in China, especially in wetter area of China.

The study on the irrigation impact by satellite observations in Jilin Province and North China proved that satellite observations are sufficiently valid to determine

the impact of irrigation on land surface parameters, and provide another valuable method for understanding the impact of irrigation on local climate, especially in those regions where direct observations are limited or obscured by other factors, such as urbanization in China. However, the performance of satellite observations in studying the irrigation impact in wetter areas was not validated in this dissertation. In wet areas, supplemental irrigation is the main irrigation method and the difference in soil moisture between non-irrigated and irrigated areas is likely to be very slight. As a result, the climate difference caused by extra irrigation water in an irrigated area with a wetter climate may be not as clear as that in irrigated areas with a dry climate, which contributes to the difficultly of validating the performance of satellite observations in wet areas. In future, the performance of satellite observations in studying the irrigation impact in wetter areas needs to be validated.

Besides, there are still some other limitations to my irrigation simulations. First, I developed time series gridded datasets of annual irrigation water withdrawal in China from 1978 to 2008 and used this dataset to control irrigation amount in modeling. However, there are some uncertainties in this dataset due to several factors:

1) Agricultural water is withdrawn not only for irrigation purposes but also for other agricultural sectors such as fisheries. Irrigation is not only applicable to cropland management, but also to forestry and pasture management. In my method, I collected the ratio of irrigation water withdrawal to agricultural water withdrawal for the year 2000, and used this data over the whole study period. However, the ratio of irrigation water withdrawal for farmland is estimated to decrease with time, as more and more agricultural water is consumed by forestry, pasture, and fishery sectors

because of changes in the agricultural structure. As a result, the irrigation water withdrawal before 2000 calculated using my method might be underestimated.

2) In my method, I used the irrigation map of China for 2000 to represent the irrigated area from 1978 to 2008 and ignored the changes in the irrigated area over the past 31 years. The lack of archived information makes it impossible to obtain a time-series irrigation map in China for this period. The extent of the irrigated area in 2000 is clearly larger than that in 1978; consequently, the irrigation water for irrigated pixels in 1978 is expected to be overestimated. Conversely, the irrigation water of irrigated pixels in 2008 is expected to be underestimated.

3) The irrigated area in the irrigation maps shows areas that were equipped for irrigation (it is also called as effective irrigation area (EIA), not the real irrigated area. The real irrigated area might be larger or smaller than the EIA. Accordingly, the real irrigation water consumption will be slightly different from my estimation.

4) The irrigation percentages of the paddy fields and dryland in each irrigated pixel in 2000 derived from the new irrigation map of China are used as an estimate of the same ratio over the whole study period (1978-2008). However, the area of irrigated paddy fields and dryland changed during those years.

5) In my method, I used the irrigation requirements for the main crops reported by Liu et al. (2009) to estimate the irrigation water consumption for each main crop in a given province. The irrigation requirements reported by Liu et al. are provincial average estimates from 1970 to 2000. However, the real irrigation requirements vary year–by-year and pixel-by-pixel, as a function of the different climate and soil conditions.

Second, to simulate irrigation impact in the future, I first estimated the irrigation requirement (IR) in two future time periods (2050 and 2100) under three scenarios (B1, A1B and A2) and further calculated the irrigation water withdrawal in the future by combining the future IR and mean irrigation water withdrawal during 1978-2008. There are some limitations in IR estimation:

1) I assumed that the cropland area and growing season would remain unmodified by climate change. Considering the higher temperatures of the future, however, both cropland area and sowing date might change. Increased CO2 concentrations may also directly affect crop transpiration by decreasing bulk stomatal conductance and influence the evapotranspiration generated by crops in the future. These considerations are beyond the scope of my current study.

2) I estimated IR simply from the difference between evapotranspiration and effective precipitation. IR is impacted not only by climate factors (temperature, downward solar radiation, precipitation, etc.) but also by factors such as the water-holding capacity of soil. Information about soil type, soil context, and soil moisture are difficult to get. I ignored IR differences owing to the water-holding capacities of soil in this study.

3) I calculated the net IR, not the actual IR. Actual IR, but not net IR, can reflect actual agricultural water requirements and water stress. Actual IR is the total water requirement of the procedure of transferring irrigation water from water resources (rivers, reservoirs, and aquifers) to fields. To calculate actual IR, more information is needed, especially irrigation water use efficiency; however, changes in irrigation water use efficiency differ from province to province owing to the

differences in financial investment by local government, current development level, and the improvement potential of irrigation systems. In future, a more complex method for estimating future IR is needed.

Third, the CLM cannot simulate paddy rice which is the dominant crop type in South China. So, in this dissertation, I did not distinguish rice from other crop types, and treat all crops as the same. However, paddy rice has very different biophysics and biochemical characteristics from wheat and corn, both of which can be simulated by CLM. Paddy rice has more drainage and runoff loss and also releases more methane, an important greenhouse gas. Hence, paddy rice should be added in the CLM in a future study.

Finally, my irrigation simulation is based on the CLM offline mode rather than CLM online mode in order to save computing time. It will cost one month to do a 10-year run with coupled CLM on a server with 20 processes and 24G system memory. In my dissertation, I designed 28 experiments; 4 of them are 27-year runs and another 24 of them are 50-year runs. Finishing the 28 experiments by coupled CLM needs several years. This significant temporal component for analysis is beyond the scope of this research. Finally, I used the offline CLM in this dissertation. However, the offline mode might underestimate the irrigation impact on near surface climate because the offline mode cannot reflect the indirect cooling effect such as cooling from an increase in cloud-reflected solar radiation. As a result, the finding that at national scale, changes in land management are not comparable to changes in land cover in terms of their effects on the climate of China, need to be validated by coupling CLM with CAM.

This study has significant implications for policy making at both national- and provincial-levels makers regarding food security in China. As the most populous country in the world, China always faces challenges for food security. The country has less than 10% of the world's arable land to feed its 1.3 billion people (Wu et al. 2010). Arable land and available water resources are distributed unevenly in China. Most arable lands are concentrated near river valleys and along the southern and eastern coasts. The North China Plain is the biggest agricultural area but has access to only own 24% of the total fresh water available in China. South China has abundant water and fertile soils, but available cropland has shrunk significantly during past decades owing to the urbanization and the expansion of large-scale industry (Deng et al. 2009; Liu et al. 2008; Liu and Tian 2010). To realize self-sufficiency in food production, China has undertaken large-scale programs to increase agricultural production, such as using chemical pesticides and fertilizers, developing new strains of genetically modified crops, and investing in irrigation infrastructure. Among those measures, agricultural irrigation has been reported to have made the largest contribution to crop yield increase and poverty reduction in rural areas (Huang et al. 2006). The information about the amount and extent of currently irrigated area provides a data support for land management department to make polices related to land use/management. For example, how much irrigated area will be needed and how much rainfed cropland needs to be transformed into irrigated cropland in order to afford the increased population.

The time series gridded dataset of annual irrigation water withdrawal from 1978 to 2008 produced in this study and the future irrigation water withdrawal

estimated in this study also have some implications for policy makers on water security in China. Water use can be divided into domestic, industrial, agricultural, and ecological uses. Agricultural use includes water for farmland irrigation, forestry, animal husbandry, and fisheries. The water use structure of China is changing along with economic development. More and more water has been diverted to the industrial, ecological, and domestic sectors. The irrigation water for farmland is also shrinking. To achieve sustainable economic development and satisfy increased requirements needed to supply food for an expanding population, the government must develop appropriate water management strategies to harmonize the water use structure among different sectors as well as within the agricultural sector The information about the amount and distribution of irrigation water consumption help water management department to estimate the total water consumption and water use efficiency, locate the hotspots with high water stress, develop optimized water use structure and smartly invest in water infrastructure, irrigation systems, and irrigation equipment.

The results about impact of irrigation from this dissertation contribute to a better understanding of the irrigation impact on near-surface climate which can improve our knowledge of how human activities influence climate, guide future policies aimed at mitigating or adapting to climate change, and help design better models to project the impact of irrigation on the climate system and irrigation requirements in the future.

Reference

Adegoke, J.O., Pielke, R.A., Eastman, J., Mahmood, R., & Hubbard, K.G. (2003). Impact of irrigation on midsummer surface fluxes and temperature under dry synoptic conditions: A regional atmospheric model study of the U.S. high plains. *Monthly Weather Review, 131*, 556-564

Barnston, A.G., & Schickedanz, P.T. (1984). The effect of irrigation on warm season precipitation in the southern great plains. *Journal of Climate and Applied Meteorology, 23*, 865-888

Beltran, C.M., & Belmonte, A.C. (2001). Photogrammetric Irrigated Crop Area Estimation Using Landsat TM Imagery in La Mancha, Spain. *Engineering & Remote Sensing, 67*, 1177-1184

Biggs, T.W., Scott, C.A., Gaur, A., Venot, J.P., Chase, T., & Lee, E. (2008). Impacts of irrigation and anthropogenic aerosols on the water balance, heat fluxes, and surface temperature in a river basin. *Water Resources Research, 44*

Biggs, T.W., Thenkabail, P.S., Gumma, M.K., Scott, C.A., Parthasapadhi, G.R., & Turral, H.N. (2006). Parthasapadhi and H.N. Turral. Irrigated area mapping in heterogeneous landscapes with MODIS time series, ground truth and census data, Krishna Basin, India. *International Journal of Remote Sensing, 27*, 4245-4266

Boken, V.K., Hoogenboom, G., Kogan, F.N., Hook, J.E., Thomas, D.L., & Harrison, K.A. (2004). Potential of using NOAA-AVHRR data for estimating irrigated area to help solve an inter-state water dispute. *International Journal of Remote Sensing, 25*, 2277 — 2286

Bondeau, A., Smith, P.C., Zaehle, S., Schaphoff, S., Lucht, W., Cramer, W., & Gerten, D. (2007). Modelling the role of agriculture for the 20th century global terrestrial carbon balance. *Global Change Biology, 13*, 679-706

Bonfils, C., & Lobell, D. (2007). Empirical evidence for a recent slowdown in irrigation-induced cooling. *Proceedings of the National Academy of Sciences of the United States of America, 104*, 13582-13587

Boucher, O., Myhre, G., & Myhre, A. (2004). Direct human influence of irrigation on atmospheric water vapour and climate. *Climate Dynamics, 22*, 597-603

Carlson, T.N., & Arthur, S.T. (2000). The impact of land use - land cover changes due to urbanization on surface microclimate and hydrology: a satellite perspective. *Global and Planetary Change, 25*, 49-65

Chow, K.C., Tong, H.W., & Chan, J.C.L. (2008). Water vapor sources associated with the early summer precipitation over China. *Climate Dynamics, 30*, 497-517

Christy, J.R., Norris, W.B., Redmond, K., & Gallo, K.P. (2006). Methodology and results of calculating central California surface temperature trends: Evidence of human-induced climate change? *Journal of Climate, 19*, 548-563

Ciganda, V., Gitelson, A., & Schepers, J. (2009). Non-destructive determination of maize leaf and canopy chlorophyll content. *Journal of Plant Physiology, 166*, 157-167

de Rosnay, P., Polcher, J., Laval, K., & Sabre, M. (2003). Integrated parameterization of irrigation in the land surface model ORCHIDEE. Validation over Indian Peninsula. *Geophysical Research Letters, 30*

Deng, J.S., Wang, K., Hong, Y., & Qi, J.G. (2009). Spatio-temporal dynamics and evolution of land use change and landscape pattern in response to rapid urbanization. *Landscape and Urban Planning, 92*, 187-198

Devries, D.A. (1959). The influence of irrigation on the energy balance and the climate near the ground. *Journal of Meteorology, 16*, 256-270

Dheeravath, V., Thenkabail, P.S., Chandrakantha, G., Noojipady, P., Reddy, G.P.O., Biradar, C.M., Gumma, M.K., & Velpuri, M. (2010). Irrigated areas of India derived using MODIS 500 m time series for the years 2001-2003. *Isprs Journal of Photogrammetry and Remote Sensing, 65*, 42-59

Dirmeyer, P.A., & Shukla, J. (1994). Albedo as a modulator of climate response to tropical deforestation. *Journal of Geophysical Research-Atmospheres, 99*, 20863-20877

Doll, P., & Siebert, S. (2002). Global modeling of irrigation water requirements. *Water Resources Research, 38*

Döll, P., & Siebert, S. (1999). A Digital Global Map of Irrigated Areas. *Report A9901, Center for Environmental Systems Research, University of Kassel, Kurt Wolters Strasse 3, 34109 Kassel, Germany.*

Douglas, E.M., Beltran-Przekurat, A., Niyogi, D., Pielke, R.A., & Vorosmarty, C.J. (2009). The impact of agricultural intensification and irrigation on land-atmosphere interactions and Indian monsoon precipitation - A mesoscale modeling perspective. *Global and Planetary Change, 67*, 117-128

Douglas, E.M., Niyogi, D., Frolking, S., Yeluripati, J.B., Pielke, R.A., Niyogi, N., Vorosmarty, C.J., & Mohanty, U.C. (2006). Changes in moisture and energy fluxes due to agricultural land use and irrigation in the Indian Monsoon Belt. *Geophysical Research Letters, 33*

Durbin, J., & Watson, G. (1950). Testing for Serial Correlation in Least Squares Regression, I. *Bimoetrika, 37*

El-Magd, Abou, I., & Tanton, T.W. (2003). Improvements in land use mapping for irrigated agriculture from satellite sensor data using a multi-stage maximum likelihood classification. *International Journal of Remote Sensing, 24*, 4197-4206

FAO (1992). CROPWAT-A Computer Program for Irrigation Planning and Management. *FAO Irrigation and Drainage Paper NO.46*: Food and Agriculture Organization, Rome

FAO (2003). World Agriculture: Towards 2015/2030. *Food and Agricultural Organization (FAO), Viale delle Teme di Caracalla, 00100 Rome, Italy. ISBN 92 5 104835 5 (FAO paperback).*

Fensholt, R., Sandholt, I., & Rasmussen, M.S. (2004). Evaluation of MODIS LAI, fAPAR and the relation between fAPAR and NDVI in a semi-arid environment using in situ measurements. *Remote Sensing of Environment, 91*, 490-507

Geerts, B. (2002). On the effects of irrigation and urbanisation on the annual range of monthly-mean temperatures. *Theoretical and Applied Climatology, 72*, 157-163

Goldewijk, K.K., Beusen, A., van Drecht, G., & de Vos, M. (2011). The HYDE 3.1 spatially explicit database of human-induced global land-use change over the past 12,000 years. *Global Ecology and Biogeography, 20*, 73-86

Gordon, L.J., Steffen, W., Jonsson, B.F., Folke, C., Falkenmark, M., & Johannessen, A. (2005). Human modification of global water vapor flows from the land surface. *Proceedings of the National Academy of Sciences of the United States of America, 102*, 7612-7617

Haddeland, I., Lettenmaier, D.P., & Skaugen, T. (2006). Effects of irrigation on the water and energy balances of the Colorado and Mekong river basins. *Journal of Hydrology, 324*, 210-223

Hargreaves, G.H., & Samani, Z.A. (1982). Estimating of potential evapotranspiration. *J.of Irrg. Drainage DIv., Proceeding of American Society of Civil Engineers, 108*, 223-230

He, R.Z., & Lu, X.P. (2007). Analysis of potential agricultural water-saving and efficient agrcitural countermeasure in Sichuan Province. *3rd Technique Youth Forum of Chinese Hydraulic Engineering Society.(In chinese)*

Hijmans, R.J., Cameron, S.E., Parra, J.L., Jones, P.G., & Jarvis, A. (2005). Very high resolution interpolated climate surfaces for global land areas. *International Journal of Climatology, 25*, 1965-1978

Houghton, R.A., & Hackler, J.L. (2003). Sources and sinks of carbon from land-use change in China. *Global Biogeochemical Cycles, 17*

Huang, Q.Q., Rozelle, S., Lohmar, B., Huang, J.K., & Wang, J.X. (2006). Irrigation, agricultural performance and poverty reduction in China. *Food Policy, 31*, 30-52

Hurtt, G.C., Frolking, S., Fearon, M.G., Moore, B., Shevliakova, E., Malyshev, S., Pacala, S.W., & Houghton, R.A. (2006). The underpinnings of land-use history: three centuries of global gridded land-use transitions, wood-harvest activity, and resulting secondary lands. *Global Change Biology, 12*, 1208-1229

Jackson, T.L., Feddema, J.J., Oleson, K.W., Bonan, G.B., & Bauer, J.T. (2010). Parameterization of Urban Characteristics for Global Climate Modeling. *Annals of the Association of American Geographers, 100*, 848-865

Kalnay, E., & Cai, M. (2003). Impact of urbanization and land-use change on climate. *Nature, 423*, 528-531

Kanamaru, H., & Kanamitsu, M. (2008). Model Diagnosis of Nighttime Minimum Temperature Warming during Summer due to Irrigation in the California Central Valley. *Journal of Hydrometeorology, 9*, 1061-1072

Kendy, E., Zhang, Y.Q., Liu, C.M., Wang, J.X., & Steenhuis, T. (2004). Groundwater recharge from irrigated cropland in the North China Plain: case study of Luancheng County, Hebei Province, 1949-2000. *Hydrological Processes, 18*, 2289-2302

Khan, S., Hanjra, M.A., & Mu, J.X. (2009). Water management and crop production for food security in China: A review. *Agricultural Water Management, 96*, 349-360

Kucharik, C.J., Brye, K.R., Norman, J.M., Foley, J.A., Gower, S.T., & Bundy, L.G. (2001). Measurements and modeling of carbon and nitrogen cycling in agroecosystems of southern Wisconsin: Potential for SOC sequestration during the next 50 years. *Ecosystems, 4*, 237-258

Kueppers, L.M., Snyder, M.A., & Sloan, L.C. (2007). Irrigation cooling effect: Regional climate forcing by land-use change. *Geophysical Research Letters, 34*

Kueppers, L.M., Snyder, M.A., Sloan, L.C., Cayan, D., Jin, J., Kanamaru, H., Kanamitsu, M., Miller, N.L., Tyree, M., Due, H., & Weare, B. (2008). Seasonal temperature responses to land-use change in the western United States. *Global and Planetary Change, 60*, 250-264

Lawrence, P.J., & Chase, T.N. (2007). Representing a new MODIS consistent land surface in the Community Land Model (CLM 3.0). *Journal of Geophysical Research-Biogeosciences, 112*, 17

Lean, J., & Rowntree, P.R. (1997). Understanding the sensitivity of a GCM simulation of Amazonian deforestation to the specification of vegetation and soil characteristics. *Journal of Climate, 10*, 1216-1235

Lee, E., Chase, T.N., Rajagopalan, B., Barry, R.G., Biggs, T.W., & Lawrence, P.J. (2009). Effects of irrigation and vegetation activity on early Indian summer monsoon variability. *International Journal of Climatology, 29*, 573-581

Li, Q.S., Willardson, L.S., Deng, W., Li, X.J., & Liu, C.J. (2005). Crop water deficit estimation and irrigation scheduling in western Jilin province, Northeast China. *Agricultural Water Management, 71*, 47-60

Liang, S. (2004). Quantitative Remote Sensing of Land Surfaces *John Wiley and Sons, Inc*, 534

Liu, J., Liu, M., Deng, X., Zhuang, D., Zhang, Z., & Luo, D. (2002). The land use and land cover change database and its relative studies in China. *Journal of Geographical Sciences, 12*, 275–282

Liu, J., Liu, M., Tian, H., Zhuang, D., Zhang, Z., Zhang, W., Tang, X., & Deng, X. (2005a). Spatial and temporal patterns of China's cropland during 1990–2000: An analysis based on Landsat TM data. *Remote Sensing of Environment, 98*, 442-456

Liu, J.Y., Liu, M.L., Tian, H.Q., Zhuang, D.F., Zhang, Z.X., Zhang, W., Tang, X.M., & Deng, X.Z. (2005b). Spatial and temporal patterns of China's cropland during 1990-2000: An analysis based on Landsat TM data. *Remote Sensing of Environment, 98*, 442-456

Liu, J.Y., Tian, H.Q., Liu, M.L., Zhuang, D.F., Melillo, J.M., & Zhang, Z.X. (2005c). China's changing landscape during the 1990s: Large-scale land transformations estimated with satellite data. *Geophysical Research Letters, 32*, 5

Liu, M.L., & Tian, H.Q. (2010). China's land cover and land use change from 1700 to 2005: Estimations from high-resolution satellite data and historical archives. *Global Biogeochemical Cycles, 24*, 18

Liu, Y., Wang, L., Ni, G.H., & Cong, Z.T. (2009). Spatial distribution characteristics of irrigation water requirement for main crops in China. *Transactions of the CSAE, 25*, 6-12. (In Chinese)

Liu, Y.S., Wang, L.J., & Long, H.L. (2008). Spatio-temporal analysis of land-use conversion in the eastern coastal China during 1996-2005. *Journal of Geographical Sciences, 18*, 274-282

Lobell, D., Bala, G., Mirin, A., Phillips, T., Maxwell, R., & Rotman, D. (2009). Regional Differences in the Influence of Irrigation on Climate. *Journal of Climate, 22*, 2248-2255

Lobell, D.B., Bala, G., Bonfils, C., & Duffy, P.B. (2006a). Potential bias of model projected greenhouse warming in irrigated regions. *Geophysical Research Letters, 33*

Lobell, D.B., Bala, G., & Duffy, P.B. (2006b). Biogeophysical impacts of cropland management changes on climate. *Geophysical Research Letters, 33*, 4

Lobell, D.B., & Bonfils, C. (2008). The effect of irrigation on regional temperatures: A spatial and temporal analysis of trends in California, 1934-2002. *Journal of Climate, 21*, 2063-2071

Lobell, D.B., Bonfils, C.J., Kueppers, L.M., & Snyder, M.A. (2008). Irrigation cooling effect on temperature and heat index extremes. *Geophysical Research Letters, 35*

Lohar, D., & Pal, B. (1995). The effect of irrigation on premonsoon season precipitation over south-west Bengal, India. *Journal of Climate, 8*, 2567-2570

Mahmood, R., Foster, S.A., Keeling, T., Hubbard, K.G., Carlson, C., & Leeper, R. (2006). Impacts of irrigation on 20th century temperature in the northern Great Plains. *Global and Planetary Change, 54*, 1-18

Mahmood, R., Hubbard, K.G., & Carlson, C. (2004). Modification of growing-season surface temperature records in the northern Great Plains due to land-use transformation: Verification of modelling results and implication for global climate change. *International Journal of Climatology, 24*, 311-327

Maisongrande, P., Duchemin, B., & Dedieu, G. (2004). VEGETATION/SPOT: an operational mission for the Earth monitoring; presentation of new standard products. *International Journal of Remote Sensing, 25*, 9-14

Menon, S., Hansen, J., Nazarenko, L., & Luo, Y.F. (2002). Climate effects of black carbon aerosols in China and India. *Science, 297*, 2250-2253

Mitchell, A. (2005). The ESRI Guide to GIS Analysis. *ESRI Press, 2*

Moore, N., & Rojstaczer, S. (2001). Irrigation-induced rainfall and the great plains. *Journal of Applied Meteorology, 40*, 1297-1309

Njoku, E.G. (2005). AMSR-E/Aqua daily L3 surface soil moisture, interpretive parms, & QC EASE-Grids,Jan 2005 to Dec 2006. *Boulder, CO, USA: National Snow and Ice Data Center.Digital media. Availabe at https://wist.echo.nasa.gov/api/*.

Nobre, C.A., Sellers, P.J., & Shukla, J. (1991). Amazonian deforestation and regional climate change. *Journal of Climate, 4*, 957-988

Owen, T.W., Carlson, T.N., & Gillies, R.R. (1998). An assessment of satellite remotely-sensed land cover parameters in quantitatively describing the climatic effect of urbanization. *International Journal of Remote Sensing, 19*, 1663-1681

Ozdogan, M., & Gutman, G. (2008). A new methodology to map irrigated areas using multi-temporal MODIS and ancillary data: An application example in the continental US. *Remote Sensing of Environment, 112*, 3520-3537

Ozdogan, M., Rodell, M., Beaudoing, H.K., & Toll, D.L. (2010). Simulating the Effects of Irrigation over the United States in a Land Surface Model Based on Satellite-Derived Agricultural Data. *Journal of Hydrometeorology, 11*, 171-184

Pachauri, R.K., & Reisinger, A. (Eds.) (2007). *Climate Change 2007: Synthesis Report*: IPCC, Geneva, Switzerland

Paruelo, J.M., Epstein, H.E., Lauenroth, W.K., & Burke, I.C. (1997). ANPP estimates from NDVI for the Central Grassland Region of the United States. *Ecology, 78*, 953-958

Paul, M.J., & Meyer, J.L. (2001). Streams in the urban landscape. *Annual Review of Ecology and Systematics, 32*, 333-365

Piao, S.L., Fang, J.Y., Zhou, L.M., Guo, Q.H., Henderson, M., Ji, W., Li, Y., & Tao, S. (2003). Interannual variations of monthly and seasonal normalized difference vegetation index (NDVI) in China from 1982 to 1999. *Journal of Geophysical Research-Atmospheres, 108*, 13

Portmann, F.T., Siebert, S., & Doll, P. (2010). MIRCA2000-Global monthly irrigated and rainfed crop areas around the year 2000: A new high-resolution data set for agricultural and hydrological modeling. *Global Biogeochemical Cycles, 24*, 24

Pu-te, W. (2010). Strategic considerations for Chinese agricultural water and food safety: Issues, challenges and suggestions. *African Journal of Biotechnology, 9*, 5251-5261

Puma, M.J., & Cook, B.I. (2010). Effects of irrigation on global climate during the 20th century. *Journal of Geophysical Research-Atmospheres, 115*, 15

Qian, T.T., Dai, A., Trenberth, K.E., & Oleson, K.W. (2006). Simulation of global land surface conditions from 1948 to 2004. Part I: Forcing data and evaluations. *Journal of Hydrometeorology, 7*, 953-975

Ramankutty, N., Evan, A.T., Monfreda, C., & Foley, J.A. (2008). Farming the planet: 1. Geographic distribution of global agricultural lands in the year 2000. *Global Biogeochemical Cycles, 22*

Rangwala, I., Miller, J.R., & Xu, M. (2009). Warming in the Tibetan Plateau: Possible influences of the changes in surface water vapor. *Geophysical Research Letters, 36*, 6

Rind, D. (1998). Climate change - Just add water vapor. *Science, 281*, 1152-1153

Rind, D., Chiou, E.W., Chu, W., Larsen, J., Oltmans, S., Lerner, J., McCormick, M.P., & McMaster, L. (1991). Positive water-vapor feedback in climate models confirmed by satellite data. *Nature, 349*, 500-503

Sacks, W.J., Cook, B.I., Buenning, N., Levis, S., & Helkowski, J.H. (2009). Effects of global irrigation on the near-surface climate. *Climate Dynamics, 33*, 159-175

Segal, M., Pan, Z., Turner, R.W., & Takle, E.S. (1998). On the potential impact of irrigated areas in North America on summer rainfall caused by large-scale systems. *Journal of Applied Meteorology, 37*, 325-331

Shiklomanov, I.A. (2000). Appraisal and Assessment of World Water Resources. *Water International, 25*, 11-32

Siebert, S., & Döll, P. (2008). The Global Crop Water Model (GCWM): Documentation and first results for irrigated crops. In: Frankfurt Hydrology Paper 07, Institute of Physical Geography, University of Frankfurt, Frankfurt am Main, Germany.

Siebert, S., Döll, P., Feick, S., Frenken, K., & Hoogeveen, J. (2007). Global map of irrigated areas version 4.0.1. *Rome, Italy: University of Frankfurt (Main), Germany / Food and Agriculture Organization of the United Nations*

Siebert, S., Döll, P., Hoogeveen, J., Faures, J.-M., Frenken, K., & Feick, S. (2005a). Development and validation of the global map of irrigation areas. *Hydrology and Earth System Sciences,, 9*

Siebert, S., Doll, P., Hoogeveen, J., Faures, J.M., Frenken, K., & Feick, S. (2005b). Development and validation of the global map of irrigation areas. *Hydrology and Earth System Sciences, 9*, 535-547

Siebert, S., Feick, S., Döll, P., & Hoogeveen, J. (2005c). Global map of irrigation areas Version 3.0. *versity of Frankfurt (Main), Germany, and FAO, Rome, Italy*.

Simelton, E. (2011). Food self-sufficiency and natural hazards in China. *Food Security, 3*, 35-52

Song, Z.W., Zhang, W.J., & Chen, F. (2010). Research on agricultural water resource balance and its optimal utilization in Beijing. *Water Saving Irrigation*, 30-34. (In Chinese)

Thenkabail, P.S., Biradar, C.M., Noojipady, P., Dheeravath, V., Li, Y.J., Velpuri, M., Gumma, M., Gangalakunta, O.R.P., Turral, H., Cai, X.L., Vithanage, J., Schull, M.A., & Dutta, R. (2009). Global irrigated area map (GIAM), derived from remote sensing, for the end of the last millennium. *International Journal of Remote Sensing, 30*, 3679-3733

Thenkabail, P.S., Biradar, C.M., Noojipady, P., Dheeravath, V., Li, Y.J., Velpuri, M., Reddy, G.P.O., Cai, X.L., Gumma, M., Turral, H., Vithanage, J., Schull, M., & Dutta, R. (2008). A Global Irrigated Area Map (GIAM) Using Remote Sensing at the End of the Last Millennium. *International Water Management Institute.*, 63

Thenkabail, P.S., Biradar, C.M.T., H., , Noojipady, P.L., Y. J.,, Vithanage, J., Dheeravath, V., Velpuri, M., Schull, M., Cai, X.L., & Dutta, R. (2006). An irrigated area map of the world (1999) derived from remote sensing. *Research Report 105. Colombo, Sri Lanka: International Water Management Institute.*

Thenkabail, P.S., Schull, M., & Turral, H. (2005). Ganges and Indus river basin land use/ land cover(LULC) and irrigated area mapping using continuous streams of MODIS data. *Remote Sensing of Environment, 95*, 317-341

Thomas, A. (2008). Agricultural irrigation demand under present and future climate scenarios in China. *Global and Planetary Change, 60*, 306-326

Wa, D. (2009). Prediction and analysisi of water demand in Tibet. *Yantze River, 40*, 37-38,45.(In Chinese)

Wang, K.C., & Liang, S.L. (2008). An improved method for estimating global evapotranspiration based on satellite determination of surface net radiation, vegetation index, temperature, and soil moisture. *Journal of Hydrometeorology, 9*, 712-727

Wang, K.C., Wang, J.K., Wang, P.C., Sparrow, M., Yang, J., & Chen, H.B. (2007). Influences of urbanization on surface characteristics as derived from the Moderate-Resolution Imaging Spectroradiometer: A case study for the Beijing metropolitan area. *Journal of Geophysical Research-Atmospheres, 112*, 12

Wang, Y.B., Wu, P.T., Zhao, X.N., & Li, J.L. (2010). Development tendency of agricultural water structure in China. *Chinese Journal of Eco-Agriculture, 18*, 399-404.(In Chinese)

Wauer, B. (2007). Climate response to irrigation in the American west. In, *Departmetn of Atmospheric and Oceanic Science* (p. 16). College Park: University of Maryland

Weare, B.C., & Du, H. (2008). Modelling regional climate changes: influences of recent global warming and irrigation in California. *International Journal of Climatology, 28*, 1201-1212

Wriedt, G., van der Velde, M., Aloe, A., & Bouraoui, F. (2009). A European irrigation map for spatially distributed agricultural modelling. *Agricultural Water Management, 96*, 771-789

Wu, P.T., Jin, J.M., & Zhao, X.N. (2010). Impact of climate change and irrigation technology advancement on agricultural water use in China. *Climatic Change, 100*, 797-805

Xue, Y.K. (1996). The impact of desertification in the Mongolian and the Inner Mongolian grassland on the regional climate. *Journal of Climate, 9*, 2173-2189

Xue, Y.K., & Shukla, J. (1993). The influence of land-surface properties on sahel climate .1. desertification. *Journal of Climate, 6*, 2232-2245

Yang, Y.M., Yang, Y.H., Moiwo, J.P., & Hu, Y.K. (2010). Estimation of irrigation requirement for sustainable water resources reallocation in North China. *Agricultural Water Management, 97*, 1711-1721

Yao, Z., Liu, X., Li, X., Yang, F., Sun, L., & Wen, B. (2009). Analysis of agroecosystems in Jilin Province based on energy theory. *Chinese Jouranl of Ecology, 28*, 2076-2081

Yu, L., & Zuo, T. (2010). The transition of rural economics and agricultural production in China from 1978 to 2008. *Reform of Economic System*, 93-98

Zhao, M.S., Heinsch, F.A., Nemani, R.R., & Running, S.W. (2005). Improvements of the MODIS terrestrial gross and net primary production global data set. *Remote Sensing of Environment, 95*, 164-176

Zhou, L.M., Dickinson, R.E., Tian, Y.H., Fang, J.Y., Li, Q.X., Kaufmann, R.K., Tucker, C.J., & Myneni, R.B. (2004). Evidence for a significant urbanization effect on climate in China. *Proceedings of the National Academy of Sciences of the United States of America, 101*, 9540-9544

Zhu, X., Liang, S., & Pan, Y. (2011a). Agricultural irrigation requirement under future climate scenarios in China. *Agricultural Water Management* (in revision)

Zhu, X., Liang, S., & Pan, Y. (2011b). Comparing land management impacts with land cover change impacts on climate in China (in preparion)

Zhu, X., Liang, S., & Pan, Y. (2011c). The impacts of land cover and land use change on climate in China. *Journal of Geophysical Research-Atmospheres* (submitted)

Zhu, X., Liang, S., & Pan, Y. (2011d). Mapping Irrigated Areas in China from Remote Sensing and Statistical Data. *Ieee Transactions on Geoscience and Remote Sensing* (in revision)

Zhu, X., Liang, S., & Pan, Y. (2012). Observational evidence of the cooling effect from agricultural irrigation in Jilin, China. *Climatic Change* (accepted)

Zhu, X., Liang, S., Pan, Y., & Zhang, X. (2011e). Agricultural irrigation impacts on land surface characteristics detected from satellite data products in Jilin Province,

China. *IEEE Journal of Selected Topics in Applied Earth Observations and Remote Sensing, 4*, 721-729